

UNIVERSITÀ DEGLI STUDI DI SALERNO
Dipartimento di Fisica “E.R. Caianiello”



XXXIII CICLO DI DOTTORATO IN
MATEMATICA, FISICA ED APPLICAZIONI

Tesi di Dottorato in

*Methodologies for environmental risks
assessment related to the exploitation of
energy geo-resources*

Tutor

prof. Paolo Capuano

Co-Tutor

dott. Guido Maria Adinolfi

Coordinatore

prof. Carmine Attanasio

Dottoranda

Elvira Battimelli

Elvira Battimelli

ANNO ACCADEMICO 2020-2021

Abstract

The increasing exploitation of geo-energy resources to satisfy the needs of the world's population has also led to a focus on the risks associated with this type of human activity. It is in this context that this thesis is to be carried out with the purpose to study TechNa (Technological Hazard Triggering Natural Disaster) and NaTech (Natural Hazard Triggering Technological Disaster) events. The natural phenomenon that is a consequence of an industrial activity or acts as a hazard for the industrial accident is considered to be an earthquake. The entire thesis, carried out following a multidisciplinary approach, aims to provide a contribution to the development of methodologies for the assessment of environmental risks potentially related to the technological activities of geo-resources exploitation.

Three case studies and different specific methodologies are considered to explore a broad spectrum of analyses, i.e., the seismic characterization of an area, the statistical correlation between the industrial and seismic activity, and finally a multi-hazard risk assessment.

The TechNa event considered is the induced seismicity that is studied in the offshore area of Porto San Giorgio (Italy) and for the Cooper Basin geothermal site (Australia). In the first case, a probabilistic approach (Lomax et al., 2000) is used to relocate the 1987 Porto San Giorgio seismic sequence, which occurred in the Adriatic offshore near the Santa Maria a Mare hydrocarbon field. The ambiguity on the mainshock depth, already known in the literature, is solved by developing a technique that uses the macroseismic intensity field data based on a grid-search of the magnitude-depth space. The results show that the seismic sequence (about 30 events) developed in the first 15 km of the crust activating thrust faults and the mainshock has depth of 5.7 km and local magnitude equal to 5. Subsequently, to investigate whether there is a relationship between anthropogenic activity and seismicity, a statistical correlation analysis is carried out using the binomial and Mann-Whitney tests. It provides

statistically significant values in correspondence with the 1987 Porto San Giorgio seismic sequence.

The second study on induced seismicity carried out in this thesis concerns the unconventional geothermal site of Cooper Basin. Unconventional techniques involve creating fractures for the circulation of fluids, but sometimes they can reach pre-existing faults by undesirable pathways, triggering strong earthquakes. In this work the relationship between technological parameters and the potential for seismicity to build undesirable pathways for fluid migration is investigated through a modern methodology (Lasocki & Orlecka-Sikora, 2020). A new parameter ZZ , degree of disordering of sources, quantifies this potential. It is calculated as the distance between seismic events in an eight-dimensional space consisting of three hypocentral coordinates, T- and P-axis plunges, T-axis trend, and polar and azimuthal angles in the spherical system of coordinates beginning at the open hole of the Habanero 4 well. A Spearman correlation test is performed between technological parameters and ZZ showing that the higher the injection rate and wellhead pressure was, the less probable was the ability to create unwanted paths for fluid migration.

The third case study in this work is the analysis of a NaTech event. A multi-hazard risk analysis is conducted on the gas storage site of San Potito and Cotignola (Italy) simulating the failure of a pipeline generated by an earthquake and/or the material fatigue of the material. A bow-tie approach is followed to calculate the probability of occurrence of an accident, i.e., the leakage of gas from a pipeline. A Fault Tree is quantitatively solved using a new, very important tool, i.e., the MERGER application (Garcia-Aristizabal et al., 2019) available on the IS-EPOS platform (Orlecka-Sikora et al., 2020). Conversely, the Event Tree is only represented qualitatively.

Contents

	<i>page</i>
List of figures	7
List of tables	11
Introduction	13
Chapter 1: Risks and energy technologies	19
1.1 TechNa events: focus on induced/triggered seismicity	20
1.1.1 <i>Oil and gas extraction</i>	25
1.1.2 <i>Geothermal energy</i>	29
1.1.3 <i>Wastewater injection and Carbon capture and storage</i>	30
1.1.4 <i>Water reservoir impoundment</i>	32
1.1.5 <i>IS-EPOS Platform</i>	33
1.2 NaTech events	34
1.2.1 <i>Earthquake-triggered NaTech events</i>	36
Chapter 2: Methodologies	39
2.1 Seismological methodologies	40
2.1.1 <i>Earthquake location</i>	43
2.1.1.1 <i>The NonLinLoc Software</i>	47
2.1.2 <i>Transformation to Equivalent Dimensions of earthquake parameters</i>	51
2.2 Statistical methodologies	54
2.3 Multi-hazard risk analysis	58
2.3.1 <i>Merger application</i>	60
Chapter 3: Study of seismicity in areas subject to hydrocarbon extraction	63
3.1 Seismotectonic setting	64
3.2 Porto San Giorgio seismic sequence 1987	70
3.2.1 <i>Earthquake relocation of the Porto San Giorgio 1987</i>	

<i>mainshock</i>	72
3.2.2 <i>Earthquake relocation of Porto San Giorgio seismic sequence</i>	79
3.2.3 <i>Results and discussion</i>	80
3.3 Statistical correlation analysis in Porto San Giorgio area	84
3.3.1 <i>Results and discussion</i>	87
3.3.1.1 Analysis of annual data	89
3.3.1.2 Analysis of monthly data	91
3.4 Conclusions	93
Chapter 4: Study of seismicity in area subject to geothermal exploration	97
4.1 The Cooper Basin geothermal field case study	98
4.2 Seismic and industrial dataset	101
4.3 Method	106
4.4 Results and discussion	111
4.5 Conclusions	119
Chapter 5: A multi-hazard risk analysis of an industrial plant: the San Potito and Cotignola gas storage field	121
5.1 The San Potito and Cotignola gas storage field	123
5.2 Risk pathway scenario	125
5.3 Earthquake – related failure of an asset	127
5.3.1 <i>Seismic hazard analysis</i>	128
5.3.2 <i>Earthquake – related fragility and failure of gas pipelines</i>	132
5.4 Fault Tree analysis	135
5.5 Conclusions	138
Conclusions	141
Appendix A	147
Bibliography	161
Web references	177

List of figures

<i>Figure</i>	<i>page</i>
1.1 Schematization of the possible initiating causes of anthropogenic seismicity.	20
1.2 Trend over time (1966-2016) of the number of publications on induced seismicity.	21
1.3 Normalized number of worldwide and Italian Google searches for the words "fracking earthquake", "drilling", "gas extraction and storage" and "fracking."	22
1.4 World map showing 1229 projects with reported induced seismicity.	23
1.5 Graphic representation of fluid injection into a permeable rock surrounded by impermeable elastic material.	24
1.6 Schematic representation of Enhanced oil recovery through the injection of CO ₂ .	26
1.7 Schematic representation of fracking technique.	27
1.8 Schematic representation of oil-gas production and wastewater injection.	31
1.9 Geographical distribution of the episodes available on the IS-EPOS platform.	34
2.1 Graphical representation of the fault plane geometry.	41
2.2 Schematic representation of a focal mechanism through a beach-ball diagram for different types of faults.	42
2.3 The Oct-Tree method: sampling of cells in 3D space.	49
2.4 Graphical representation of the Oct-Tree sampling procedure.	50
2.5 Graphical representation of the Oct-Tree results.	50
2.6 Graphical representation of the equivalent-dimensional transformation.	54
2.7 Bow-tie schematic structure.	59
2.8 Example of bow-tie structure for a Top Event identified as leakage of fluid, that is, in turn, the Basic Event of the Event Tree.	60
2.9 MERGER application interface on the IS-EPOS platform.	61
3.1 Geological structural map of the Central Adriatic basin.	66
3.2 Epicentral distribution of Italian seismicity.	67
3.3 Historical and instrumental seismicity in the Porto San Giorgio area.	69
3.4 Seismic network map at distance up to 400 km from Porto San Giorgio.	71

3.5 Modified Wadati diagram obtained considering the dataset recorded by seismic stations within 150 km of Porto San Giorgio.	71
3.6 Histograms of the weighting factors associated to the P- and S-wave arrival-time catalog.	73
3.7 Relocation of the PSG mainshock using different 1D P-velocity models taken from the literature and $V_p/V_s=1.70$.	75
3.8 Macroseismic intensity map of the ML 5, Porto San Giorgio earthquake and results of the grid-search performed in the magnitude-depth space.	78
3.9 Histograms of the 91 seismic events distributions to evaluate the quality of locations of the PSG seismic sequence.	79
3.10 Epicentral and hypocentral distribution of the relocated 1987 Porto San Giorgio seismic sequence.	82
3.11 Map of seismicity in Porto San Giorgio area (1985-2015).	86
3.12 Orthogonal regression line to extrapolate a magnitude conversion rule in the study area.	87
3.13 Magnitude distribution of 247 seismic events after the application of the transformation rule on 190 values of duration magnitude.	87
3.14 Annual production (oil, water, and gas) and values of injected water since 1985 to 2015 considering all wells in the field.	89
3.15 Trend of monthly production technological parameters (oil, water, and gas) from 9 wells in the period 1985 – March 1992.	92
4.1 Map of Australia showing Cooper Basin.	98
4.2 Schematic representation of Habanero wells intersecting the ‘Habanero Fault’.	99
4.3 Map of station network in Habanero field.	100
4.4 Spatio – temporal distribution of seismicity after Habanero 4 well stimulation.	101
4.5 Time evolution (step 1 day) of the seismic events occurred in the Cooper Basin geothermal field from November to December 2012.	102
4.6 Magnitude distribution of the 20734 seismic events occurred in the Cooper Basin geothermal field from November to December 2012.	102
4.7 Map of the 489 seismic events used in this study.	103
4.8 Moment magnitude distribution with step 0.1.	104
4.9 Distribution of earthquake parameters: longitude, latitude, and respective relative errors; elevation and respective relative error; strike, dip, and rake.	105

4.10 Trend of injection rate and wellhead pressure (17-30 November 2012) in the Habanero 4 well of the Cooper Basin geothermal field.	106
4.11 Variation of the ZZ parameter in windows 1:45.	109
4.12 Variation of Δ_r in windows 1:45.	109
4.13 Variation of Δ_m in windows 1:45.	110
4.14 Variation of Δ_ϕ in windows 1:45.	110
4.15 Variation of the average injection rate in windows 1:35.	111
4.16 Variation of the average wellhead pressure in windows 1:35.	111
4.17 Variation of injection rate, wellhead pressure with a delay of two windows with respect to injection, ZZ with a delay of two windows with respect to wellhead pressure.	118
5.1 Map of the area where the San Potito and Cotignola gas storage field is located.	123
5.2 Schematization of San Potito and Cotignola gas storage facility.	124
5.3 Fault tree in which there are two basic events (B01 and B02), and the top event is the spill of gas in the air.	126
5.4 Simplified Event Tree in which there are three nodes: the spill of gas in the air as initiating event (i.e., the top event of the Fault Tree), the ignition and the incident outcome.	127
5.5 Graphical schematization of the mesh used to calculate the value of the intensity parameter at point X, known the value that it assumes in nodes 1, 2, 3 and 4 and the distances d_i .	129
5.6 Seismic hazard curve in term of annual frequency of exceedance of PGA for the point Cluster A of coordinates (11.9472°, 44.4203°).	130
5.7 Seismic hazard curve in term of annual frequency of exceedance of PGA for the point Cluster B of coordinates (11.9472°, 44.4203°).	131
5.8 Seismic hazard curve in term of annual frequency of exceedance of PGA for the point Cluster C of coordinates (11.9194°, 44.3710°).	131
5.9 Earthquake-related fragility curve calculated for a natural gas pipeline in the 1st case study (Cluster A) of the gas storage site.	133
5.10 Earthquake-related fragility curve calculated for a natural gas pipeline in the 2nd case study (Cluster B) of the gas storage site.	134
5.11 Earthquake-related fragility curve calculated for a natural gas pipeline in the 3rd case study (Cluster C) of the gas storage site.	134

5.12 Results of the annual probability of occurrence of the top event obtained in cluster A of the gas storage site.	136
5.13 Results of the annual probability of occurrence of the top event obtained in cluster B of the gas storage site.	137
5.14 Results of the annual probability of occurrence of the top event obtained in cluster C of the gas storage site.	137
A.1 Tests on instrumental earthquakes of the 2009 L'Aquila seismic sequence to verify the reliability of the methodology to get information about depth and magnitude of pre-instrumental earthquake from the macroseismic intensity field.	154
A.2 Results of the grid searching for test 1, test 2, and test 3.	156

List of tables

<i>Table</i>	<i>page</i>
3.1 Location of the mainshock of the PSG seismic sequence obtained by different seismological institutes	72
3.2 Results of the mainshock relocation using six different 1D P-velocity models and V_p / V_s equal to 1.70.	76
3.3 Relocation results obtained for 30 events of the PSG seismic sequence (July – December 1987).	81
3.4 Annual results of binomial and U-test.	90
3.5 Results of binomial and Mann Whitney U-test obtained by considering summarized monthly data from nine wells.	93
4.1 Mean and standard deviation of injection rate and wellhead pressure in the three phases of the technological process.	112
4.2 Results of Spearman rank correlation between injection rate and the degree of disordering of sources, ZZ , and its components.	113
4.3 Results of Spearman rank correlation between wellhead pressure and the degree of disordering of sources, ZZ , and its components.	114
4.4 Results of Spearman rank correlation - injection rate and wellhead pressure.	115
5.1 PGA values (expressed in g) and annual frequency of exceedance for the point cluster A of coordinates (11.9472°, 44.4203°).	130
5.2 PGA values (expressed in g) and annual frequency of exceedance for the point cluster B of coordinates (11.9692°, 44.3617°).	130
5.3 PGA values (expressed in g) and annual frequency of exceedance for the point Cluster C of coordinates (11.9194°, 44.3710°).	131
5.4 Values of the annual rate of failure (λ) due to an earthquake for the pipelines considered in each case study of the gas storage site.	135
5.5 Values of the annual probability of occurrence of the top event, considering the 50th, 5th and 95th percentiles in each cluster of the gas storage site.	136
A.1 Macroseismic intensity data of Porto San Giorgio (PSG) mainshock (3 July 1987, 10:21.57 UTC).	147
A.2 The final solutions of grid-searching for the three tests performed.	157
A.3 Cumulative delay list for P and S phases at each station.	157

INTRODUCTION

The Sustainable Development Goals included in the 2030 Agenda, approved by the United Nations (UN) General Assembly, represent an important challenge and opportunity for a dialogue between scientists, society, and political institutions to achieve environmental, economic, and social goals. The 2030 Agenda is an international program of action for people, planet, and prosperity with the goal of creating a better and sustainable future. Science becomes the engine of change by playing a fundamental role in the acquisition and dissemination of knowledge necessary for its realization (Schneider et al., 2019). Moving towards sustainable development requires also strengthening resilience and adaptive capacity to risks associated with climate change and natural disasters (Goal 13 UN Agenda 2030) by mitigating the impacts on the economy, cities, people, and the environment. Although natural events occur in a short period of time, their impact is durable over time, such as the post-earthquake scenarios that heavily affects the country's economy and the whole society. This is further complicated when the natural and industrial worlds meet in a particularly vulnerable area resulting in major incidents (Krausmann & Cruz, 2017) as happened in Fukushima in 2011.

With the purpose of reducing disaster-related risks, the state governments and international disaster risk communities signed a 15-year international agreement in Sendai, Japan, in 2015 (Mysiak et al., 2015). It consists of four priority areas, thirteen guiding principles, and seven goals that aim to reduce loss of life and economic loss and damage to critical infrastructures (e.g., schools, hospitals, etc.) by increasing the implementation of early warning systems and improving understanding of disaster risk. At the global level, it is necessary to increase knowledge and studies to better understand which risks arise from the occurrence of natural disasters, developing scientific methodologies to study available data and implement strategies for the mitigation of future risks (UN, 2015).

The exploitation of geo-resources inevitably involves risks even when so-called clean and renewable energy sources are considered. These risks can

cause harmful effects on the surrounding environment and the industrial apparatus itself with consequent economic losses and fatalities in extreme cases. The events that produce the most damage are rare events, i.e., they occur with low probability, while routine operations that occur with greater frequency are manageable. A distinction can be made between TechNa (Technological Hazard Triggering Natural Disaster) and NaTech (Natural Hazard Triggering Technological Disaster) events depending on whether the natural phenomenon is a consequence of anthropogenic industrial-type activity or acts as a hazard of an accidental industrial event.

Considering as an industrial activity the exploitation of geo-resources and as a natural phenomenon the earthquake, it follows that the TechNa event is represented by anthropogenic seismicity, also known as induced seismicity. This phenomenon occurs as a result of changes in the pore pressure of subsurface rocks that, in turn, create increased stress that can exceed the threshold value for fracture. Such a situation may arise from underground extraction or injection of fluids, work in the mining industry, filling or emptying of reservoirs, gas or CO₂ storage. The issue of induced seismicity is much debated in the scientific, political, and social scene (Ellsworth, 2013) as it can lead to significant damage especially in highly urbanized areas. It is, therefore, necessary to carry out detailed studies of seismicity occurred in areas of geo-resources exploitation to expand knowledge of this phenomenon and develop safety protocols.

On the other hand, the earthquake, as other natural phenomena, can be a hazard for the occurrence of industrial-type accidents with the release of hazardous substances into the environment due to material spills from plant elements, explosions or fires giving rise to a domino effect (Krausmann & Cruz, 2017). It is the so called NaTech event. A lot of past NaTech accidents underline how society is unprepared to deal with the impact of natural events on highly vulnerable industrial activities with damage to human health, environment, and economy. The occurrence of an extreme phenomenon such as an earthquake can generate a series of cascading events that amplify the damage of the natural event itself. In

fact, it can generate, for example, collapses of the escape routes of the industrial plant, the breakdown of the safety systems and the fall of the houses surrounding the industrial activity complicating the arrival of the rescues. In addition, in case of a toxic spill into the environment special safety measures to protect people living in the vicinity of the facility should be provided. The increasing urbanization and industrialization and the increasing occurrence of rare events, also due to climate change, make necessary the development of methodologies for the prevention and mitigation of risks due to NaTech events with the formulation of emergency-response plans. To develop disaster plans for both NaTech and TechNa events, it is important to consider every phase of the industrial activity, from construction to decommissioning. Moreover, it is necessary to properly inform and educate the population about the possible risks and benefits resulting from the presence of a particular industrial facility in an area.

The aim of this thesis is to study TechNa and NaTech events considering three case studies and different methodologies: the Porto San Giorgio offshore area (Italy), where hydrocarbon exploitation is carried out; the geothermal site of Cooper Basin (Australia) and the gas storage site of San Potito and Cotignola (Italy). This work wants to give a contribution to the development and research of methodologies for the assessment of environmental risks potentially related to the technological activities of exploitation of geo-resources.

Frequently, studies of induced seismicity are performed, but rarely the industrial aspect is investigated. In this thesis the whole spectrum of possible analyses has been covered: 1) seismicity characterization (localizations, focal mechanisms,...); 2) statistical correlations to study induced seismicity by using different tests, 3) multi-hazard analysis related to the failure of components of the industrial plant. The innovation lies in the fact that the whole procedure was followed, although each part is treated separately in the three different case studies. This choice is related to the availability of data and is linked to the individual cases analyzed. Each point was analyzed specifically, with recent and specific

methodologies (e.g., Lomax et al., 2000; Lasocki, 2014, Garcia-Aristizabal et al., 2019).

The study carried out in the Porto San Giorgio offshore area (Italy) fits into the re-analysis of past seismicity in areas of geo-resources exploitation in view of new knowledge on induced seismicity. It wants to provide an innovative contribution to seismotectonic of the area, already investigated (Riguzzi et al., 1989; Console et al., 1992), and new insights on the possible link between seismicity and anthropogenic activity in the area. On 3 July 1987, a seismic sequence, with a mainshock of M_L 5, took place in the Adriatic offshore, close to the coast of Porto San Giorgio municipality (PSG). In this work an accurate relocation of the PSG seismic sequence using a nonlinear probabilistic approach (Lomax et al., 2000) is presented. The trade-off between the hypocentral location and the velocity model is exhaustively explored using six different velocity models available for the area provided by previous studies. To solve the ambiguity of the mainshock depth, a technique that uses the macroseismic intensity field data is used. Because the offshore of Adriatic Sea hosts several hydrocarbon (mainly gas) production fields, located near active faults, with some of them in the area of this study, analyzing the past and instrumental seismicity is necessary to better understand the seismicity generated by the seismogenic faults and improve the assessment of the area's seismic hazards. The study of analyzing a possible correlation between seismicity and industrial activity is conducted statistically using the binomial and Mann-Whitney tests by analyzing the change in seismicity rates and medians of the magnitudes of seismic events with the simultaneous change in the trends of production parameters.

In the Cooper Basin area there is an Enhanced Geothermal System that apply the pressurized fluid injection to fracture impermeable rocks to form pathways in which water circulates, as required by the industrial process. However, the induced fractures may coalesce into unwanted paths that allow the fluids to reach pre-existing faults, triggering major seismic events. To study the relationship between injection and seismicity, in particular the potential of seismicity to build these “undesirable” paths

a Spearman correlation analysis is performed between industrial parameters and a new quantity, namely ZZ, focusing on the Habanero 4 well stimulation. ZZ is the degree of disordering of sources and quantifies the potential of seismicity to build pathways for fluid migration. The analysis is carried out using the technique recently proposed by Lasocki (2014), in which the limitation of comparing different physical quantities was overcome through an equivalent-dimensional transformation. Mathematically, ZZ is calculated as the distance between seismic events in an eight-dimensional parameter space consisting of three hypocentral coordinates, T- and P-axis plunges, T-axis trend, and polar and azimuthal angles in the spherical system of coordinates beginning at the open hole of the Habanero 4 well. An increasing hazard of forming far-reaching migration pathways occurs in correspondence with a decrease in ZZ. The methodology used is the same as that developed and applied by Lasocki & Orlecka-Sikora (2020) to study the geothermal field at The Geysers.

The third and last case study treated in this work is the San Potito and Cotignola gas storage site located in the Emilia-Romagna region (Northern Italy). When an earthquake occurs, pipelines are the elements of a facility that require the most attention. Since they often extend over long distances, damage to them can cause the release of toxic and flammable materials with disastrous consequences. In this work, a multi-hazard risk analysis was performed with the aim of assessing the probability of occurrence of an accident, identified as the leakage of gas from a pipeline located within the storage site. The study is conducted following a bow-tie approach in which earthquake, as a natural hazard, and material fatigue are considered as potential accident triggering events. The calculation of the pipeline rupture probability is carried out according to the methodology reported in Porter (2021) knowing the values of the seismic excitation (i.e., PGA) and having properly calculated the fragility function. The annual probability of occurrence of the incident event was calculated by computational resolution of the Fault Tree using the MERGER application (Garcia Aristizabal et al., 2019) available on the Induced Seismicity - European Plate Observing System (IS-EPOS; Orlecka-Sikora et al., 2020) platform.

This thesis work is structured with a total of five chapters, of which the first two provide the necessary notions to introduce the topic to be discussed. Chapter 1 discusses TechNa events with detailed explanation of all possible causes of anthropogenic seismicity related to the exploitation of energy geo-resources and NaTech events with particular attention to what can happen in the case where the natural hazard is an earthquake. The seismological, statistical, and multi-hazard risk analysis methodologies employed in the work to analyze each case study are presented in Chapter 2. In Chapter 3 the whole seismological and statistical study carried out in the Porto San Giorgio offshore area is presented, considering the 1987 seismic sequence and the anthropogenic activity in the area. The statistical correlation analysis related to the Cooper Basin geothermal field to understand the relationship between the probability of creating undesirable fluid migration paths and industrial parameters is presented in detail in Chapter 4. Finally, Chapter 5 illustrates the multi-hazard risk analysis carried out on the San Potito and Cotignola gas storage site to determine the probability of occurrence of an accidental event. At the end, the Conclusions are reported.

The whole thesis work was performed in the framework of “MIUR-PON R&I Azione I.1 Dottorati innovativi con caratterizzazione industriale” and of the S4CE (“Science for Clean Energy”) project, funded from the European Union’s Horizon 2020–R&I Framework Programme, under Grant Agreement Number 764810, and of the PRIN-MATISSE (20177EPPN2) project funded by Italian Ministry of Research. In addition, this thesis work was carried out with the following partners of the PhD project: Edison S.p.A., an Italian electric utility company, and the Department of Seismology - Institute of Geophysics of the Polish Academy of Sciences.

RISKS AND ENERGY TECHNOLOGIES

The growth of the world population has led to an ever-increasing demand for energy with a consequent massive exploitation of natural fossil resources (i.e., coal, oil, and gas). In recent years, international climate agreements have given a great boost to the development of renewable energies, whose primary sources are the sun, wind, sea, biomass, water, and heat. All these energy activities bring improvements to human life but at the same time there is no energy production without any risk on the environment, society, and economy. It is therefore necessary to talk about energy as a complex system of issues concerning different areas such as technological, environmental, financial, economic, and social sectors (De Michele, 2014). Mathematically, this could be expressed by the equation (Ehrlich & Holdren, 1972):

$$I = P \times A \times T$$

This means that the human impact on the environment (I) is the result of the product between the human population (P), the affluence (A), i.e., consumption per person, and the impact of technology on the environment (T). The impact, i.e., routine impacts and incidents, can be minimized by acting on factors A and T by modifying consumption and their quality (Greco, 2014). In the last century, the population has increased exponentially and economic prosperity in wealthy parts of the world has led to an increase in affluence generating an increase in the impacts. In order to reduce the human impact, it is very important to understand what level of risk is considered acceptable for each form of energy exploitation in relation to the objectives to be achieved (Leone, 2014).

The purpose of this chapter is to provide an overview of what happens when the natural and technological worlds interact. In particular, the NaTech (Natural Hazard Triggering Technological Disaster) and TechNa

(Technological Hazard Triggering Natural Disaster) events are considered with a special focus on anthropogenic seismicity. The former occurs when the natural phenomenon generates a technological accident while, vice versa, the latter when the technological activity is at the origin of a problem concerning the natural environment.

1.1 TechNa events: focus on induced/triggered seismicity

It is possible that anthropogenic activities linked to the use of industrial equipment can have effects on the surrounding environment. In this case we talk about TechNa (Technological Hazard Triggering Natural Disaster) events. Examples are air or groundwater pollution due to industrial activities and anthropogenic seismicity that is the TechNa event on which this thesis work is focused.

The technological activities that exploit geo-resources are all potential causes of anthropogenic seismicity. These include oil and gas extraction, geothermal energy production, underground mining, underground storage of CO₂, filling and emptying of water reservoirs (Figure 1.1).

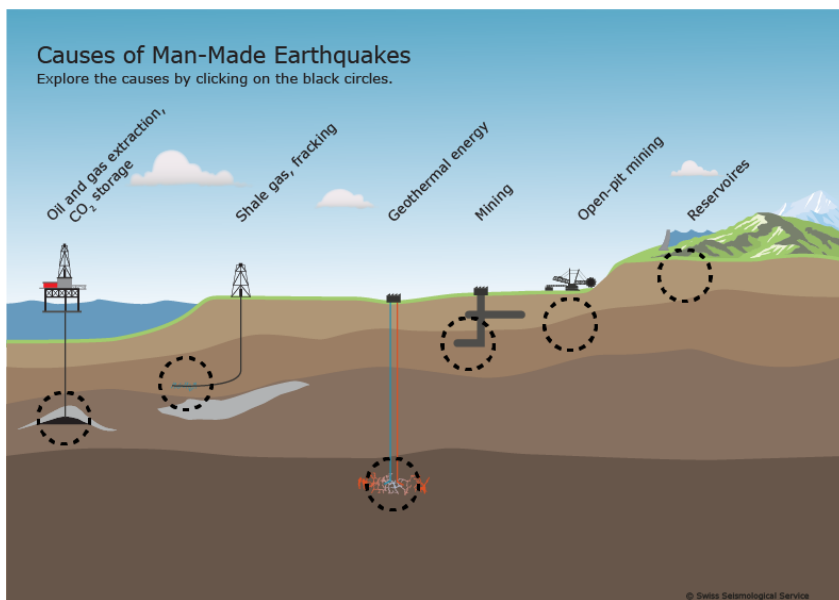


Figure 1.1 - Schematization of the possible initiating causes of anthropogenic seismicity. Source: Swiss Seismological Service (SED) ETH Zurich (<http://www.seismo.ethz.ch>; last accessed, March 2021)

When we talk about anthropogenic seismicity, we refer to:

- induced seismicity - the earthquake is generated due to variations in the stress field caused only by anthropogenic activities in an area that is generally not tectonically active. In this case, earthquakes are of low magnitude and detectable only by instruments, with few exceptions;
- triggered seismicity - the seismic event occurs in an active seismic area and the system shift from a critical state to instability by means of human activity. Earthquakes activating pre-existing faults can be of high magnitude and they would have happened in any case but in a longer time.

However, induced seismicity is generally used for both definitions by many researchers and in common language.

Although the first case of induced seismicity dates to the early decades of the 1900s, interest in this topic has grown in recent years, not only in the scientific community (Figure 1.2) but worldwide in politics, society, and institutions due to the damage that these events can generate (Ellsworth, 2013). A study carried out by Grigoli et al. (2017) shows how the online search for words like “fracking earthquakes”, “drilling” or “gas extraction” has increased after the widespread use of the fracking technique in the United States with re-injection of wastewater and simultaneously to the Emilia-Romagna (Italy, 2012) seismic sequence (Figure 1.3) in Italy.

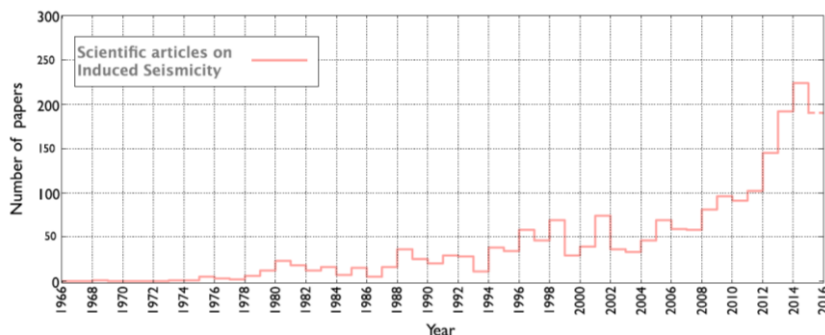


Figure 1.2 – Trend over time (1966-2016) of the number of publications on induced seismicity. Source: Grigoli et al. (2017)

This ever-growing interest and the multiplication of cases led to the creation in 2017 of The Human-Induced Earthquake Database (HiQuake) which to date contains 1229 projects worldwide reporting induced seismicity (The Human Induced Earthquake Database (HiQuake): <https://inducedearthquakes.org/>, Figure 1.4). The database, initially funded by Nederlandse Aardolie Maatschappij BV (NAM) to Durham University (UK) and Geenergy Durham Ltd, is freely accessible and groups variable quality data from scientific articles, government and industrial relations, academic activities (Wilson et al., 2017).

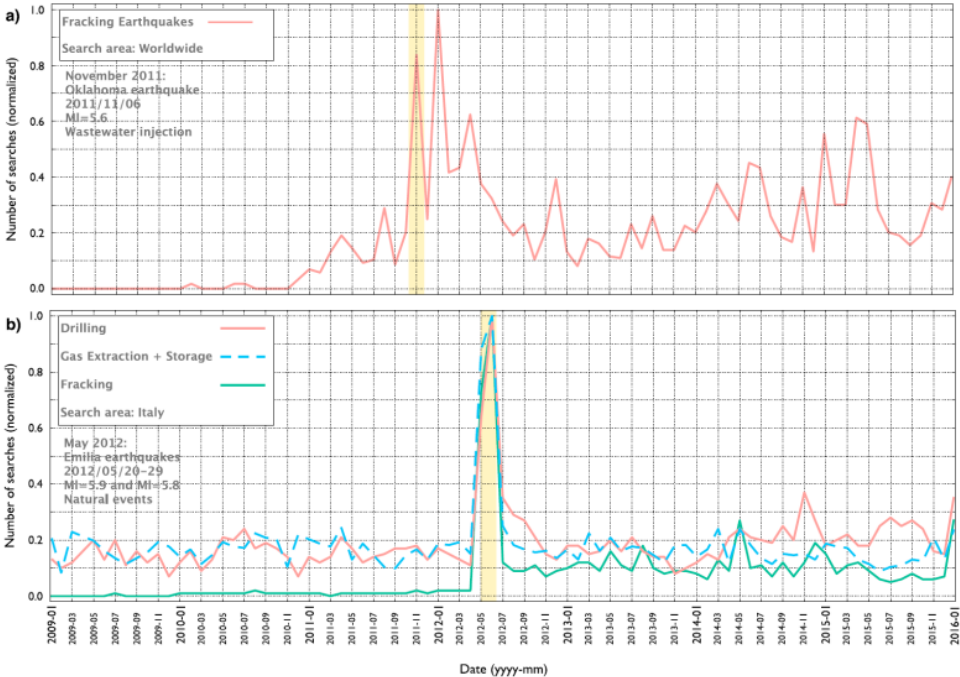


Figure 1.3 – a) Normalized number of worldwide Google searches for the word "fracking earthquake", the yellow band identifies the 2011 Oklahoma earthquake occurred after wastewater injection following a fracking operation; b) Normalized number of Italian Google searches for the words "drilling", "gas extraction and storage" and "fracking"; the yellow band identifies the 2012 Emilia-Romagna earthquakes. Source: Grigoli et al. (2017)



Figure 1.4 - World map showing 1229 projects with reported induced seismicity. Source: The Human-Induced Earthquake Database (HiQuake - <https://inducedearthquakes.org/>, last accessed March 2021)

The potential of the above-mentioned technological activities to generate seismicity is inherent in their ability to change the physical parameters of the underground rocks. It should be remembered that an earthquake occurs when an effort acting on a point of the Earth's lithosphere exceeds a threshold value, generating a fracture that propagates as long as the stress and friction conditions allow it. The relationship that quantifies this critical condition was established experimentally in 1773 by Coulomb, who formulated the fracture criterion that generally applies to any type of rock. It is expressed by the following equation:

$$\tau_{crit} = \mu(\sigma_n - P) + \tau_0 \quad Eq.1.1$$

where τ_{crit} is the shear stress that generates the fracture, μ is the internal friction coefficient, $(\sigma_n - P)$ the difference between the normal stress and the pore pressure, called the effective normal stress. Finally, τ_0 is the cohesion or cohesive strength.

It is easy to understand how a small variation of the parameters present in equation 1.1 can perturb the system. In particular, process involving the extractions and injections of fluid not only modifies the pore pressure of the reservoir but also leads to a change on the stress field of the surrounding volume. To understand the physical mechanism, we can consider the permeable rock as a porous elastic sphere that is located

inside a waterproof and elastic body. Injecting a certain volume of fluid into the sphere the process generates an increase Δp of the pore pressure in the permeable rock and a variation $\Delta\sigma$ of its stress in the nearby formation. Since the sphere is caged, the expansion is blocked by the presence of an external force. Extracting fluids, on the other hand, may result in a contraction of the reservoir due to the decrease of the pore pressure even by about 100 bar (Figure 1.5; National Research Council, 2013).

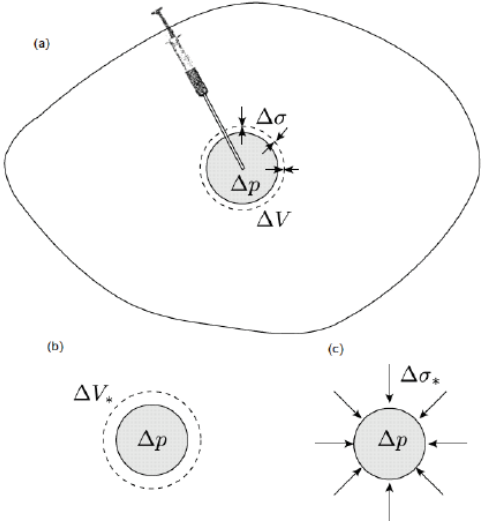


Figure 1.5 – a) Graphic representation of fluid injection into a permeable rock surrounded by impermeable elastic material. Inside the sphere the pore pressure increases by an amount Δp , while due to a volumetric expansion (ΔV) both inside and outside the sphere there is a stress perturbation ($\Delta\sigma$). b) The rock sphere due to the increase in pressure tends to increase its volume and if there aren't external constraints the expansion would be free. (c) An external stress is applied on the sphere to constrain the expansion. Source: National Research Council (2013)

In the following subsections the technological processes potentially capable of generating seismicity are illustrated in detail; for each of them significant case studies are reported. In addition, the induced seismicity-European plate observing system (IS-EPOS) is described in the last subsection. Its web portal offers to its user's access to data, applications, and documents to facilitate the study of anthropogenic seismicity.

1.1.1 Oil and gas extraction

Hydrocarbons extraction can take place via two techniques: traditional (or conventional) and unconventional, commonly known as fracking (Ellsworth, 2013). The traditional technique consists of drilling permeable rocks and generally includes primary, secondary, and tertiary recoveries (National Research Council, 2013). In the first recovery, hydrocarbons rise to the surface spontaneously thanks to the high pressures to which they are subjected until the pressure inside the reservoir reaches the hydrostatic condition. This process can cause a contraction of the reservoir giving rise to changes in stress in the surrounding rocks and neighboring fault systems. The extraction of hydrocarbons with the sole natural push allows the recovery of about 50-80% of gas and a low quantity of oil, equal to about 30% (Shepherd, 2009; Ahmed, 2010; National Research Council, 2013). It is therefore necessary to use artificial practices to increase production and compensate for the pressure inside the reservoir injecting fluids in the subsurface. The most common secondary recovery method is water flooding which involves a controlled injection of water to avoid exceeding the critical pressure, i.e., the initial reservoir pore pressure. Nevertheless, it may happen that the threshold value is exceeded and therefore the conditions of the stress field can vary. At this point, the reservoir is generally not completely emptied, and the remaining hydrocarbons are extracted by means of a third recovery, called enhanced oil or gas recovery (EOR - EGR). This process aims to facilitate the mobility of hydrocarbons by introducing a solvent that reduces their viscosity altering the chemical-physical properties of the reservoir (Shepherd, 2009). One of the most common EOR methodologies employs the use of CO₂ (Figure 1.6) and in these cases, it is considered a type of CCS (Carbon Capture and Storage, see subsection 1.1.3). A peculiarity of the EOR-EGR process is to keep the extracted and injected fluids balanced and the pore pressure at values like the initial ones. In this way, the possibility of generating earthquakes is reduced but it could lead to pollution of the aquifers.

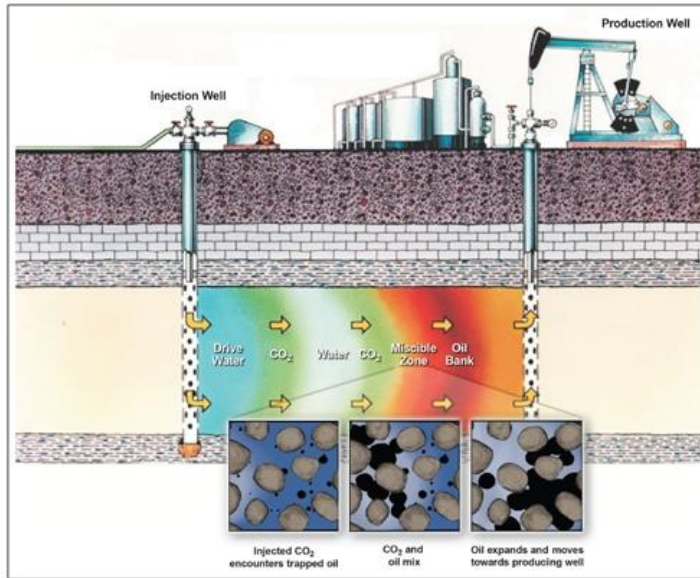


Figure 1.6 – Schematic representation of Enhanced oil recovery through the injection of CO₂. Carbon dioxide penetrating the pores of the rock reduces the viscosity of the oil making it flow towards the production well. Source: National Research Council (2013)

The fracking technique, on the other hand, consists in extracting oil and gas by hydro-fracturing rock formations with low permeability (e.g. oil shales or black shales). The fluid pumped at high pressure breaks the rock creating pathways in which the hydrocarbon can pass. To prevent the fractures created from closing, proppant is added to the injected water (90% of the total injected fluid). It is a solid substance, generally quartz sand or ceramic microspheres, which represents 9% of the total injected. The remaining 1% is made up of chemicals (Dayal, 2017). The fracking process lasts from hours to days during which a network of horizontal fractures connected to the borehole are created. They can extend up to three kilometers away (National Research Council, 2013). This technique intentionally generates a micro-seismicity ($M_w < 1$; Ellsworth, 2013) that serves as a guide to understand the geometry of the fractured area (Figure 1.7). After the fracturing, the well is opened and the phenomenon of flowback begins. The previously injected water and other substances (e.g. chemical, debris) collected during the process come back to the surface where they are disposed of properly or reused in a new fracking process. Only later the production begins. The fracking technique is an issue of

great concern in the scientific community as it can have a great impact on the environment. It is widely used in the United States where the shale gas and shale oil industry has allowed the country to become relatively independent from the import of hydrocarbons (Dayal, 2017). In many other countries, like Italy, this technique is forbidden.

Although the fracturing caused by fracking induces earthquakes generally of very low magnitude there are also cases of events felt by the population, often due to the activation of pre-existing faults in the areas surrounding the reservoir.

Among the seismic events reported in the scientific literature in relation to fracking activities, there is the seismic event of magnitude 2.3 felt in Blackpool, England, in 2011. After this mainshock an event of M 1.5 and other 48 weaker events occurred (De Pater & Baisch, 2011).

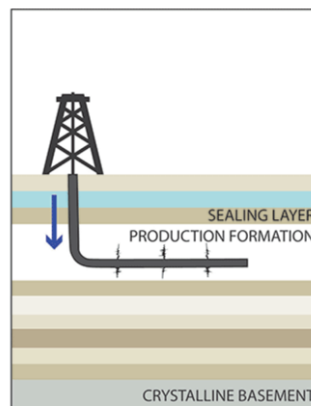


Figure 1.7 - Schematic representation of fracking technique. The blue arrow shows the direction of fluid injected. In the production formation microfractures are formed because of high pressure hydrofracturing of low-permeability rocks. Source: Rubinstein & Mahani (2015)

A study conducted by Holland (2013) revealed a strong temporal correlation between fracking and a seismic sequence ($0.6 \leq M_L \leq 2.9$) that took place in 2011 in Oklahoma.

One of the stronger seismic events (M_L 3.8) currently known related to this technology was felt in British Columbia, Canada, in a remote zone without causing damage (BC Oil and Gas Commission, 2014).

In the Rangely oil field, Colorado, some researchers from the USGS (United States Geological Survey) conducted a controlled experiment of induced seismicity from 1970 to 1974 (Raleigh et al., 1976, National Research Council, 2013). They measured the parameters involved in the Coulomb relationship, with aiming to test the theory for the activation of pre-existing faults due to the increase in pore pressure. The interest in the experiment arose because in 1957 secondary recovery operations began in the field. Since 1962, the injection of water into the well increased the pore pressure exceeding in some areas the original value before production (about 170 bar). In the same period, numerous seismic events with $M \geq 0.5$ were recorded in the areas close to Rangely. The maximum magnitude (M 3.4) was reached in 1964.

Among the best documented cases of induced seismicity by gas extraction there are the fields of Lacq, in France, and Gazli, in Uzbekistan (National Research Council, 2013). In the first case, at the beginning of production, in 1957, the reservoir had a pressure of 660 bar which over the years began to decrease in conjunction with the increase of seismicity. A study carried out on the location of events with magnitude greater than 3 (Grasso & Wittlinger, 1990) showed that 95% of them have epicentral coordinates that fall within the field. In the case of Gazli, large quantities of water were injected into the reservoir to facilitate extraction but, despite this, there was a consistent decrease in pressure (from 70 atm in the 1960s to about 30-35 atm since 1976 and to 15 atm since 1985). This situation caused three seismic events of magnitude 7 that occurred in 1976 and 1984 in the northern area of the production field that was previously seismically silent.

Even the northern area of the Netherlands, naturally at low seismic risk, has had to deal with the increase in seismicity due to the extraction of gas using the conventional method. In the Groningen field, in operation since 1963, the first earthquake felt by the population occurred in 1991 with a

local magnitude 2.4. In 2012, an earthquake with M_L 3.6 caused significant damage to homes in the neighborhood area (van Thienen-Visser & Breunese, 2015).

1.1.2 Geothermal energy

Geothermal energy exploits the internal heat of the Earth and is considered a form of green energy as it does not use fossil fuels and CO₂ emissions produced by geothermal plants are generally very low. Geothermal systems are characterized by the presence of water, rock permeability and high temperature. They are divided in vapor-dominated and liquid-dominated in which steam or hot water is extracted respectively from natural fractures within hot permeable rocks. Generally, the process uses water from atmospheric precipitation but where this is not enough, it must be artificially introduced (National Research Council, 2013).

The geothermal unconventional technique is known as Enhanced Geothermal Systems (EGS). It involves the creation of artificial fractures or opening of pre-existing faults in hot dry rocks to reduce the reservoir permeability and form pathways in which water can circulate (Grigoli et al., 2017). Cold fluids are pumped into deep well, heat up in contact with the hot rock and then rise to the surface. The creation of fractures causes intentionally micro-seismicity that allow to understand the path of the water in the subsurface, also indicating the areas where there is an increase in permeability. The earthquakes caused are generally of low magnitude but sometimes they could be felt by population and generate damages especially in highly urbanized areas. Both conventional and unconventional geothermal techniques have the potential to induce earthquakes as the introduction of cold water can create thermoelastic deformation of the rock and the pore pressure can increase due to the water injected in the subsurface (National Research Council, 2013).

The best-known case of induced seismicity connected with EGS occurred in Basel, Switzerland. In December 2006 the project involved the injection of high-pressure water into the crystalline basement rock at a depth of about 5 km with the aim of create a geothermal reservoir and increase its

permeability. Micro-seismicity linked to hydro-fracturing was recorded by the regional network of the Swiss Seismological Service (SED) and a local borehole array (Grigoli et al., 2017). On December 8 an earthquake of M_L 2.6 occurred. Within six days the project was stopped. Nonetheless, a few hours after the project shot down, another seismic event (M_L 3.4) occurred and was even perceived by population. The seismic activity continued in the following months with three events with magnitude greater than 3 (Deichmann & Giardini, 2009). In 2009, the project was permanently suspended.

A similar case occurred at the Soultz-Sous Forêts geothermal field (France) where 114000 seismic events ($-2.0 \leq M \leq 2.9$) occurred during the stimulation of the well and in the shut-in period (Baisch et al., 2010; Evans et al., 2012).

Similarly, in 2017 in Pohang, Korea, a seismic swarm occurred after stimulation of the well and the strongest event (M_w 5.5) was recorded two months after the cessation of activity (Yeo et al., 2020).

Earthquakes induced by conventional geothermal energy production have been documented in The Geysers field (California), the largest and best known in the world. The site has been operational since the 1960s but in the 1990s the natural steam production was aided by fluid injections. The seismicity in the field has increased over the years, reaching its peak in 2006 with an annual number of earthquakes equal to 1384, maximum magnitude 4.6 (National Research Council, 2013).

1.1.3 Wastewater injection and Carbon capture and storage

The previously described energy technologies also produce by-products called wastewater. In some cases, they are cleaned and used for other purposes, in others they are discarded by re-injecting them into the subsurface at depths greater than those of the extraction wells and in nearby areas (Figure 1.8; Rubinstein & Mahani, 2015). Wastewater consist of:

- produced water extracted together with hydrocarbons. They contain both organic and inorganic compounds and sometimes toxic substances that must be removed before re-injection;

- injection waters which are the water previously injected into the well to maintain high pressure in the reservoir and facilitate the production.

The re-injection process takes years or decades in new wells without a balance between extracted and injected fluids, leading to an increase in the pore pressure and a subsequent variation of the stress field. Therefore, this technique has a high potential to generate seismicity.

The first documented and known earthquake caused by wastewater injection occurred in Denver, Colorado, in the 1960s in an area considered to be of low seismicity. The injection activity began in 1962 and lasted until 1966 despite the hundreds of tremors recorded in that period by the Bergen Park seismic station.

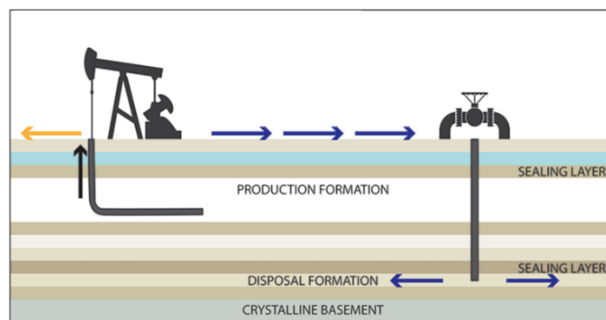


Figure 1.8 – Schematic representation of oil-gas production (on the left) and wastewater injection (on the right). From the extracted fluid (black arrow) the oil- gas (yellow arrow) is separated from the by-products which are re-injected into a new deeper well (blue arrows). Source: Rubinstein & Mahani (2015)

The three strongest events of magnitude 5, however, occurred in 1967, more than a year after the end of the fluid pumping activities, causing extensive structural damage (National Research Council, 2013).

In 2011, seismic events induced by wastewater injection occurred in Trinidad, Colorado, and Prague, Oklahoma with magnitudes 5.3 and 5.6 respectively (Rubinstein & Mahani, 2015). It is precisely this re-injection following fracking operations that has led the Oklahoma to an increase in seismicity in the last decade.

In 2006, in Val d'Agri (Italy) a seismic swarm began a few hours after the first wastewater injection in the Costa Molina 2 well (Improta et al., 2017).

One of the challenges that modern society must face is the reduction of carbon dioxide (CO₂) into the atmosphere. Engineers and researchers are developing different methodologies to achieve this goal, among them is the Carbon Capture and Storage (CCS). This new technology involves the capture of carbon dioxide produced by industries before it reaches the atmosphere and the subsequent underground storage in geological formations suitable for this purpose (National Research Council, 2013). Although the advantage of using CCS is high, it must be considered that there is a risk of generating seismicity. In fact, the injection of high rates of CO₂ at high pressure for long periods of time could lead to increases in pore pressure and changes in the stress field (Eiken et al., 2011; Nicol et al., 2013). This technology will be increasingly important and more used in the future. Therefore, it is important to try to mitigate the risks associated with it as much as possible to increase the benefits.

1.1.4 Water reservoir impoundment

A cause of induced seismicity, different from the previous ones because it does not involve the injection or withdrawal of fluids from underground, can be the addition of a load on the surface, as it happens for example with the water reservoir impoundment. The filling or emptying of the reservoir causes load changes that can alter the stress conditions of the subsurface triggering pre-existing faults or producing new ones (National Research Council, 2013).

The most disastrous anthropogenic seismic event for this technology is the Great Wenchuan earthquake (M 8), in Sichuan province (China). The earthquake caused about 90000 deaths, collapse of roads and bridges.

Another strong event (M_s 6.3) with loss of about 200 human lives occurred in Konya, India, in 1967 (Foulger et al., 2018).

Other episodes with a magnitude greater than 6 occurred in Egypt (Aswan), Greece (Kremasta), Zambia/Zimbabwe, USA, and China. Cases

of induced seismicity linked to this technology are very frequent all over the world due to the large presence of dams.

In Italy, an artificial reservoir under observation is the Pertusillo lake in Val d'Agri where a micro-seismicity is recorded in an area already subject to natural seismicity (Stabile et al., 2020).

1.1.5 IS-EPOS Platform

In order to create an infrastructure that can allow the study of anthropogenic hazards related to the exploitation of geo-resources, an international synergy between research groups is born within the framework of the Thematic Core Service - Anthropogenic Hazards (TCS - AH) of the European Program Observing System (EPOS-ERIC) (Orlecka-Sikora et al., 2020). In this context the Induced Seismicity-European Plate Observing System (IS-EPOS) web portal comes to life (<https://tcs.ah-epos.eu/>) in 2016. To study induced seismicity, not only seismological but also industrial data are needed, which are often inaccessible to researchers as they are the prerogative of energy companies alone. IS-EPOS platform overcomes this barrier as it contains multidisciplinary datasets related to anthropogenic seismicity cases (episodes) due to oil-gas and geothermal energy production, CO₂ sequestration, reservoir impoundment, underground mining, underground gas storage and wastewater injection (Figure 1.9).

Each episode is identified by the technological activity, the project to which it is associated, the area where the site is located and the provider that made the data available. The information is accessible to all, but only registered users can analyze the datasets. They are present on the portal or uploaded by the user, within their own virtual space (My Workspace) using applications on the platform itself (Leptokarpoulos et al., 2019).

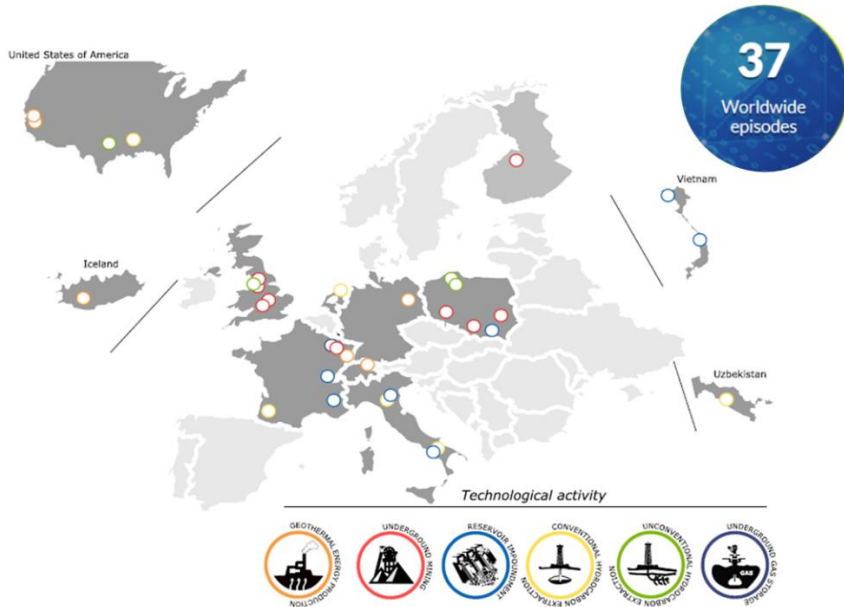


Figure 1.9 – Geographical distribution of the episodes available on the IS-EPOS platform. The circles of different colors identify the respective industrial activity shown below. Source: Orlecka-Sikora et al. (2020)

1.2 NaTech events

Whenever a natural hazard impacts an industrial plant causing accidents (e.g., release of toxic substances, fires, and explosions) we refer to NaTech events or Natural Hazard Triggering Technological Disaster (Krausmann et al., 2019). Often, it is possible that a chain of events, called cascade or domino effects, is generated. The key elements of this process are a first accident that trigger the sequence, a propagation vector and one or more secondary accidents (Cozzani et al., 2005). The study of cascade effects is very complex as it is necessary to consider several variables and the different probability of the occurrence of secondary events (Huang et al., 2020). Obviously, all this is further complicated if the initial sources are more than one.

NaTech events can be triggered by minor hazards such as storms, lightning, and freeze or by major hazards such as earthquakes, tsunamis, volcanic eruptions, and hurricanes. The first studies date back 1970s but only in recent years this type of accidents has become known due to their

greater frequency of occurrence attracting international political media attention for their great economic and social impact (Krausmann & Cruz, 2017). This rate will increase more in the next few years due to climate changes that increasingly give rise to extreme events and to industrial growth in natural hazard densely populated region (UNISDR, 2017). For this reason, it is very important to know the risks connected to NaTech events, also taking into account the accidents that occurred in the past, in order to be able to prevent and-or mitigate risks in the future by making appropriate changes to government protocols and industrial safety reports.

In general, after conventional technological accidents, safety systems are activated, and emergency plans are implemented. Unfortunately, they cannot be applied equally in the case of NaTech events as they are totally different from other types of accidents and require specific emergency plans. As a result of the occurrence of the natural phenomenon, there could be damage to lifelines and the simultaneous release of hazardous substances in a large area at different points of the plant. In addition, the natural hazard may have caused disruption to surrounding homes and roads, making the implementation of evacuation plans much more complicated (Krausmann & Cruz, 2017). The consequences of a NaTech event can be multiple and different depending on the material released from the facilities, the area in which the plant is located and the vulnerability of the component of the system that suffers the failure. There can be loss of human lives (both workers and residents), health problems, environmental damage, and of course huge economic losses (Krausmann et al., 2019).

Despite this, NaTech risks are overlooked compared to conventional ones as they occur with a lower probability and furthermore their analysis requires multidisciplinary knowledge. A NaTech risk assessment at national and international level turns out to be very important. In Europe, the Seveso Directive is in force to control the danger of major accidents associated with dangerous substances. It was first introduced in 1982 following the 1976 accident in a reactor of a chemical industry in the

province of Milan, Italy. The current third version of the directive (Seveso III) was issued by the European Community in 2012 and implemented by member states since 2015. It provides that for certain types of industrial sites (i.e., upper-tier establishment) the drafting of a safety report is required with the aim of assessing the remaining risks after prevention and protection activities. Important updates foreseen in this directive are the addition in the safety report of the analysis of risk due to natural hazard such as earthquake or flood and greater interaction with the resident population around the plants. Seveso III includes the involvement of residents in decisions relating to industrial sites providing them adequate information about the risks involved in the activity and educate them in emergency plans (European Union, 2012).

1.2.1 Earthquake-triggered NaTech events

Earthquakes are the first natural hazard on which scientific research is focused for the study of NaTech events. Especially in areas with high seismic risk they are considered the greatest hazard for industrial plants containing dangerous chemicals (Huang et al., 2020). This can lead to the quick trigger of domino effects and damage to safety systems. Furthermore, they can affect several components of the system in a short time and in a big area generating collapses of industrial structures and surrounding houses blocking emergency exits. A study of 78 NaTech events due to earthquakes showed that the most damaged structures are the atmospheric storage tanks (Campedel, 2008). Generally, these structures contain large quantities of flammable hazardous substances that in case of earthquake can easily give rise to fires and explosions, becoming vectors of propagation (UNISDR, 2017).

Experience shows that to minimize accidents, it would be optimal to build industrial facilities outside highly seismic areas, but if this is not possible, it is necessary to use seismic safety codes as well as a careful NaTech risk assessment. In fact, studying past earthquake - triggered NaTech events it has been noted that in areas where careful earthquake design codes are implemented, the damages are due to cascading effects and not to the seismic event itself (Cruz et al., 2017).

An example of recent NaTech event in which earthquake prevention measures proved effective is the Tohoku or Great East Japan earthquake (M_w 9.0, March 2011). The seismic event occurred in the offshore Pacific Ocean, at 130 km east of Sendai, triggering a tsunami with waves of 40 m high giving birth to cascading effects. Many industrial facilities were affected by the tsunami, the best known is the Fukushima nuclear power plant. This last accident caused radioactive releases and has drawn world population and political attention to the risks associated with the use of this form of energy (Yamamura, 2012). The emergency in the nuclear power plant became a priority over accidents occurring in chemical plants with explosions and fires that led to evacuation of 1142 residents nearby the facilities (Krausmann & Cruz, 2017). This big disaster killed 16000 people and other 3000 were missing with an economic loss of more than \$US 210 billion.

Sometimes the source of a cascading effect can be a TechNa event as happened in Wenchuan, China, 2008. An earthquake of magnitude 8 was induced by the emptying of an artificial basin (Foulger et al., 2018) giving rise to NaTech events and other geological phenomena. The US Geological Survey estimated the collapse of 5 million buildings and the damage of more 20000 with over than \$US 140 billion in economic losses (Krausmann et al., 2010). The great human disaster has obscured the accidents in the chemical industries that caused environmental pollution due to the release of ammonia and sulfuric acid (Cruz & Suarez-Paba, 2019).

The third and last earthquake - triggered NaTech event occurred in Kocaeli, Turkey. An earthquake of moment magnitude 7.4 was recorded in August 1999 in a populated and industrialized area damaging roads, bridges, ports and killing over 15000 people. The study carried out by Steinberg & Cruz (2004) on 19 industrial facilities identify releases of anhydrous ammonia, spill of diesel, leakage of acrylonitrile in air, soil and water, release of cryogenic liquid and LPG leakages. Another accident occurred in a refinery in the Izmit Bay that was subject to strong ground motion, a tsunami wave and surface faulting triggering three fires and hazardous material releases (Krausmann & Cruz, 2017).

METHODOLOGIES

TechNa and NaTech events can produce impacts even of considerable magnitude on the surrounding environment and, in extreme cases, can lead to important consequences for the society and the economy. To mitigate and forecast risks, it is essential to study each phase of the industrial project developing methodologies, sometimes multidisciplinary, that can lead to a revision of safety protocols.

It is essential to conduct site-specific studies because the seismic activity in an area can greatly influence the magnitude of impacts. In addition, the effect of a NaTech or TechNa event is highly dependent on the exposed elements (e.g., homes, schools, industrial plants, hospitals, etc.) located in the impact areas (Capuano et al., 2017).

When considering earthquakes as a hazard of a NaTech event or a consequence of a TechNa event, it is crucial to prevent damages and fatalities as those derived by: 1) the collapse of the industrial plant itself or of the surrounding houses, 2) the loss of containment of hazardous materials from one of the elements of the plant (Krausmann, 2017).

To study a TechNa event such as induced seismicity requires the knowledge of the historical and current seismicity of the area under examination, as well as the industrial data, such as volumes and pressures of hydrocarbons injected or withdrawn.

The study of a NaTech event, instead, needs information on the elements that constitute an industrial plant to perform a multi-hazard risk analysis that estimates the probability of occurrence of accidents and, therefore, consequent impacts.

This chapter is divided into three paragraphs in which the seismological, statistical, and multi-hazard analysis methodologies used within the thesis work are reported. They will be applied in the following chapters

to study induced seismicity in the area of Porto San Giorgio (Italy) and Cooper Basin (Australia) and to perform a multi-hazard analysis on the San Potito and Cotignola gas storage facility (Italy).

2.1 Seismological methodologies

Each time an earthquake occurs, the release of energy resulting from the rupture process generates seismic waves that travel within the Earth following different paths and reach the surface where they are recorded by receivers i.e., seismic stations, as seismograms. The installation of an increasing number of instruments and the technological advancement in data acquisition have led to the recording of a large amount of seismic data in recent decades (Havskov & Ottemöller, 2010).

A primary problem that seismologists encounter in the study of instrumental seismicity is the accurate determination of the earthquake location, i.e., latitude, longitude, depth at which the earthquake occurs, and the origin time, i.e., the time when the earthquake rupture began (Havskov et al., 2009). It is possible to perform an absolute or relative location. In the first case (see subparagraph 2.1.1) the earthquake is located in a fixed geographic and temporal (UTC) system; in the second case the event position is given with respect to a fixed point, e.g., a well located earthquake that is considered to be a reference point (Husen & Hardebeck, 2010; Havskov & Ottemöller, 2010). The reliability of the earthquake location depends on the geometry of seismic network, the accuracy of the crustal model used and the number and quality of phase readings (Husen & Hardebeck, 2010). The parameter that can be particularly influenced by uncertainty is the hypocentral depth (Florez & Prieto, 2017). The most recent and accredited developments for obtaining the greatest possible accuracy of the localization parameters involve the use of techniques based on differential arrival times (e.g., Waldhauser & Ellsworth, 2000) or the use of waveform-based, picking-free location methods (e.g., Grigoli et al., 2018). Both methods involve the use of waveforms: for the first method, the best usage condition is to employ the differential arrival times estimated through the waveforms cross-correlations; the picking-free methods work directly on the characteristics of the waveforms.

An important quantity that can be routinely calculated from seismograms is the earthquake magnitude. This value defines the size of an earthquake and is expressed, in its general form, as follows (e.g., Zollo & Emolo, 2011; Lay & Wallace, 1995)

$$M = \log\left(\frac{A}{T}\right) + f(\Delta, h) + C_R + C_S \quad \text{Eq.2.1}$$

where A and T are the amplitude and period of the ground displacement, respectively; $f(\Delta, h)$ is a correction function of the epicentral distance and the hypocentral depth. The last two terms represent correction factors for the site effects (C_R) and source (C_S).

There are several magnitude scales although the most widely used and known is the Richter magnitude, also known as the local magnitude scale. (Zollo & Emolo, 2011).

In addition, from the seismograms, it is possible to understand the kinematic of the seismic rupture by calculating the focal mechanism associated with the earthquake. It is possible to get information about the geometry of the fault with respect to a geographic coordinate system by specifying three angles: strike, dip, and rake (Figure 2.1).

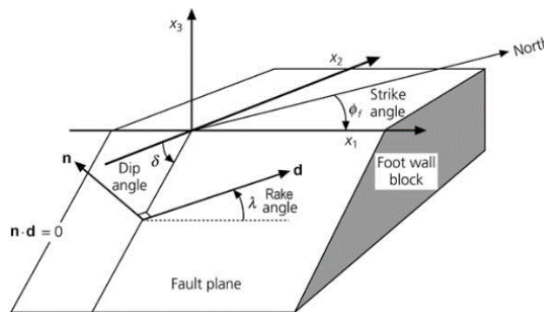


Figure 2.1 – Graphical representation of the fault plane geometry. The coordinate system identifies x_1 as the strike direction, x_2 the dip direction, and x_3 as the perpendicular axis to the other two. The strike angle is measured clockwise with respect to the North direction, the dip is the angle the fault forms with the Earth's surface. These two angular quantities define the orientation of the fault. The vector \mathbf{d} is called the slip vector and represents the direction of motion along the fault plane; it is defined by the rake which is an angle measured counterclockwise from the strike direction. Source: Havskov & Ottemöller (2010)

Graphically, the focal mechanism of an earthquake is represented by the beach-ball diagram (Figure 2.2). It is a sphere with light and dark portions that represent volumes of rock near the source subject respectively to compression and distension. Through the beach-ball is possible to have the representation of the focal mechanisms for different types of faults.

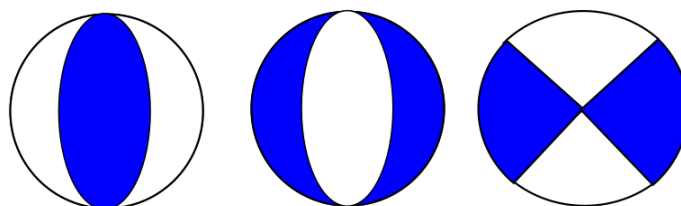


Figure 2.2 - Schematic representation of a focal mechanism through a beach-ball diagram for different types of faults: normal (on the left), reverse (in the middle) and strike-slip (on the right).

Sometimes, especially in the study of historical earthquakes, it is not possible to use digital waveforms and it is necessary to analyze catalog data. Since the data could be affected by systematic or reading errors in the arrival times of the P and S phases, it is important to perform a preliminary quality study (Husen & Hardebeck, 2010). Moreover, accurate studies on earthquake locations and fault geometry can be performed by analyzing macroseismic data (e.g., Sirovich & Pettenati, 2001, Emolo et al., 2004, Convertito & Pino, 2014). Several methods that use macroseismic intensity data have been proposed to investigate earthquake source locations, and magnitude or fault parameters (physical dimension and spatial orientation; Gasperini et al., 2010 and references therein).

The macroseismic field includes useful information for estimations, although with variable uncertainty, of the quantitative parameters of historical earthquakes and allow to obtain a more robust catalogue for correct hazard assessments. Macroseismic estimates may be affected by large uncertainties related to inaccurate intensity data as reported by historical information; this inaccuracy is mainly due to the lack of a physical definition for macroseismic intensity. Although these methods can be very useful for studying historical seismicity, their principal aim is

to define the epicenter location and estimate the earthquake magnitude (Gasperini et al., 2010 and references therein) and source parameters (Sirovich et al., 2001). The epicenter location can be obtained 1) by calculating the barycenter of the spatial distribution of the sites that show the largest intensities or 2) by predicting the intensity data through an attenuation relationship and finding the best fit for different values of unknown parameters (such as epicenter location and depth). To estimate the magnitude of earthquakes, macroseismic data may be used to find an empirical relationship between instrumental magnitude and one of three factors: 1) the maximum epicentral intensity, 2) the maximum areal extent where the earthquake was felt or 3) a combination of these factors. These approaches are biased by the earthquake depth, whose value is unknown and influences the magnitude estimate through opposing directions. The determination of the earthquake depth with macroseismic data is crucial and must be handled carefully. In fact, in modern seismology, many factors can lead to an erroneous estimate of source depth, including poor coverage of a seismic network, errors during arrival time readings, and a complex geology causing uncertainties related to the used velocity models. These elements introduce degrees of bias into the attenuation laws used to derive the macroseismic depth of historical earthquakes, generally providing an unreliable estimate of the hypocentral depths that are greatly underestimated when compared with instrumental earthquakes (Gasperini et al., 2010).

2.1.1 Earthquake location

Location is a typical non-linear, inverse problem. The quantitative formulation of an inverse problem is expressed by the functional relationship:

$$G(\mathbf{m}) = \mathbf{d} \tag{Eq.2.2}$$

in which \mathbf{d} is the observed data set and \mathbf{m} the set of parameters to be estimated, both represented as vectors.

Consider a homogeneous medium with velocity v and suppose that an earthquake occurs at an instant of time t_0 in a point inside the Earth having

Cartesian coordinates $\mathbf{x}_0 = (x_0, y_0, z_0)$. These four unknown quantities identify the hypocenter and the origin time of the seismic event, constituting the set \mathbf{m} of model parameters. Let n_i be the number of seismic stations with coordinates $\mathbf{x}_i = (x_i, y_i, z_i)$ that record the time of the first arrivals of the P and S waves. At the i -th station the P wave arrives at a time t_i which depends on the origin and travel time of the seismic waves from the hypocenter to the receiver:

$$t_i = t_0 + t(\mathbf{x}_0, \mathbf{x}_i) \quad \text{Eq.2.3}$$

Explicitly this equation can be rewritten as

$$t_i = t_0 + \frac{\sqrt{(x_i - x_0)^2 + (y_i - y_0)^2 + (z_i - z_0)^2}}{v} \quad \text{Eq.2.4}$$

with t_i element of the vector data \mathbf{d} . It is evident that there is no linear dependence between data and parameters and that to solve the inverse problem it is necessary to know a priori the velocity model. Through this classic-linearized approach, also known as Geiger's method, the problem is solved by perturbing the set of parameters and making a first-order Taylor series expansion of the data around an initial set \mathbf{m}^0 . With this procedure we obtain a system of n linear equations:

$$\Delta \mathbf{d} = \mathbf{G} \Delta \mathbf{m} \quad \text{Eq.2.5}$$

The unknown quantities are the four parameters corresponding to the space-time coordinates of the hypocenter. They are less in number than the observed data, therefore the inverse problem is overdetermined and therefore resolvable with the least squares method. The procedure continues by iteration until the prediction error is of the same order of the average error on the data or the perturbations are no longer significant. Although this type of methodology is widely used in many location codes, it has some limitations. The convergence of the algorithm is strongly dependent on the choice of the initial solution. It may also happen that the perturbative process stops when the number of iterations established is reached, obtaining a wrong solution, i.e., that corresponds not to the global, but to a local minimum. All these difficulties are overcome if the

problem of hypocentral location is solved by following a probabilistic approach that provides an exhaustive exploration of parameters space. In this case a probability density function (PDF) is calculated for the unknown parameters: origin time and spatial coordinates of the hypocenter in a predefined and discretized volume. In this case the inverse problem (Eq.2.2) is expressed defining a probability density $\Theta(\mathbf{d}, \mathbf{m})$ given the probability densities of the parameters $\mu_M(\mathbf{m})$ and the data $\mu_D(\mathbf{d})$:

$$\Theta(\mathbf{d}, \mathbf{m}) = \mu_D(\mathbf{d})\mu_M(\mathbf{m}) \quad \text{Eq.2.6}$$

According to probability theory, the equation is rewritten as the product between the conditional probability of \mathbf{m} given \mathbf{d} and the marginal probability of \mathbf{m}

$$\Theta(\mathbf{d}, \mathbf{m}) = \theta(\mathbf{d}|\mathbf{m})\mu_M(\mathbf{m}) \quad \text{Eq.2.7}$$

Following the probabilistic formulation of the inverse problem illustrated in Tarantola (2005) and Tarantola & Valette (1982), the solution is provided by a marginal probability density function in the parameter space

$$\sigma_M(\mathbf{m}) = \int \sigma(\mathbf{d}, \mathbf{m}) d\mathbf{d} \quad \text{Eq.2.8}$$

known $\sigma(\mathbf{d}, \mathbf{m})$, that is an a posteriori probability density function calculated considering the theoretical relationship between the data and the parameters $\Theta(\mathbf{d}, \mathbf{m})$ and a quantity enclosing the a priori information about the parameters and the observed data.

The following treatment describe the probabilistic formulation of an earthquake location presented in Tarantola & Valette (1982) and used in this thesis work.

The unknown quantities of the problem are the space-time hypocentral coordinates (X, Y, Z, T) while the data are the P- and S- wave arrival times (\mathbf{t}) at the stations. Within the problem there are other important quantities such as the coordinates of the stations or the parameters describing the velocity model but, since they are accurate enough, are considered

constants. The theoretical relationship between data and parameters is given by:

$$\mathbf{t} = \mathbf{g}(X, Y, Z, T) \quad \text{Eq.2.9}$$

Let C_g be the covariance matrix that determines an estimate of the errors obtained by calculating the arrival times. Assuming, for simplicity, that they are of the Gaussian type, the theoretical probability density function is:

$$\theta(\mathbf{t}|X, Y, Z, T) = \exp\left\{-\frac{1}{2}[\mathbf{t} - \mathbf{g}(X, Y, Z, T)]^T C_g^{-1}[\mathbf{t} - \mathbf{g}(X, Y, Z, T)]\right\} \quad \text{Eq.2.10}$$

Similarly, consider that also the observed arrival times have Gaussian uncertainties with covariance matrix C_d , therefore the a priori probability density function is:

$$\rho(\mathbf{t}) = \exp\left\{-\frac{1}{2}(\mathbf{t} - \mathbf{t}_0)^T C_d^{-1}(\mathbf{t} - \mathbf{t}_0)\right\} \quad \text{Eq.2.11}$$

The solution of the inverse problem solved with a probabilistic approach is given by the posterior probability density function which for the problem under examination becomes:

$$\begin{aligned} \sigma(X, Y, Z, T) &= \quad \text{Eq.2.12} \\ &= \rho(X, Y, Z, T) \exp\left\{-\frac{1}{2}[\mathbf{t}_0 - \mathbf{g}(X, Y, Z, T)]^T (C_g + C_d)^{-1}[\mathbf{t}_0 - \mathbf{g}(X, Y, Z, T)]\right\} \end{aligned}$$

This equation is the general solution of the hypocentral location problem with Gaussian uncertainties on the data and parameters. It represents a four-dimensional probability density function. The PDF of the only spatial coordinates is obtained by integrating on the time variable and it is expressed by

$$\begin{aligned} \sigma(X, Y, Z) &= \quad \text{Eq.2.13} \\ &= K \rho(X, Y, Z) \exp\left\{-\frac{1}{2}[\tilde{\mathbf{d}} - \tilde{\mathbf{h}}(X, Y, Z)]^T (C_g + C_d)^{-1}[\tilde{\mathbf{d}} - \tilde{\mathbf{h}}(X, Y, Z)]\right\} \end{aligned}$$

Where K is a normalization constant, $\tilde{\mathbf{d}}$ is the vector of the observed arrival times minus their weighted average, $\tilde{\mathbf{h}}$ is the vector of the theoretical arrival times minus their weighted average. The weights are given by

$$w_i = \sum_j w_{ij} \quad w_{ij} = [(C_g + C_d)^{-1}]_{ij} \quad \text{Eq.2.14}$$

The posterior probability density function includes information relating to uncertainties on observed arrival times, errors in the theoretical calculation and those due to the velocity model used, thus representing a complete probabilistic solution.

2.1.1.1 The NonLinLoc Software

The NonLinLoc (Non-Linear Location) software, used in this work, consists of a set of programs for the definition of velocity model grid, calculation of travel times and probabilistic hypocentral location (Lomax et al., 2000). The NonLinLoc program aims to solve the problem of location. The solution is provided by the point of maximum probability of the PDF obtained by scanning the entire space of the model by a grid search. The code calculates the travel times between each station and each node of a three-dimensional grid using the Podvin & Lecomte (1991) algorithm which exploits a finite differences approximation of the Huygen's principle. The Probability Density Function can, on the other hand, be calculated using two types of misfit functions:

- the first is a function of norm L2 constructed starting from the treatment of the hypocentral location problem reported in Tarantola & Valette (1982). The uncertainties on the observations and the errors due to the theoretical calculation are assumed to be Gaussian. This allows to estimate the maximum likelihood origin time as the weighted average of the origin times obtained considering the arrival times of the seismic phases to the single receivers (Moser et al., 1992). Considering X , Y and Z as the spatial coordinates of the hypocenter and known the theoretical travel

time $h_i(X, Y, Z)$ for an i -th station, the maximum likelihood origin time is:

$$T_{ml}(X, Y, Z) = \frac{\sum_i \sum_j w_{ij} [d_i - h_i(X, Y, Z)]}{\sum_i \sum_j w_{ij}} \quad \text{Eq.2.15}$$

- the second type of misfit function is based on Zhou's (1994) Equal Differential Time (EDT) and its generalization by Font et al. (2004) proving to be a more robust technique in the presence of outliers. The PDF calculated following this formulation appears to be independent of the time origin and in this case both the theoretical errors that the experimental uncertainties are assumed to have Gaussian trend.

The searching technique for the "optimal" hypocenter can be carried out in NonLinLoc by choosing one of the three proposed sampling algorithms: Oct-Tree, used in this thesis work, Grid-Search, and Metropolis - Gibbs.

The Oct-Tree algorithm, developed by Lomax et al. (2009), provides a complete and accurate mapping of the PDF to a three-dimensional volume, resulting in a more exhaustive exploration than Metropolis-Gibbs algorithm and converging faster than Grid-search algorithm. The method performs a recursive subdivision in a 3D space following an octant scheme. It starts from an initial volume which is then partitioned into eight sub-cells. The PDF is calculated at the center point of each subcell (Figure 2.3).

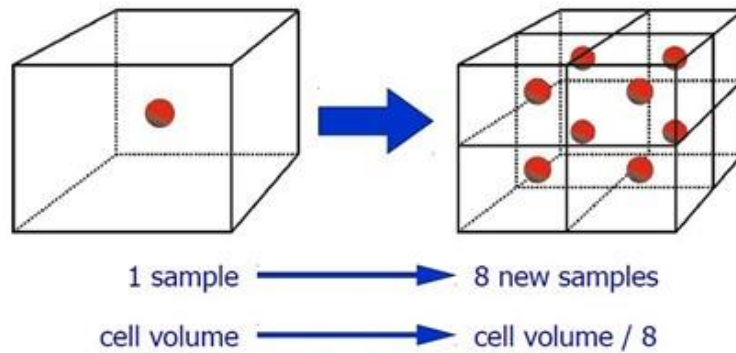


Figure 2.3 - The Oct-Tree method: sampling of cells in 3D space. Source: The NonLinLoc Software Guide (<http://alomax.free.fr/nlloc/>; last accessed March 2021)

For each cell, known its volume V_i , the algorithm calculates the probability that the location of the earthquake is just in it:

$$P_i = V_i PDF(x_i) \quad Eq.2.16$$

and this quantity is inserted together with the corresponding cell in an ordered list which is updated as the sampling proceeds.

The procedure can be summarized as follows: 1) the cell C_{max} in which the probability value (P_{max}) is greater is divided into octants; 2) for each sub-cell, the PDF in the center and the P_i are calculated and the values are entered in the list; 3) the method continues recursively, progressively selecting and dividing the high PDF cells and converging quickly to the solution. (Figure 2.4). All samples in three-dimensional space can be reproduced graphically, giving a complete and compact representation of the PDF (Figure 2.5).

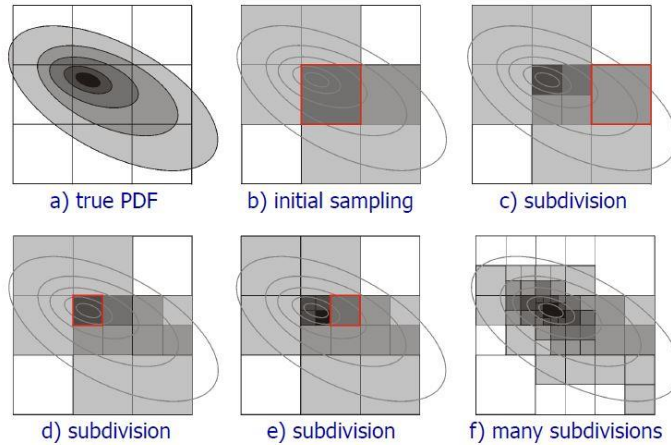


Figure 2.4 - Graphical representation of the Oct-Tree sampling procedure. Source: The NonLinLoc Software Guide (<http://alomax.free.fr/nlloc/>; last accessed March 2021)

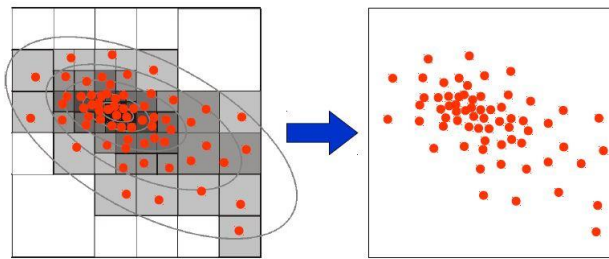


Figure 2.5 - Graphical representation of the Oct-Tree results; the samples give a representation of the PDF. Source: The NonLinLoc Software Guide (<http://alomax.free.fr/nlloc/>; last accessed March 2021)

The Grid-Search algorithm proceeds with the PDF calculation in finer nested grids after an initial three-dimensional grid is defined. This procedure has the advantage of exhaustively cover all the space and being able to identify optimal multiple solutions and highly irregular volumes. The main disadvantage is to converge to the final solution in a very long time compared to other algorithms. Furthermore, it is necessary to carefully select the size and the number of the node of both initial and subsequent grids to have neither too large nor to small volume to sample avoiding cases of low resolution or truncated PDF exploration, respectively.

Metropolis-Gibbs is a sampling procedure that performs a random walk in the solution space going towards the areas in which the PDF turns out to be higher. A current sampling location, \mathbf{x}_{curr} , is perturbed by a vector quantity $d\mathbf{x}$, according to an arbitrary direction and length l , to reach a new sampling location (\mathbf{x}_{new}). In the latter, the posterior probability density function $\sigma(\mathbf{x}_{\text{new}})$ is calculated and compared with the previous $\sigma(\mathbf{x}_{\text{curr}})$. If $\sigma(\mathbf{x}_{\text{new}}) \geq \sigma(\mathbf{x}_{\text{curr}})$ the new location is accepted, becoming current, otherwise it is accepted with a probability $P = \sigma(\mathbf{x}_{\text{new}})/\sigma(\mathbf{x}_{\text{curr}})$. The algorithm is about 100 times faster than Grid-Search and only 10 times slower than linearized techniques.

Whatever the research technique used, the NLLoc program calculates the Gaussian estimators such as the expectation value and the covariance matrix, knowing the values of the PDF at the nodes of the location grid. The covariance matrix by means of singular value decomposition can be represented graphically as a confidence ellipsoid to 68%. In this way, it is possible to plot the confidence ellipsoid as scatter cloud representing the errors associated to the earthquake location. The Gaussian estimators can be considered good indicators for the uncertainty of earthquake location especially when the PDF shows an ellipsoidal shape.

2.1.2 Transformation to Equivalent Dimensions of earthquake parameters

In seismology, several parameters are used to describe the earthquake source, such as hypocentral coordinates, magnitude, or focal mechanisms. We refer to these as direct parameters. It is possible to derive other parameters to characterize the seismic events such as spatial distance from a particular geographical point or from the location of an earthquake, selected as reference. If all the parameters are taken into account to characterize a seismic event, a vector that locates the earthquake in a multidimensional space of parameters can be defined. Since the parameters do not have the same metric, a systematic comparison among several earthquakes, as in the case of seismic clusters, in this multidimensional space cannot be performed. Therefore, it is necessary to find a new strategy to overcome this limitation. With this aim, in this

work, the transformation to equivalent dimensions of the earthquake parameters developed by Lasocki (2014) is used.

The goal of this transformation is to have all parameters in a Euclidean space so that the distances between them can be calculated easily. Let consider a seismic dataset that constitutes a population of seismic events described by parameters, for which there are related populations of parameters with their own probabilistic distribution. The latter are assumed to be equivalent as they are related to the same population. Let X_1, \dots, X_p earthquake parameters with cumulative distributions F_{X_1}, \dots, F_{X_p} . For each pair of parameters $X_k, X_l: k, l \in \{1, \dots, p\}, k \neq l$ or $k = l$, two intervals of the parameter values $[x_k(i), x_k(j)], [x_l(i'), x_l(j')]$, are equivalent if $\Pr(X_k \in [x_k(i), x_k(j)]) = \Pr(X_l \in [x_l(i'), x_l(j')])$.

If $U_k = F_{X_k}(X_k)$ and $U_l = F_{X_l}(X_l)$, then the distances between parameter values are equivalent when $|u_k(i) - u_k(j)| = |u_l(i') - u_l(j')|$ with $u_k \in U_k$ and $u_l \in U_l$. U_1, \dots, U_p are the parameters transformed to Equivalent Dimension (ED). All these U quantities are uniformly distributed in the interval $[0,1]$, constituting a vector of parameters $\mathbf{U}(U_1, \dots, U_p)$ that identifies a seismic event in a space where the metric is Euclidean. In this new space, the distance between two earthquakes i, j is:

$$d(i, j) = \sqrt{\sum_{k=1}^p [u_k(i) - u_k(j)]^2} \quad Eq.2.17$$

Because the cumulative F_{X_k} distributions of earthquake parameters are generally not known, the treatment of Lasocki (2014) requires that they are evaluated by means of kernel estimators (Silverman, 1986), using Gaussian kernel function.

Given a continuous parameter X , defined in \mathfrak{R}^1 whose values for the entire population of events are $\{x_i, n\} = \{x_1, x_2, \dots, x_n\}$, then the kernel estimator of the cumulative distribution function F_X is

$$\widehat{F}_X(x|\{x_i, n\}) = \frac{1}{n} \sum_{i=1}^n \Phi\left(\frac{x-x_i}{\lambda_i h}\right) \quad Eq.2.18$$

in which h represents the smoothing factor, i.e., the solution of the following equation (Kijko et al., 2001):

$$\sum_{i,j} \left\{ 2^{-0.5} \left[\frac{(x_i - x_j)^2}{2h^2} - 1 \right] \exp \left[-\frac{(x_i - x_j)^2}{4h^2} \right] - 2 \left[\frac{(x_i - x_j)^2}{h^2} - 1 \right] \exp \left[-\frac{(x_i - x_j)^2}{2h^2} \right] \right\} = 2n$$

Eq.2.19

while λ_i are the local bandwidth factors as reported in Orlecka-Sikora & Lasocki (2005)

$$\lambda_i = \left[\frac{\hat{f}^*(x_i | \{x_j, n\})}{g} \right]^{-0.5}$$

Eq.2.20

where

$$\hat{f}^*(x_i | \{x_j, n\}) = \frac{1}{\sqrt{2}hn} \sum_{j=1}^n \exp \left[-\frac{(x_i - x_j)^2}{2h^2} \right]$$

Eq.2.21

$$g = \left[\prod_{i=1}^n \hat{f}^*(x_i | \{x_j, n\}) \right]^{\frac{1}{n}}$$

Eq.2.22

Finally, Φ is the Gaussian cumulative distribution function.

The formulations here are valid only if the parameter X is defined on a non-finite interval, otherwise they need to be modified appropriately. Moreover, equation 2.18 is written assuming that the parameters are continuous random variables without the presence of repeated values. If the latter are present, it is recommended to randomize parameter values within their rounding range to avoid local increases in the kernel density estimate that will affect the cumulative distribution (Lasocki, 2014).

A graphical example of the transformation to ED for two parameters, magnitude and latitude, is shown in Figure 2.6.

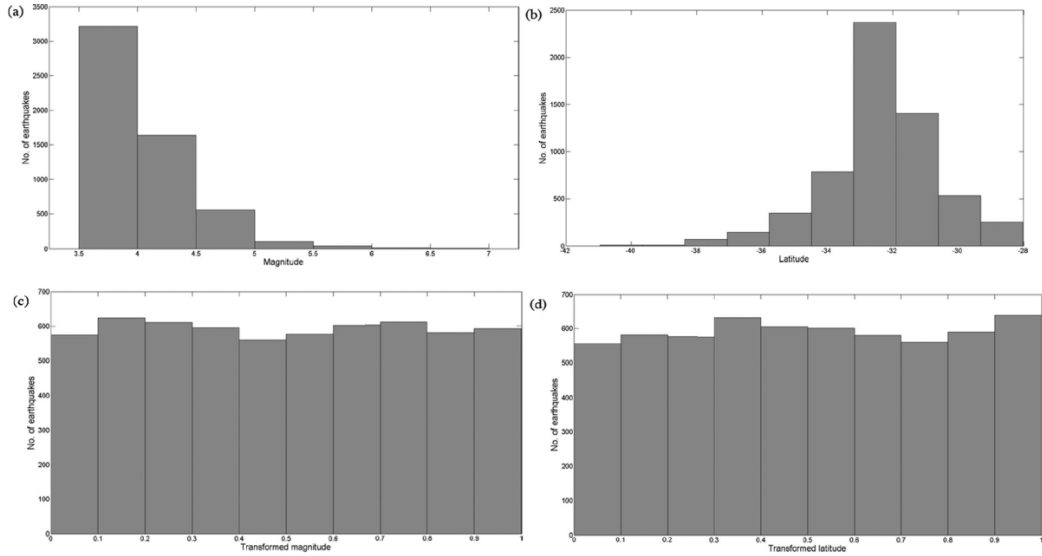


Figure 2.6 – Graphical representation of the equivalent-dimensional transformation. Figures (a) and (b) show the magnitude and latitude distributions, respectively, for a set of 5930 seismic events in the Flinn – Engdhal’s area #135 for a time range from 1991 to 2010. Figures (c) and (d) illustrate the distribution of the two parameters transformed to ED. Source: Lasocki (2014)

2.2 Statistical methodologies

Earth scientists are increasingly resorting to the use of statistics as it is often necessary to manipulate datasets and look for similarities between populations of events (McKillup & Darby Dyar, 2010). For a preliminary study of the induced/triggered seismicity, statistical tests can be used to have a first clue about the possible relationship between the seismicity in a specific area and the operational data due to the exploitation of geo-energy resources. One of the characteristics of the hypothetico-deductive scientific method (Popper, 1968) is to observe the natural world and then formulate, with the available information, a logical hypothesis about how a particular phenomenon occurs (McKillup & Darby Dyar, 2010). Often the objective of statistical analysis is to test the validity of the hypothesis. It is necessary, therefore, to formulate the so-called null hypothesis, usually indicated with H_0 , which represents the opposite of the objective of the study. Its verification is carried out through the application of a test that according to the type has its own logic and computational

methodology (Sardanelli & Di Leo, 2008). The null hypothesis is rejected when the probability p is less than a threshold value called the statistical significance level, usually set at 5% (Fisher, 1954). This allows the complementary hypothesis to be considered true.

The choice of which test to use is often arbitrary and depends on the specific case to be analyzed. When small samples are used and it is not possible to prove the normality of the distribution, it is preferable to use non-parametric tests (Soliani, 2008). This type of test has advantages in that it does not require rigid assumptions on the initial data and is therefore more versatile.

In the following, the binomial test, Mann-Whitney U test, and Spearman rank correlation are presented in detail. They are applied in the next chapters to investigate a relationship between seismic activity and production parameters.

The binomial test operates on a dichotomic scale (yes/no, success/failure, true/false) to assess the significance of changes in the quantity to be analyzed. Considering having n independent tests, for example the launch of n coins, it is possible to define with p the probability of success in each trial (i.e., to obtain the desired output, e.g., head) and with $q=1-p$ the probability of failure (i.e., to obtain an output different from the desired one). The probability of obtaining ν successes in n trials is given by the binomial distribution (e.g., Taylor, 1999)

$$B_{n,p}(\nu) = \binom{n}{\nu} p^{\nu} q^{n-\nu} \quad \text{Eq.2.23}$$

When the binomial test is applied to evaluate the variation of the seismicity rate in correspondence of an increase or decrease of the production parameters (e.g., oil or gas production), t_0 , T_1 and T_2 , the reference time, and the times preceding and following t_0 , respectively, must be defined. Let n_1 the number of seismic events in the time interval $[t_0 - T_1; t_0]$ and n_2 in $[t_0; t_0 + T_2]$. While $N = n_1 + n_2$ stands for the number of total events in $[t_0 - T_1; t_0 + T_2]$.

If the total number of events in the two intervals is significantly different from a randomly subdivision, then a correlation between the rate of seismicity and the variation of production parameters is to be expected. At this point it is possible to formulate the following null hypothesis

H_0 : n_2 events could be obtained randomly from N with probability

$$P = \frac{T_2}{T_1 + T_2} \quad \text{Eq.2.24}$$

The verification of this hypothesis through the binomial test allows to determine the probability p_1 , that if N events occur randomly in the time interval $[t_0 - T_1; t_0 + T_2]$, the number of seismic events in $[t_0; t_0 + T_2]$ is less than or equal to the value n_2 . Similarly, it is possible to calculate the probability p_2 of obtaining in the considered interval a number of events greater or equal to n_2

$$p_1 = \Pr(n \leq n_2 | N, P) = \sum_{n=0}^{n_2} \binom{N}{n} P^n (1 - P)^{N-n} \quad \text{Eq.2.25}$$

$$p_2 = \Pr(n \geq n_2 | N, P) = 1 - \sum_{n=0}^{n_2-1} \binom{N}{n} P^n (1 - P)^{N-n} \quad \text{Eq.2.26}$$

If the value of p_1 is less than the chosen significance level (0.05), it is possible to conclude that the seismicity rate in $[t_0; t_0 + T_2]$ decreased compared to the previous interval. The opposite is true, if p_2 is less than 0.05.

When the difference of the median for two independent samples is to be tested, it is possible to use the non-parametric Mann-Whitney U test. It is also called the robust rank order test and was introduced to generalize the Wilcoxon method (Mann & Whitney, 1947).

Given two samples X and Y , the null hypothesis to be tested, in general, is that the medians of the two groups are equal. The data are combined into a single sample, arranged in ranks of ascending order and keeping memory of the group they belong to. The sums of the ranks of each sample X and Y are denoted by R_1 and R_2 , respectively. In this way two indicators U_1 and U_2 , are calculated (e.g., McKillup & Darby Dyar, 2010):

$$U_1 = n_1 n_2 + \frac{n_1(n_1+1)}{2} - R_1 \quad \text{Eq.2.27}$$

$$U_2 = n_1 n_2 + \frac{n_2(n_2+1)}{2} - R_2 \quad \text{Eq.2.28}$$

in which n_1 and n_2 are the number of data in X and Y , respectively. The smallest value between U_1 and U_2 is called U . It is the Mann-Whitney statistic and is compared to a tabulated value for the level of significance considered. The null hypothesis is rejected when the calculated value is less than or equal to the tabulated value. The p-value is also obtained from the tables.

In this thesis work, the Mann-Whitney U-test was used to compare the medians of the magnitudes of two groups of seismic events to determine if there is some correspondence with the variation in industrial parameters.

Moreover, to evaluate the "strength" of the link between seismicity and anthropogenic activity, the Spearman's rank correlation test was employed (Spearman, 1904). It is the non-parametric alternative to the Pearson test. The Spearman correlation coefficient is generally denoted by the Greek letter ρ and takes values between -1 and +1. Values tending to one of the two extremes reveal a negative or positive correlation, while it is null for values close to zero. Samples to be tested must be paired and measured with an ordinal scale. The null hypothesis to be tested is that there is no correlation between the two variables under analysis.

Given two samples X and Y , in each it is necessary to sort the data and then associate each variable value with the corresponding rank. For each pair, the square of the difference (d_i) between the ranks is calculated and then all quantities are summed. It is possible, at this point, to define the Spearman's correlation coefficient ρ as follows (e.g., Soliani, 2008):

$$\rho = 1 - \frac{6 \sum d_i^2}{n(n^2-1)} \quad \text{Eq.2.29}$$

in which n denotes the sample size. For small samples, the obtained value is compared with the tabulated ones of Spearman's ρ in correspondence of

chosen n and α . The null hypothesis is rejected for ρ values greater than the value shown in the table. From the latter it is possible to obtain the value of the probability.

2.3 Multi-hazard risk analysis

Industrial facilities are often subject to routine operations that can generate impacts on the surrounding environment. While these events are easily managed as they are frequent, much more complicated is the management of impacts due to the occurrence of accidents caused by system failures or even more extreme events that have the potential to generate unexpected and disastrous consequences (Capuano et al., 2017). They are, therefore, of considerable importance in a multi-hazard risk assessment that aims to assess the probability of occurrence of accidents and consequent impacts considering various initial hazards (Garcia-Aristizabal et al., 2017). This study must be carried out for each phase of an industrial project, i.e., plant construction, hydrocarbon exploration, plant operation, and decommissioning. It must also consider several aspects such as the possibility of having multiple hazards as initial triggering mechanisms, different cascading event scenarios, and types of elements exposed to risk, e.g., population, buildings, industrial plant, and ecosystem (Gasparini et al., 2016; Garcia-Aristizabal et al., 2017; Capuano et al., 2017).

The first task of a multi-hazard risk assessment is to develop risk pathway scenarios, consisting of chains of events that may occur as the result of natural or anthropogenic hazards and their possible interactions. An initial qualitative treatment leads to a selection of major incidents that can then be analyzed quantitatively using a bow-tie approach (Capuano et al., 2017; Garcia-Aristizabal et al., 2019; 2017, Khakzad et al. 2013, 2014; Yang et al. 2013), which allows to define a pathway of type: source-mechanism-receptor (Figure 2.7). It simplifies the structuring of incident scenarios by first identifying the critical event, called the Top Event (TE), which must be defined and characterized in detail by answering the questions what happens and where (Capuano et al., 2017). It can affect a primary risk receptor, that is usually identified as an environmental element like the

groundwater, the soil, or the air (Garcia-Aristizabal et al, 2019; 2017). From the TE with a backward mechanism, the Fault Tree (FT) is built defining the initial and intermediate events which in cascade lead to the occurrence of the accident. This latter (TE) is, in turn, the initial event of the Event Tree (ET), which enables the examination of the consequences and the impacts on the final risk receptors (Figure 2.8).

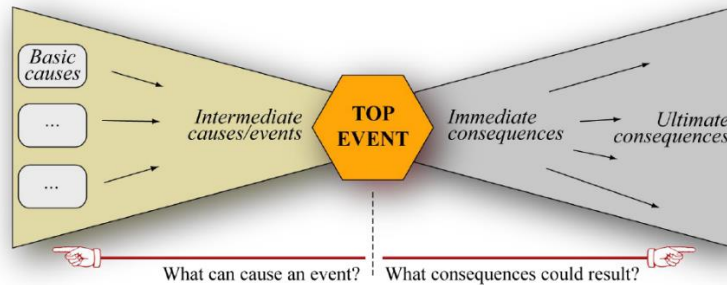


Figure 2.7 - Bow-tie schematic structure, on the left there is the Fault Tree in which the initial causes and intermediate events that lead to the occurrence of the Top Event are reported. On the right there is the Event Tree in which the consequences that originate due to the occurrence of the critical event are described. Source: Gasparini et al. (2016)

The probability of occurrence of the TE is quantitatively calculated starting from the probabilities assigned to the Basic Events (BE), that are connected among them through Boolean logical operators. The probability of the consequences is, instead, calculated from the probability of occurrence of the TE and assigning probabilities to the nodes of the ET. In this phase it is necessary to consider the presence of any safety systems installed inside industrial plants (Garcia-Aristizabal et al., 2019). Since rare events are often considered in this analysis and few literature data are available, it is preferred to implement in Bayesian statistical data analysis the probability models of the basic events (Garcia-Aristizabal et al., 2019). Analytical resolution of the bow-tie often proves to be complex, requiring the aid of computational methods, such as the Monte Carlo simulations. The assessment of FT is performed sampling the probability distributions defined for the BEs to obtain the empirical distribution of the probability of the critical event. Using again the Monte Carlo simulations, it is possible to reach the probability distributions of the outcomes of the ET.

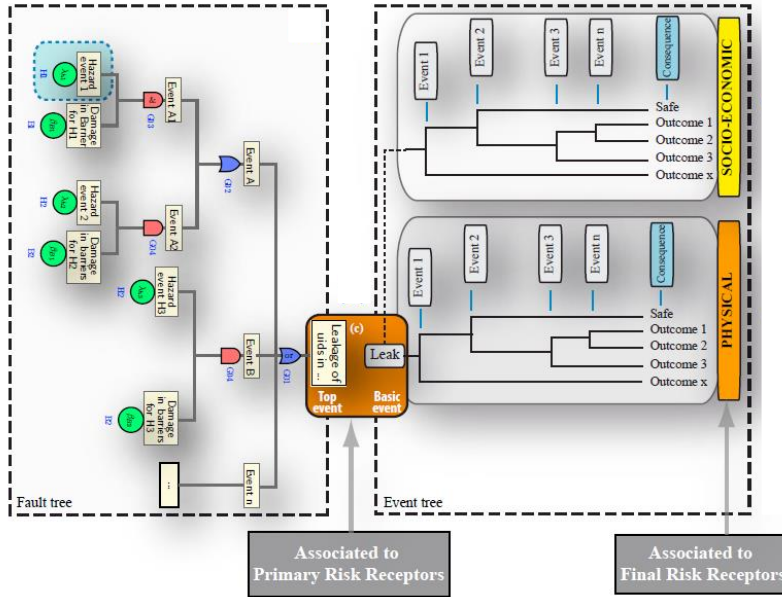


Figure 2.8 - Example of bow-tie structure for a Top Event identified as leakage of fluid, that is, in turn, the Basic Event of the Event Tree. On the left there is the Fault Tree with six Basic Events (green circles) originating intermediate events. All the events in Fault Tree are interconnecting through Boolean logical gates (or in blue, and in pink). Source: Garcia-Aristizabal et al. (2017)

2.3.1 Merger application

An open-source computational tool, useful to solve a quantitative multi-hazard risk analysis described by a bow-tie structure, is the Simulator for Multi-hazard risk assessment in ExploRation/exploitation of GEOResources (MERGER; Garcia-Aristizabal et al., 2019). This application is available on the IS-EPOS Platform (Orlecka-Sikora et al., 2020) allowing, to date, to solve only the Fault Tree using a Monte Carlo approach. Like other applications on the platform, it is possible to load MERGER into the own workspace in order to have a virtual space in which the analysis can be carried out. The first step is defining the top event to study and then introduce as input the information about the basic events and any intermediate events (Figure 2.9). In detail, for each event it is necessary to insert the description and the model typology for the basic event, i.e., 'Binomial class', 'Homogeneous Poisson process' or 'Weibull failure class' (Garcia-Aristizabal et al., 2019). Finally, it is necessary to set the

parameters of the distributions and logical Boolean gates as “and/or” for the event interconnections. Moreover, it is possible to perform time-dependent or independent calculations and choose the number of iterations to obtain the probability of occurrence of the Top Event. After running the application, the results are automatically uploaded in the workspace, available for the download or to be viewed by the user. The results include files with information on the input setting, the processing and the probability values obtained for the top event (the best estimate, 50th percentile, 5th and 95th percentile as uncertainty limits) and a histogram of the top event probability.

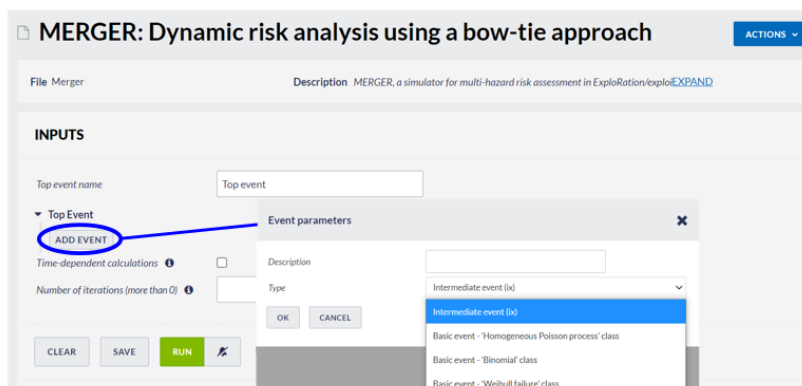


Figure 2.9 – MERGER application interface on the IS-EPOS platform. Source: IS-EPOS Platform (<https://tcs.ah-epos.eu/>)

STUDY OF SEISMICITY IN AREAS SUBJECT TO HYDROCARBON EXTRACTION

In recent years, seismicity originating by active fault zones close to hydrocarbon fields has become a topic of debate and study (Bertello et al., 2010; Braun et al., 2018). In these areas, instrumental and historical seismicity studies allow to infer new insights to discriminate between anthropogenic and natural seismicity (Caciagli et al., 2015; López Comino et al., 2018). An Italian area seismically active where the link between industrial activities and seismicity can be studied is the Adriatic Sea. Hydrocarbon exploration began in 1970 in the Adriatic Sea that represents the main target area of gas production in Italy, producing approximately 10 billion m³/year (Casero & Bigi, 2013). Most of the oil and gas fields in this area are associated with the geodynamic evolution of the Apennine thrust belt and the North African margin, where a complex paleogeographic system of deep-water basins and open shallow platforms developed during the Mesozoic and Early Paleogene. The Adriatic Sea is the youngest sector that experienced different flexural phases forming foredeep basins filled by huge volumes of siliciclastic sediments during the Pliocene-Pleistocene. Three main systems of hydrocarbon lithologies are recognized: 1) biogenic gas in siliciclastic Plio-Pleistocene deposits 2) mixed oil and gas in terrigenous deposits and Cretaceous slope-to-basin sediments 3) oil in carbonate rocks of the Meso-Cenozoic. Currently, the main activities of the petroleum industry in the central Adriatic are focused on the exploitation of existing fields, which are in some cases close to active faults. Therefore, the knowledge of the seismic activities of the Adriatic offshore faults and their link with industrial activities must be improved through detailed studies on instrumental seismicity and statistical correlation to be able to correctly assess the seismic hazard and, where possible, try to mitigate it by making changes to industrial safety protocols.

The aim of this chapter is to improve understanding of the seismicity of the Central Adriatic offshore area. Interest is focused on the 1987 Porto San Giorgio seismic sequence because it occurred in an area where hydrocarbon fields are exploited. In this chapter a refined relocation of the 1987 Porto San Giorgio seismic sequence (Riguzzi et al., 1989; Console et al., 1992) using an earthquake location technique based on nonlinear, global-search, and probabilistic approach (Lomax et al., 2000) is performed. The ambiguity encountered in evaluating the mainshock depth is overcome through a novel approach that uses macroseismic intensity data to constrain the depth of seismic events through a grid search technique in a magnitude-depth space. In addition, since the proximity of the seismic sequence to the Santa Maria a Mare hydrocarbon field, a statistical analysis is performed to better understand if a correlation between anthropogenic activity and seismicity exists.

3.1 Seismotectonic setting

The geodynamic evolution of the Adriatic Sea is related to the active tectonic processes along the Central and Northern Apennines that led to Quaternary thrust belt formations and Padana-Adriatic foredeep domains (Doglioni, 1993; Scrocca et al., 2007; Casero & Bigi, 2013). Due to the counterclockwise rotation of the Adriatic block, a crustal thickening and the mountain building of the Apennines happened to the east while to the west a crustal thinning and rift-zone developed along the Tyrrhenian Sea. During the Miocene-Pleistocene, thrust sheets were progressively transported eastward, according to the Adriatic vergence, and were stacked to form fold and thrust belt structures. In the Late Pliocene-Pleistocene, extensional faults were developed upon the thrust sheet, and extensional and contractional deformations were active at the same time, side by side, and then progressively migrated over time from west to the east (Lavecchia et al., 1994; Scrocca et al., 2007). The fold-thrust sheet system of eastern-central Italy is characterized by minor contractile structures that experienced coherent mechanical and kinematic deformations (Lavecchia et al., 1994 and references therein). These well-defined tecto-stratigraphic units overthrust adjacent units to the east,

showing progressively younger ages as indicated by the syntectonic foredeep deposits. Moving from west to east, the deformational phase date spans from Late-Middle Pliocene to Pliocene-Pleistocene. Contractional structures mostly correspond to dip-slip or oblique-slip reverse shear zones with the arc-shape and convexity to the east, as characterized by several structures at different scales from the thrust-related folds with the Adriatic vergence and coeval strike-slip faults. The extensional deformation was accommodated by high-angle normal faults that developed upon the preexisting folds-and-thrust belt structures. The results of the later extensional deformation are several interconnected grabens and half-grabens with NW-SE or N-NW-S-SE elongation, as exposed in Tuscany or western Umbria, or intramontane small basins bounded by high-angle west-dipping normal faults, as exposed in eastern Umbria, Marche, and Abruzzo (Chiaraluce 2012; Lavecchia et al., 2017). Pliocene-Pleistocene continental deposits fill the basins, showing a deformation dating later than the folding and thrusting phases. Westward contraction and eastward extension were paired chronologically and kinematically; they were simultaneously active along adjacent areas at different times. Three contraction-extension pairs were identified by the researchers (Lavecchia et al., 1994), and the fronts of their deformative phases both migrated eastward over time. The surface positions of the fronts are indicated in Figure 3.1. Based on structural kinematic evidence, earthquake distributions and focal mechanism data, seismotectonic zones, such as the Apennines Mountain zone and Central Adriatic coastal zone, can be identified as having homogeneous tectonic features and seismic activity (Figures 3.1, 3.2). These seismotectonic zones correspond to a simplified and schematic representation common to models proposed by several researchers (Lavecchia et al., 1994; Frepoli & Amato, 1997; Ghisetti & Vezzani, 2002; Montone et al., 2004; Scrocca et al., 2007; Chiaraluce et al., 2017b), although they might differ in terms of the number of tectonic domains and their boundaries. The Apennines Mountain Zone (AMZ) corresponds to the axial sector of the Apennine chain, between the Tuscan boundary region of the thinned crust (west) and the outer-most part of the Pliocene Quaternary extensional fault zone. This zone shows the highest

seismic activity with magnitude up to 6.5 (Norcia earthquake, Mw 6.5, 30 October 2016) with a maximum depth of about 10-15 km (Chiaraluce et al, 2017a; Chiaraluce et al., 2017b).

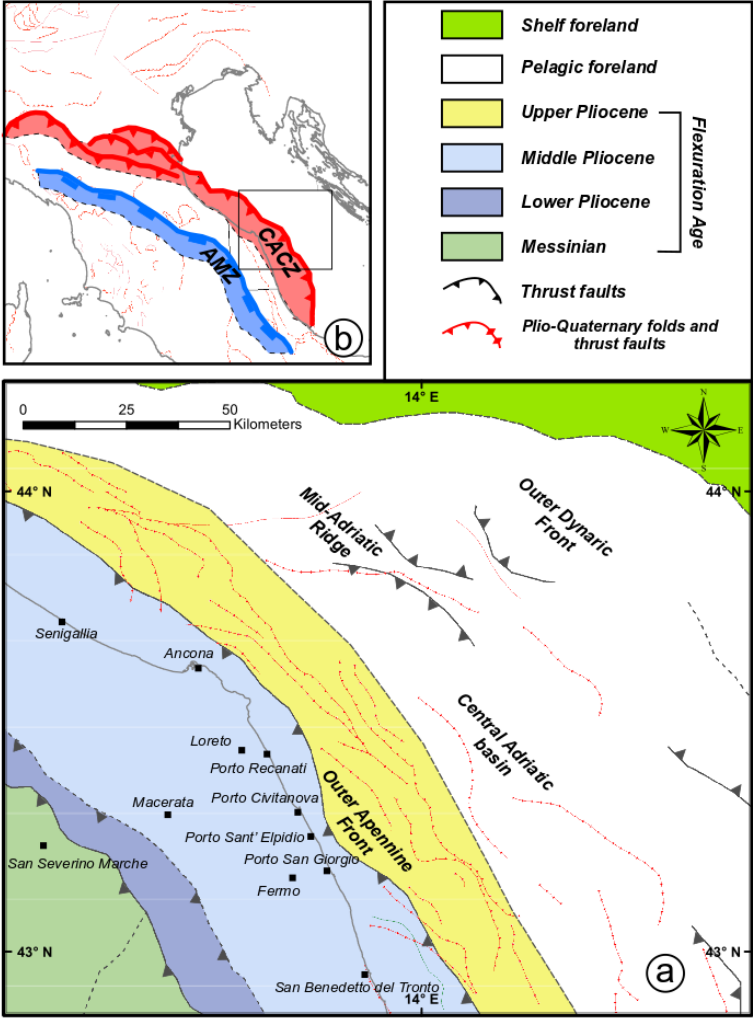


Figure 3.1 - a) Geological structural map of the Central Adriatic basin (redrawn from Casero, 2004). The tectonic units and age of deformation are reported. Adriatic Plio-quaternary folds and thrusts are indicated in red (from Italian Sea Geological Map 1:25000, Geological Survey of Italy). b) Location map with active extensional (blue) and compressional (red) fronts of deformation. AMZ stands for Apennines Mountain Zone; CACZ stands for Central Adriatic Coastal Zone.

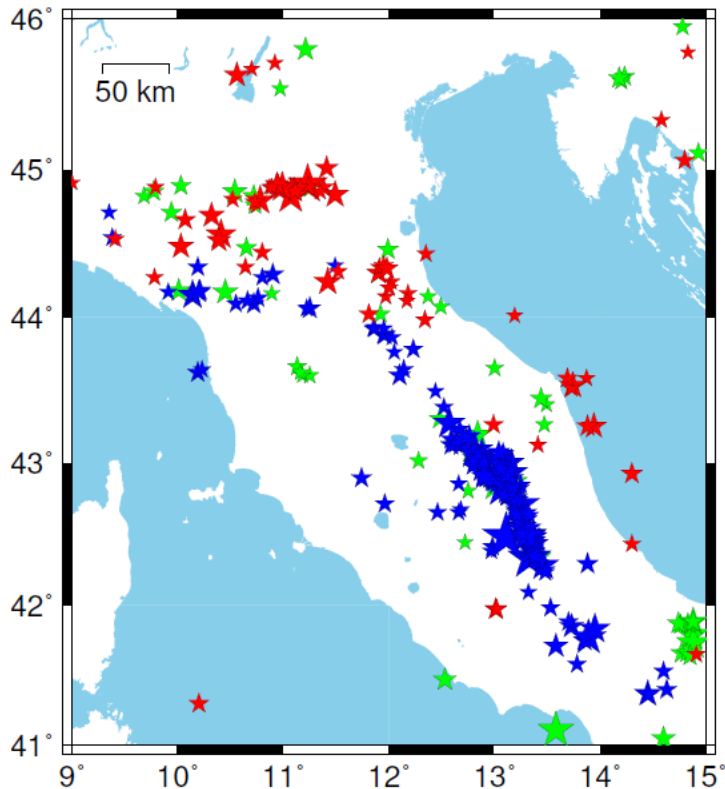


Figure 3.2 - Epicentral distribution of Italian seismicity. Earthquake with $M \geq 3.8$ occurred during 1976–2018 for which the focal mechanism solution is available (data from Pondrelli et al., 2006 and European–Mediterranean Regional Centroid-Moment Tensors Catalog). The focal mechanisms are classified according to their tectonic regimes as a function of the orientation of the P, B, and T axes. Red stars indicate earthquakes with thrust, green with strike slip, and blue with normal-fault kinematic. Thrust, strike-slip, and normal regimes are defined as in Kagan (2002).

Earthquakes (with small to strong magnitude) show focal mechanisms ranging from normal to oblique-normal kinematics, with T-axis SW-NE trending, and are consistent with the direction of the σ_3 axis (minimum principal stress) as indicated by geological data (Lavecchia et al., 1994; Charaluce et al., 2017). Small to moderate seismicity is distributed onshore and offshore along the Central Adriatic Coastal Zone (CACZ). This zone is characterized by reverse tectonics involving Pleistocene units along the Padana-Adriatic front as derived by seismic lines analysis. In Porto San Giorgio area, seismic profiles show westward dipping contractional

structures related to thrusting during the Pleistocene with Adriatic vergence. The Apennine thrust external front is located in the Adriatic offshore at a few kilometers between the towns of Ancona and Pescara (Lavecchia et al., 1994); however, a different location in the middle of the Central Adriatic Sea was proposed in recent years (Scrocca et al., 2007). Structural highs with NW-SE WNW-ESE trends form the so-called “Mid-Adriatic Ridge” that has been interpreted as thrust-related folds involving the Plio-Pleistocene layers of at least 150 km in length in the central Adriatic. Along the Marche coastline, several pieces of evidence suggest active seismogenic faults due to thrust-related folds of the outer Apennine front (Vannoli et al., 2004; DISS). Historical and instrumental seismicity indicate a compressive stress field as shown by the few available fault plane solutions. Geological evidence derived from the seismic profiles indicates that Quaternary strata were affected by the deformation due to the buried blind thrust activity, with a morphological effect on the bathymetry of the sea floor. A compressional stress field, coherent with the active reverse structures of CACZ, and containing a minimum horizontal axis with a NW-SE trend, is supported by seismological and borehole break-out data (Montone et al., 2004; Scrocca et al., 2007; Pierdominici et al., 2012). This evidence suggests that the most recent activity of the Apennine thrust front occurred during the Late Pliocene-Late Quaternary and affected the Adriatic Ridge according to forelandward (NE-) thrusting.

The Adriatic coast is characterized by small to moderate seismic activity ($M \leq 5.5$) with hypocentral depth of less than 15 km (Lavecchia et al., 2003; Maesano et al., 2013). The strongest historical earthquakes occurred in Fano (1389, M_w 5.1; Rovida et al., 2016), Senigallia (1924, M_w 5.5; 1928 M_w 5.0; 1930, M_w 5.8; Vannoli et al., 2015; Rovida et al., 2016), and Ancona (1269, M_w 5.6; 1474, M_w 5.1; 1690, M_w 5.6; 1870, M_w 5.2; 1917, M_w 5.2; 1972, M_w 4.7, Rovida et al., 2016; Figure 3.3a). A series of small to moderate earthquakes (M_L 1.3-5.0) occurred along the Adriatic coast offshore of Porto San Giorgio (hereinafter PSG) (Riguzzi et al., 1989; Console et al., 1992) from July to December 1987. Focal mechanisms show the reverse fault kinematics with a maximum stress axis at approximately W-E and

an intermediate axis at approximately N-S subhorizontal (Riguzzi et al., 1989; Pondrelli et al., 2006). The PSG mainshock (M_L 5.0) occurred on July 3, 1987, showing a Mercalli-Cancani-Sieberg (MCS) intensity value equal to the VII degree in the epicentral area, and a strong NNW-SSE elongation of the isoseismals up to the fourth degree, with an axis parallel to the coast.

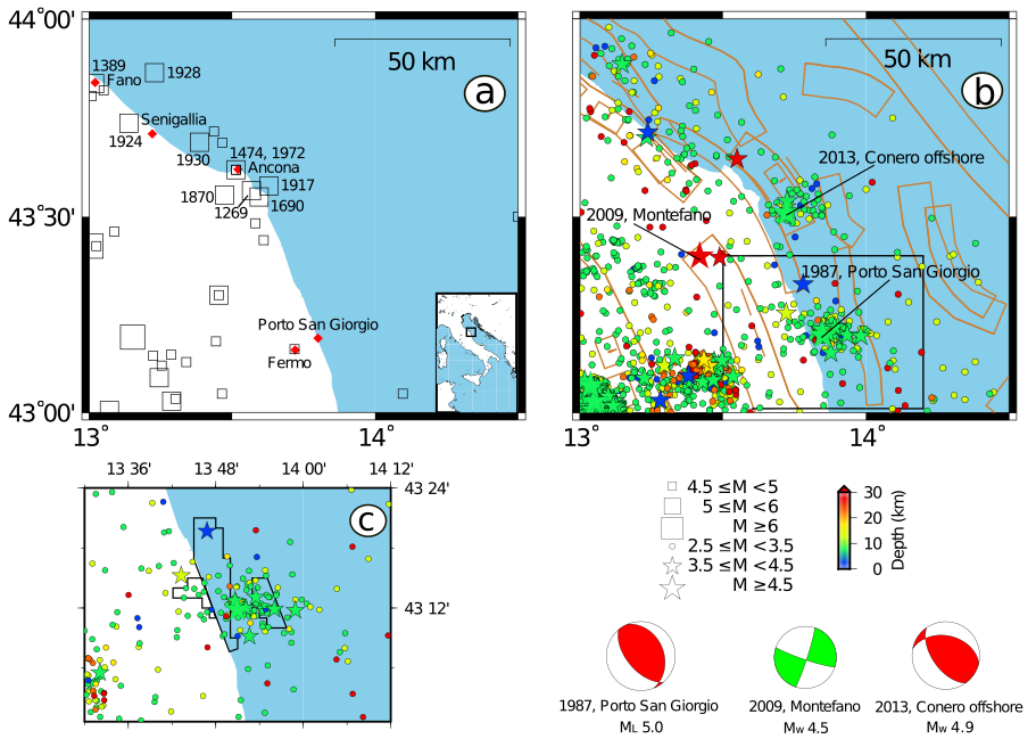


Figure 3.3 - a) Historical seismicity (1000-1984) (data from Rovida et al., 2016) with $M \geq 4.5$. The towns of Porto San Giorgio, Fermo, Fano, Senigallia and Ancona are indicated by red diamonds. The earthquakes mentioned in the text are labeled with the year in which they took place. b) Instrumental seismicity (1985-2018) (data from INGV - National Earthquake Center, <http://cnt.rm.ingv.it/>) with $M \geq 2.5$. Different symbols are used to indicate the magnitude size (see legend figure), while the color indicates the depth. The seismic events along the coastal zone with $M \geq 4.5$ and their focal mechanisms are also indicated. In orange are the mapped seismogenic faults derived from the DISS database (DISS Working group 2018). The black rectangle is the area in c. c) Zoomed view of the study area with the instrumental seismicity. The black lines are the borders of the hydrocarbon cultivation concessions B.C. 7.LF, B.C. 2.LF and Fiume Tenna.

Instrumental seismicity is distributed along the Adriatic coast with small to moderate magnitude ($M \leq 5$) and a depth less than 15 km (Figure 3.3b).

Seismic sequences often take place along this stretch of coast as in Porto San Giorgio in 1987 or Conero offshore in 2013 (M_w 4.9, Mazzoli et al., 2014). Figure 3.3c shows a view enlarged of Porto San Giorgio area, highlighting the location of instrumental seismicity and the nearby hydrocarbon fields.

3.2 Porto San Giorgio seismic sequence 1987

On 3rd July 1987, an earthquake of local magnitude 5 affected the offshore area of Porto San Giorgio, giving rise to a seismic sequence consisting of 91 events that occurred between July and December 1987 with local magnitudes ranging from 1.3 to 5.0 (Castello et al., 2006; CSTI 1.1, 2005). The events were recorded by 57 seismic stations (Figure 3.4), of which 47 belonging to the Italian seismic network of the Istituto Nazionale di Geofisica (ING, today INGV) and 10 situated in the Balkan area belonging to different seismic networks (Seismological Survey - University of Zagreb, Montenegro Seismological Observatory, Agencija Republike Slovenije za okolje - Seismological Office, Sarajevo Seismological Station). The number of first arrival times used to relocate the PSG seismic sequence was 991 for P phase and 485 for S one (CSTI 1.1, 2005).

The reliability of this dataset was assessed by creating a modified Wadati diagram (Chatelain, 1978; Chatelain et al., 1980). It consists in computing the difference between the P and S phases calculated for the fixed events at all recording stations. This representation provides an estimation of a constant V_p/V_s ¹ ratio value and does not depend on the origin time. The data recorded by seismic stations at a maximum distance of 150 km from PSG are distributed according to a linear trend with a best-fit line corresponding to a V_p/V_s ratio equal to 1.70 (Figure 3.5).

¹ V_p : P-wave velocity, V_s : S-wave velocity

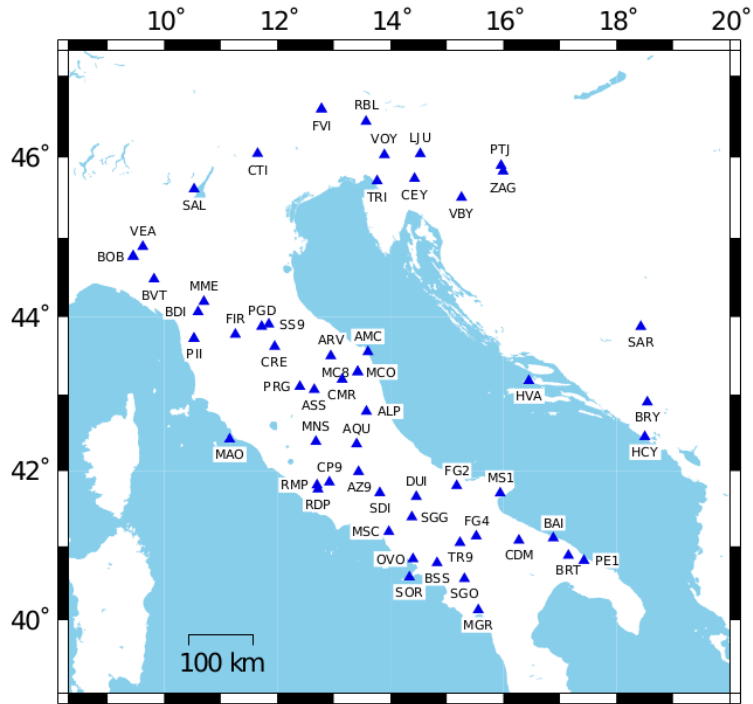


Figure 3.4 - Seismic network map at distance up to 400 km from Porto San Giorgio.

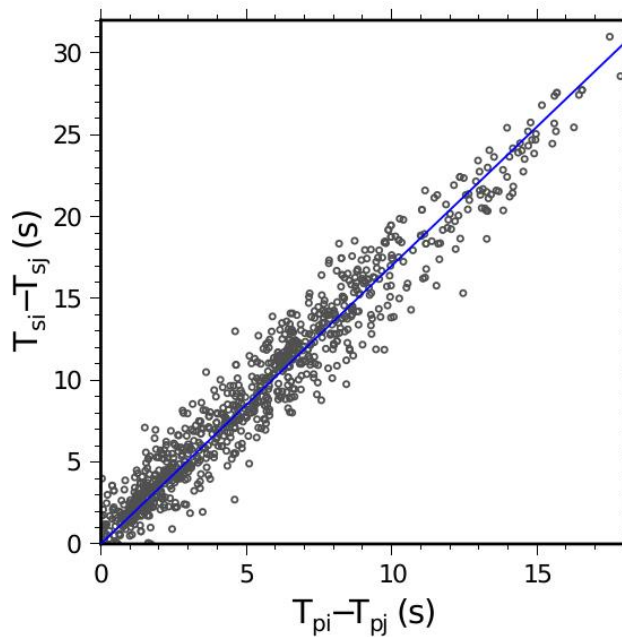


Figure 3.5 - Modified Wadati diagram obtained considering the dataset recorded by seismic stations within 150 km of Porto San Giorgio. The blue line identifies the best fit that was obtained for $V_p/V_s = 1.70 \pm 0.01$.

3.2.1 Earthquake relocation of the Porto San Giorgio 1987 mainshock

The mainshock relocation of the Porto San Giorgio seismic sequence is a very delicate issue, since in the scientific literature the depth values estimated by agencies' reports and the few studies range from 2.7 km to 33 km (Table 3.1). This variability in depth is due to the poor azimuthal coverage of the seismic network and the choice of velocity model used in the relocation process.

Latitude (°)	Longitude (°)	Depth (km)	Magnitude	Author
43.260	13.690	3.0	$M_b=5.3$ $M_s=5.1$	MOS
43.200	13.400	18.0	-----	PEK
43.254	13.936	12.0	$M_b=5.1$ $M_d=4.9$	NEIC
43.240	13.946	5.0	-----	EHB
43.300	14.100	----	$M_L=4.8$	LDG
43.310	13.970	11.0	$M_L=5.4$	TTG
43.300	15.800	33.0	$M_b=4.8$	NAO
43.270	13.960	10.0	-----	CSEM
43.233	13.925	10.0 (operator assigned)	$M_b=5.1$	ISC
43.198	13.902	2.7	$M_w=5.06$	CPTI15
43.200	13.850	5.0 (operator assigned)	$M_d=4.9$ $M_L=4.2$	INGV

Table 3.1 - Location of the mainshock of the PSG seismic sequence obtained by different seismological institutes and reported by the Bulletin of the International Seismological Centre by Rovida et al. (2016) and by Istituto Nazionale di Geofisica e Vulcanologia (INGV). CPTI15, Catalogo Parametrico dei Terremoti Italiani 2015; CSEM, Centre Sismologique Euro-Méditerranéen; EHB, Engdahl, van der Hilst, and Buland; LDG, Laboratoire de Détection et de Géophysique; ISC: International Seismological Centre; MOS, Geophysical Survey of Russian Academy of Sciences; NAO, Stiftelsen Norwegian Seismic Array (NORSAR); NEIC, National Earthquake Information Center; PEK, Peking; TTG, Titograd Seismological Station.

In this work the mainshock relocation involves a two-step procedure: the first investigates different velocity models looking for the best one while the second exploits a macroseismic analysis to determine the depth and magnitude of the seismic event considered. In the latter analysis, the dataset used consist of 212 intensity values reported in the ING Macroseismic Bulletin (Gasparini et al., 1988) and shown in Table A.1 in appendix A.

To relocate the PSG seismic sequence the NonLinLoc software (Lomax et al., 2000) was used (see Chapter 2, subsection 2.1.1.1). This technique is based on a probabilistic formulation of the inverse problem presented in Tarantola & Valette (1982) and Tarantola (2005). It allows the use of optimal hypocenters through an estimation of the posterior probability density function for the spatial coordinates (x,y,z) . An analysis of the distribution of weighting factors associated with the P- and S-wave arrival times' catalogue was performed (Figure 3.6) by associating, based on their statistics, an uncertainty in seconds (weight 0 corresponds to 0.05 s, 1 to 0.1 s, 2 to 0.2 s, 3 to 0.5 s, and a weight 4 to an unused value).

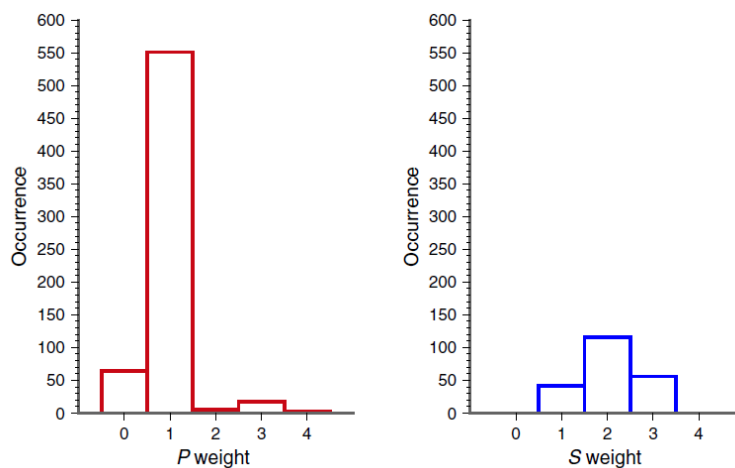


Figure 3.6 - Histograms of the weighting factors associated to the P- and S-wave arrival-time catalog.

To reduce the bias between the hypocenter coordinates and the seismic velocity related to unmodeled velocity structure, several location tests were performed for the mainshock by varying the 1D velocity model and

V_p/V_s ratio. Several researchers have produced velocity models useful to evaluating the central Adriatic.

Specifically, in Figure 3.7 the velocity models used for the localization tests of the mainshock are shown: Scognamiglio et al. (2009) defined P- and S-velocity models, on both national and Mediterranean-wide scales, that were used to calculate Green's functions to determine the moment tensor; Chiarabba & Frepoli (1997) calculated the P-velocity model for the Northern Apennines and obtained their results by inverting the P-wave arrival times relative to 135 earthquakes; Valensise's velocity model (1987) was adopted in Console et al. (1992) to relocate the PSG and Montefeltro seismic sequences (July - September 1987, Marche Adriatic coast) with the 'joint hypocenter technique'; the Carannante et al. (2013) velocity model was obtained for the Northern Central Apennines by performing seismic tomography on a regional scale; CSTI 1.1 (2005) was used to relocate the events reported in version 1.1 of the Catalogo Strumentale dei Terremoti Italiani; IASP91 (Kennett, 1991). Other tests were performed by varying the number of stations used based on their epicentral distance from the mainshock. All the tests on the mainshock were performed using a V_p/V_s value equal to 1.70, as provided by the Wadati modified diagram (Figure 3.5). The epicentral locations of the mainshock are aligned in a SW-NE direction, thus varying the P-wave velocity models. This result is an artifact introduced by the poor azimuthal station coverage in that direction. Each of the models provided different location results, showed that the depth varies from 0 to 18 km and that the horizontal errors are equal to 0.5 km while the vertical errors range between 0.2 km and 0.9 km. The rms^2 value is less than or equal to 1.05 s (Table 3.2). After this analysis, the models in which the depth was zero were excluded as they are unacceptable solutions, while the models of Scognamiglio et al. (2009) and Chiarabba & Frepoli (1997) in which the depth is equal to (2.0 ± 0.9) km and (18.0 ± 0.6) km, respectively, were considered (Figures 3.7 b-c). In this study, to discriminate between the two depths, a new method is provided

² rms (root mean square): this quantity is calculated as the quadratic deviation of times over all stations.

to investigate the earthquake depth that was consistent with the pattern of macroseismic intensity data.

Firstly, synthetic seismograms were simulated at each site in which intensity was reported. Seismic signals were modelled (Coutant, 1989) by considering a point source with a fixed reverse-fault mechanism as indicated in Riguzzi et al. (1989) and fixing the epicenter to a macroseismic solution as reported by Bollettino Macrosismico ING (Gasparini et al, 1988).

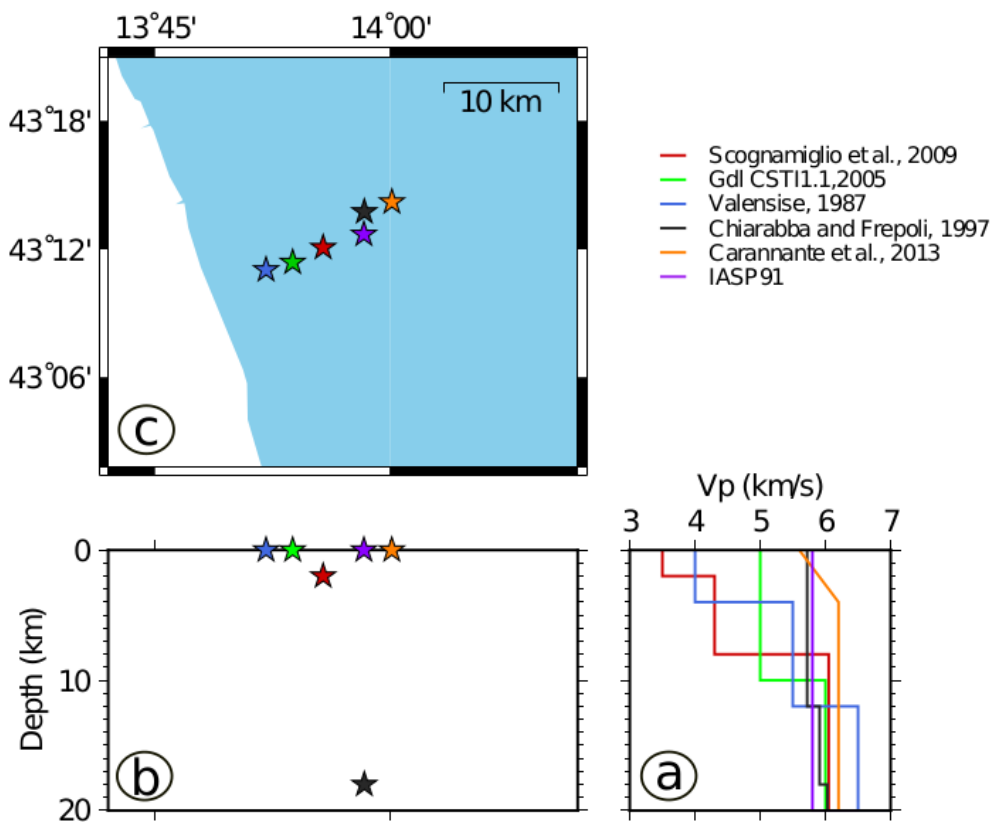


Figure 3.7 - a) Relocation of the PSG mainshock using different 1D P-velocity models taken from the literature and $V_p/V_s=1.70$. b) Vertical section of the PSG mainshock relocation showing the dependence of depth on the velocity model used. c) 1D P-velocity models taken from the literature.

<i>NonLinLoc output</i>										
Velocity model	T origin	Lat (DM)	Lon (DM)	Depth (Km)	rms (s)	ERH (km)	ERZ (Km)	Gap (°)	N phases	MinStaDist (km)
<i>Scognamiglio et al. (2009)</i>	10:21:56.43	43 12.07	13 55.74	2.0	0.69	0.5	0.9	82	47	42.50
<i>Chiarabba & Frepoli (1997)</i>	10:21:57.55	43 13.74	13 58.37	18.0	0.77	0.5	0.6	83	47	45.38
<i>Valensise (1987)</i>	10:21:58.45	43 11.03	13 52.09	0	1.05	0.5	0.2	80	47	38.31
<i>Caramante et al (2013)</i>	10:21:57.86	43 14.20	14 0.13	0	0.77	0.5	0.9	84	47	47.57
<i>Gdl CSTI 1.1 (2005)</i>	10:21:57.69	43 11.38	13 53.79	0	0.92	0.5	0.2	81	47	40.31
<i>IASP91</i>	10:21:57.76	43 12.69	13 58.34	0	0.76	0.5	0.6	82	47	45.70

Table 3.2 – Results of the mainshock relocation using six different 1D P-velocity models and V_p / V_s equal to 1.70. ERH: horizontal error; ERZ: vertical error; rms: root mean square.

Subsequently, to recover the macroseismic intensity data at sites, the Peak Ground Velocity (PGV) was selected as the maximum between the horizontal components and converted it into macroseismic intensity (MCS) following the methods of Faenza & Michelini (2010). Because of the trade-off between magnitude and depth, different combinations, ranging from 4.2 to 5.2 for magnitude and from 2 to 20 km for depth were explored. The analyzed ranges of magnitude and depth corresponded with the different estimates reported in scientific literature for the PSG mainshock (Table 3.1). Several sampling step sizes were tested during the grid-search. For the final analysis, a sampling of size equal to 0.2 and to 1 was selected for the magnitude and depth, respectively, which represented a useful compromise to limit the computation times and to denote the presence of multiple minima. The reliability of the methodology was verified through its application to different datasets (Figures A.1-A.2 and Table A.2 in appendix A), although a resolution and error analysis were not performed since it goes beyond the purpose of this work. For each magnitude-depth combination, the synthetic seismograms were modeled. Then, a grid search in the magnitude-depth space (Figure 3.8b) was carried out by comparing the real and synthetic intensity data to find the minimum root-mean-square value (rms) between the real and synthetic intensity data for each magnitude-depth couple. The minimum misfit (measured as the rms value) was obtained for an earthquake with a depth of 5 km and a magnitude (M_L) equal to 5. The grid-search result indicated a shallow source rather than a deep source as the preferred solution for the PSG mainshock, as shown in Figure 3.8, where synthetics and the real macroseismic map are compared at depths equal to 5 km and 18 km, respectively (M_L 5 and depth 5 km, Figure 3.8c; M_L 5 and depth 18 km, Figure 3.8d). According to the previous mainshock relocation analysis, the model of Scognamiglio et al. (2009) was preferred to relocate the mainshock and the whole PSG seismic sequence.

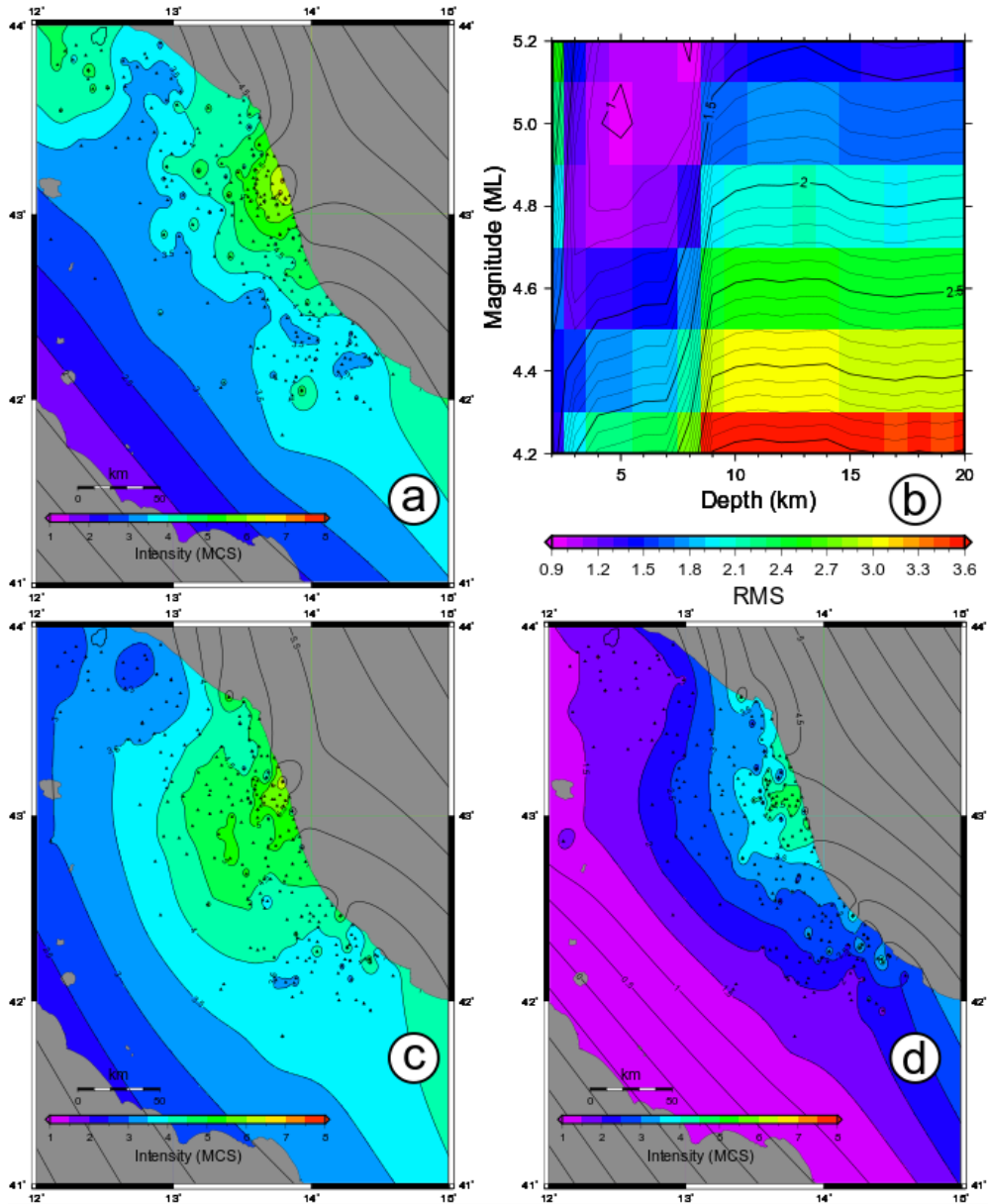


Figure 3.8 - a) Macroseismic intensity map of the M_L 5, Porto San Giorgio earthquake - July 3rd, 1987, at 10:21.57 (UTC). The Mercalli-Cancani-Sieberg scale (MCS) is used. Intensity data, whose geographical location is indicated with a black triangle, are derived from the ING Macroseismic Bulletin (1988). b) Results of the grid-search performed in the magnitude-depth space. The real and synthetic macroseismic maps for the M_L 5, 1987 Porto San Giorgio earthquake are compared by evaluating the root-mean-square value (rms) between the real and synthetic intensity data for each combination of magnitude-depth values. In c) and d), synthetic intensity maps are reported for M_L 5 depth=5 km and M_L 5 depth=18 km, respectively.

3.2.2 Earthquake relocation of Porto San Giorgio seismic sequence

In this study 91 events of the PSG seismic sequence (July - December 1987) with $1.3 \leq M_L \leq 5.0$ were relocated using the 1D velocity model reported in Scognamiglio et al. (2009) and arrival-time data from 57 seismic stations situated up to 400 km from Porto San Giorgio. The V_p/V_s ratio considered was equal to 1.75, i.e., the value obtained from the P- and S- velocity structures reported in Scognamiglio et al. (2009) and in accordance with several studies (Chiarabba & Frepoli, 1997; Carannante et al., 2013). Moreover, unmodeled local velocity changes were considered using the seismic station corrections by adopting a two-step location procedure. The sum of the average residuals provided, in the first relocation step, the cumulative delay for P and S phase at each station (Table A.3, in appendix A). These values were used as the station corrections for the second relocation step. Then, by adopting selection criteria (azimuthal gap less than 200° and vertical (ERZ) and horizontal (ERH) location errors less than 3 km (Figure 3.9)) 30 seismic events were obtained as the final earthquake locations.

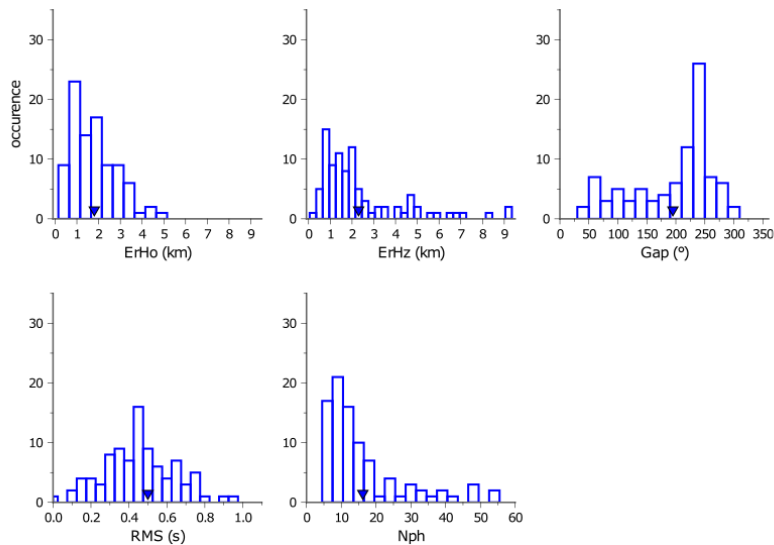


Figure 3.9 - Histograms of the 91 seismic events distributions to evaluate the quality of locations of the PSG seismic sequence. They show the horizontal (ErHo) and vertical (ErHz) errors, the Gap, the rms, and the number of phases used (Nph). The inverted triangle identifies the median of the values obtained.

3.2.3 *Results and discussion*

The relocation results for the 30 events of the sequence, selected as described above, are shown in Table 3.3. The events occurred from July to December 1987 with local magnitudes ranging from 1.3 and 5.0 (CSTI 1.1, 2005; Castello et al., 2006). The earthquakes' location calculations show a rms less than 1 s and depths between 1.6 km and 32.8 km with the maximum horizontal (ERH) and vertical (ERZ) errors equal to 1.1 km and 2.1 km, respectively. The PSG mainshock depth is equal to 5.7 km with an ERZ equal to 1.3 km, and an ERH equal to 0.5 km. The relocated PSG seismic sequence is shown in Figure 3.10 in map and along a vertical section with a SW-NE direction (azimuth $N49.64^\circ$, obtained from the strike value of the mainshock minus 90°). Notably, almost all the events were within the first 15 km of the crust and are located up to 15 kilometers from the coast.

The depth of the PSG earthquake is a crucial point of discussion. The PSG seismic sequence occurred in the offshore Adriatic, not far from the Marche region coastline. No ocean-bottom seismometers are installed in the Adriatic Sea, so the lack of coverage could be seen from the north to southeast. To cover this azimuthal gap, the data were integrated with the seismic stations of the Balkan Peninsula, regardless of whether the stations were far from the epicenter region. At the same time, in 1987, the Italian regional network managed by ING was not composed of many stations and was not as dense as at present. Therefore, considering the available data and the seismic network criteria, the PSG mainshock depth cannot be constrained within standard earthquake location methods; no data exist within 40 km of the epicenter (the closest station to the mainshock epicenter is at a distance of 41.3 km), and no S-wave readings were taken within the same distance. Moreover, the absence of seismic phases that are useful in constraining the focus depth is evident in the teleseismic data from the earthquake locations reported by several agencies in which the PSG depth was fixed to the default value as reported by ISC online bulletin (International Seismological Centre, [ISC] 2016).

<i>Date yyymmdd</i>	<i>Time hhmm ss.ss</i>	<i>M_L</i>	<i>Lat (DM)</i>	<i>Lon (DM)</i>	<i>Depth (km)</i>	<i>ERH (km)</i>	<i>ERZ (km)</i>	<i>RMS (s)</i>
870703	1021 57.05	5.0	43 12.25	13 54.86	5.7	0.5	1.3	0.55
870703	1042 24.64	2.9	43 12.07	13 56.11	11.3	0.9	1.5	0.52
870703	1155 23.58	3.3	43 12.64	13 54.48	8.0	0.6	0.8	0.72
870703	1354 1.73	2.7	43 13.00	13 48.95	14.3	0.7	0.8	0.72
870703	1738 2.87	3.6	43 12.48	13 56.15	8.0	0.5	0.5	0.50
870703	1930 11.12	2.7	43 11.86	13 52.82	13.8	0.6	0.7	0.69
870703	2110 1.58	2.7	43 11.69	13 55.02	9.1	0.7	1.1	0.73
870705	2354 17.05	3.5	43 12.84	13 54.87	8.0	0.5	0.6	0.41
870706	0337 23.11	2.8	43 13.21	13 53.99	10.6	0.7	1.0	0.44
870706	1044 55.20	2.6	43 12.59	13 52.02	2.2	0.9	1.1	0.41
870707	1735 8.82	2.5	43 15.00	13 45.74	14.9	0.8	0.7	0.40
870712	2042 24.38	1.8	43 6.02	13 24.79	15.5	0.7	1.5	0.23
870721	0225 35.35	2.6	43 12.37	13 47.96	13.6	0.7	0.8	0.61
870721	0316 40.14	2.9	43 11.42	13 57.32	8.6	0.7	0.8	0.49
870801	0341 9.56	1.8*	43 8.25	13 28.29	16.3	0.8	2.1	0.43
870807	1016 37.10	1.6	43 8.71	13 28.15	15.7	0.7	1.7	0.36
870816	0031 44.03	2.8	43 11.88	13 50.03	14.0	0.9	0.7	0.31
870820	0632 26.90	2.6	43 10.27	13 47.52	17.0	0.8	0.8	0.86
870904	1642 47.63	4.6	43 12.98	13 56.39	4.4	0.5	1.4	0.44
870910	1324 22.61	4.2	43 13.93	13 56.26	8.1	0.5	0.8	0.57
870910	1336 42.45	2.6	43 15.65	13 55.75	3.4	0.6	1.3	0.49
870922	0424 54.49	3.7	43 13.17	13 53.14	12.5	0.5	0.8	0.56
871003	0434 24.69	1.3*	43 20.54	13 23.03	16.7	0.8	1.1	0.29
871005	0738 2.01	1.5*	43 0.87	13 23.35	8.0	0.7	1.7	0.49
871010	2247 25.58	2.2	43 13.94	13 55.13	10.0	1.0	0.9	0.74
871028	2333 8.66	2.1	43 1.70	13 31.14	4.0	0.8	0.7	0.79
871114	0409 24.69	2.3	43 8.26	13 23.62	18.2	0.6	0.5	0.61
871119	1259 28.13	2.5	43 12.27	13 56.61	8.8	0.7	1.4	0.50
871129	0222 22.34	2.6	43 31.06	13 36.33	32.8	0.8	0.5	0.64
871223	0503 32.31	2.0	43 12.88	13 47.53	1.6	1.1	1.1	0.66

Table 3.3 - Relocation results obtained for 30 events of the PSG seismic sequence (July – December 1987). The magnitude values are taken from the Catalogue of the Italian Seismicity (Castello et al., 2006) and the asterisked values from CSTI 1.1 (2005).

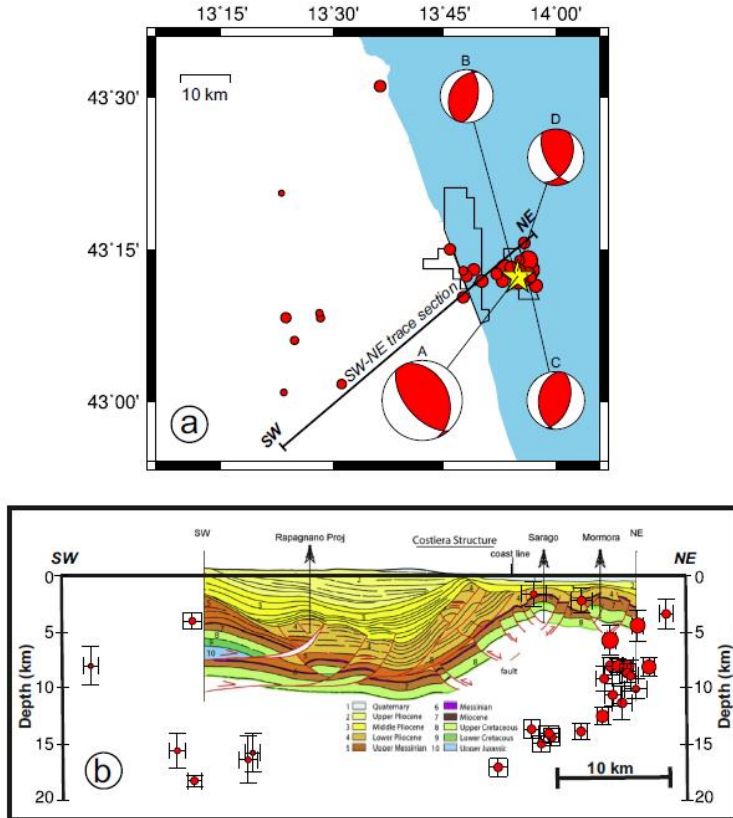


Figure 3.10 - a) Epicentral distribution and focal mechanisms (data from Riguzzi et al., 1989) of the relocated 1987 Porto San Giorgio seismic sequence. The red circles are the 30 events relocated ($1.3 \leq M_L \leq 5.0$, July-December 1987). The yellow star is the M_L 5 mainshock of the 1987 Porto San Giorgio sequence; it is at about 0.5-1 km far from the production wells. Focal mechanisms (A: M_L 5, 1987-07-03 at 10:21.57; B: M_L 3.3, 1987-07-03 at 11:55.23, C: M_L 3.6, 1987-07-03 at 17:38.02, D: M_L 3.5, 1987-07-05 at 23:54.17) indicate thrust fault kinematics. Black lines delineate the borders of the hydrocarbon cultivation concessions B.C. 7.LF, B.C. 2.LF and Fiume Tenna. b) Geological section (from Casero and Bigi, 2013) along the SW-NE direction with hypocenters of the relocated 1987 Porto San Giorgio seismic sequence. Earthquakes within 20 km on both sides of section were considered. Vertical and horizontal errors of the earthquake location are indicated. The symbol size is proportional to the earthquake magnitude.

Despite the uncertainty associated with the macroseismic data and analysis, the results suggest that the PSG mainshock occurred at a shallow depth (approximately 5 km) and had a magnitude equal to 5 (Figure 3.8). The earthquake locations describe a thrust fault structure with a northeast vergence and a listric geometry extending from 5 km to 15 km. This

geometry agrees with the SW-dipping nodal plane indicated by the PSG mainshock fault plane solution and is compatible with the available focal mechanisms when considering the uncertainties involved in the calculation. The results show a fault structure that is named in this study the Porto San Giorgio Seismogenic Thrust (PSGST), whose knowledge and attributes help in determining a correct seismic hazard assessment of the offshore Adriatic area. The fault structure is found in the external area of the Apennines foreland and thrust belt, located in the central offshore Adriatic region, where an inversion and/or reactivation occurred during the Middle and late Pliocene along a deep detachment likely seated on Triassic evaporites and involving Meso-Cenozoic carbonates (Argnani & Gamberi, 1995; Gambini et al., 1997, Casero & Bigi, 2013). As constrained by the results, the 1987 PSG seismic sequence activated a fault structure that correspond to an NE-verging, anticline related fault as evidenced by previous seismic profiles (Bally et al., 1986; ViDEPI Line B-411 (ViDEPI database) and surfaces trace located in the offshore Adriatic at 15 km from the Porto San Giorgio coast. This fault structure is compatible with the composite seismogenic source located off the coast of the southern Marche and was indicated as being responsible for the PSG seismic sequence by some authors (DISS Working Group, 2018).

The relevance in analyzing the PSG seismic sequence in this study is also due to its small distance to hydrocarbon exploitation permits, which in some cases are located close to active faults of the offshore Adriatic. Oil and/or gas fields are exploited along the so-called Costiera thrust front and are located partially onshore and offshore, as indicated by Casero & Bigi (2013). Upper Cretaceous-Paleocene limestone, resedimented, fractured bioclastics, and alternating with pelagic mudstone, produces oil and/or gas originating commercial middle-sized fields. Hydrocarbon traps can be formed by double-vergence thrust and inversion folds, with high-angle faults showing a NW-SE orientation, which were probably caused by the reactivation of old structures during the Middle-Pliocene. For the geometry, the location, and the depth of the fault structure, the PSGST might be associated with the geological structure that hosts the hydrocarbon trap of the San Giorgio a Mare field located in the external

thrust front of the Apennines. This mixed oil and gas system is characterized by an Upper Pliocene double vergence, up-thrust-like inversion folds, and a detachment level along the Triassic evaporites (Casero & Bigi, 2013).

Moreover, the tectonic activity of thrusting and folding of the external front of Apennines is debated (Bertotti et al., 1997; Di Bucci & Mazzoli, 2002; Argnani et al., 2003). For some authors, the activity likely stopped in the Adriatic Sea in the Early Pliocene, as evidenced by geological studies showing thrust structures sealed by younger deposits (from Middle Pleistocene to present). The results of this study suggest that the external front of the Apennines can produce moderate seismicity at shallow depths and is still active, as proposed by geomorphological studies, seismic profiles, and current stress field studies (Valensise & Pantosti, 2001; Vannoli et al., 2004; Scrocca et al., 2007; Montone et al., 2012). Historical and instrumental seismicity that may be associated with thrusting of the external front of Apennines developed off the Adriatic coast, at both north and south of PSG (Figure 3.3, Rovida et al., 2016; Lavecchia et al., 1994; Chiaraluce et al., 2017a; Chiaraluce et al., 2017b).

3.3 Statistical correlation analysis in Porto San Giorgio area

The Marche offshore area in Italy has been subject to hydrocarbon exploration and extraction since the 1970s. Between the municipalities of Porto Sant' Elpidio and Porto San Giorgio lies the Santa Maria a Mare field, which is located both on- and off-shore in the Fiume Tenna and B.C7.LF cultivation concessions, respectively. The field was discovered in 1974 and became operational from September 1975 until March 1992. After a period of inactivity of about 15 years, production has restarted in a minor way. The field initially consisted of eleven wells grouped into four clusters and connected by flowline to the Santa Maria a Mare treatment and storage facility. Subsequently, seven wells were closed minerally while two became injectors and two producers.

Given the proximity between the geo-resource production and the Porto San Giorgio 1987 seismic sequence, it is important to investigate if there

was a relationship between anthropogenic activity and the seismicity occurred in the area. An important initial clue in this study is provided by a statistical analysis taking into account both industrial and seismic datasets.

Industrial data were provided by Edison S.p.A. as part of the doctoral activities, while the seismic data are derived from ISIDe catalog by INGV (Italian Seismological Instrumental and parametric Database, <http://iside.rm.ingv.it/iside>). Moreover, to carry out the analysis it is important to opportunely select the area of study. In fact, if it is too large, outsider seismicity can be erroneously included in the analysis masking a possible correlation. Conversely, if the area is too small, the analysis could be distorted because it does not include the real number of seismic events. In this work a circular area with a ray of 18 km and centered on Porto San Giorgio has been considered. 18 km is three times bigger than the length of the reservoir of Santa Maria a Mare, the field of interest investigated in this work.

Although production data are available since 1975, the seismic catalog begins in 1985 and consequently the period 1985 - 2015 was considered to perform the statistical analysis. The seismic dataset consists of catalog data: hypocentral coordinates, origin time and magnitude of 247 events (Figure 3.11); 57 earthquakes are reported in the catalog with local magnitude estimations ($1.0 \leq M_L \leq 3.5$), while 190 with duration magnitude estimations ($1.7 \leq M_d \leq 4.9$). The seismic event with M_d 4.9 corresponds to the mainshock of the 1987 Porto San Giorgio seismic sequence.

With the aim of carrying out a statistical analysis, including the magnitude data of seismic events, it was necessary to define a conversion law between M_d and M_L for the study area, making the database uniform. This analysis was performed selecting the seismicity occurred in a circular area (radius of 50 km) centered on Porto San Giorgio since 1985 to October 2018 and for which both local and duration magnitude data are provided (data available on INGV - National Earthquake Center, <http://cnt.rm.ingv.it/>).

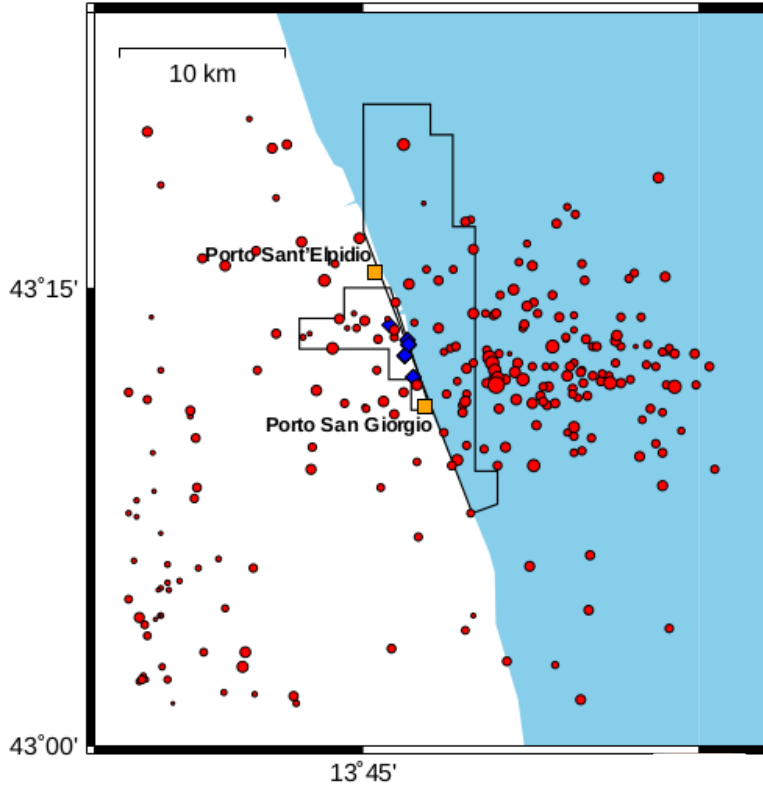


Figure 3.11 – Map of seismicity in Porto San Giorgio area (1985-2015). Red circles indicate the seismic events; their size is proportional to the magnitude. Black lines delineate the borders of the hydrocarbon cultivation concessions B.C.7.LF (offshore), and Fiume Tenna (onshore). The diamond in blue are the wells in Santa Maria a Mare field while the orange squares identify the town between which the field is located.

The number of seismic events satisfying these characteristics is equal to 790. Through the orthogonal regression (Figure 3.12), the following transformation rule was defined:

$$M_L = 1.1M_d - 0.7 \quad \text{Eq. 3.1}$$

The ‘Magnitude conversion’ application on IS-EPOS platform (Orlecka-Sikora et al., 2020) has been used providing also a 95% confidence interval for intercept and slope equal to 0.2 and 0.1, respectively, and a root mean square error of 0.4. In this way, 190 values of duration magnitude have been converted. The local magnitude distribution of the 247 seismic events, constituting the initial study dataset, is shown in Figure 3.13.

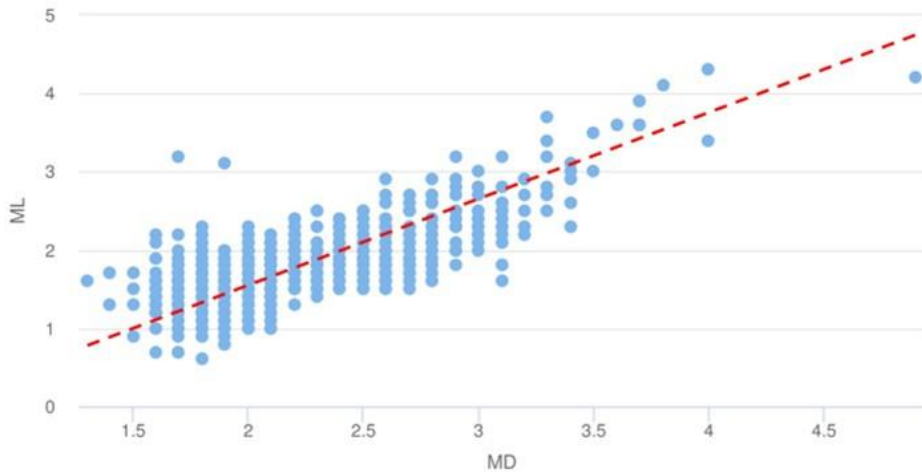


Figure 3.12 - Orthogonal regression line to extrapolate a magnitude conversion rule in the study area. On the x-axis the duration magnitude is represented while on the y-axis the local magnitude is indicated. The figure was generated using the 'Magnitude conversion' application on the IS-EPOS Platform (Orlecka-Sikora et al., 2020). The blue circles indicate the seismic events and the dotted red line the fit obtained.

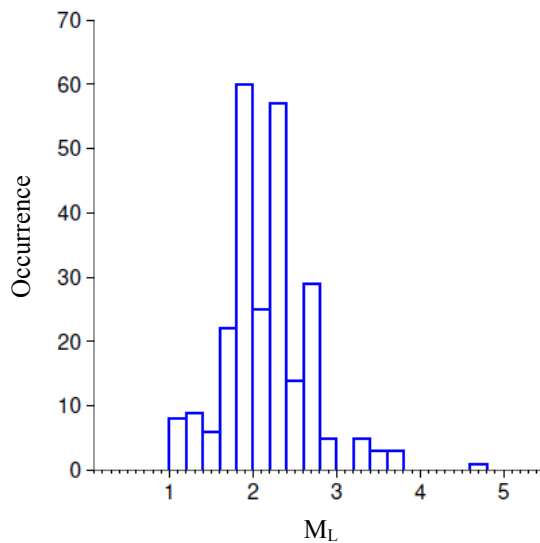


Figure 3.13 - Magnitude distribution of 247 seismic events after the application of the transformation rule on 190 values of duration magnitude.

3.3.1 Results and discussion

To study a possible link between anthropogenic activity and seismicity and to identify a potential induced/triggered seismicity in the area, a statistical analysis was performed between the seismicity and the

production parameters (oil and gas produced and injected water) using the binomial and Mann-Whitney U tests in the period 1985-2015.

The first test was implemented by considering the seismicity rate. After defining two periods as variables, T_1 and T_2 , the test evaluates if the seismicity rate is significantly different in one of the considered periods from a random process (Leptokaropoulos et al., 2018). So, the number of seismic events (n_1 and n_2) is significantly different from the number of events falling in a time interval in a random way. It is possible to define the null hypothesis as the occurrence of a random number of events n_2 in period T_2 with probability $P = T_2/(T_2 + T_1)$. A significance level of 5% was considered.

The second statistical test, Mann-Whitney U (Mann & Whitney, 1947), was applied using the magnitude data of the seismic events to verify if the difference between the medians of two samples, corresponding to two different period, is statistically significative. Given two sets of data, the null hypothesis is defined by stating that they are not different. The results of the test is evaluated at a 5% significance level.

The statistical analysis was performed in two steps: in the first, annual data from 11 wells (MAM2d, MAT3, MAM4d, MAM5d, MAM6d, MAT7, MAM8d, MAM9d, MAM10d, MAT11) are considered, while in the second, monthly data defined as the sum of the production rates of 9 wells (MAT3, MAM4d, MAM5d, MAM6d, MAM8d, MAM9d, MAM10d, MAT11) are used.

3.3.1.1 Analysis of annual data

Looking at the annual production data (Figure 3.14) since 1985 to 2015, the whole period was split into five parts in which production parameters show clear and stable trends.

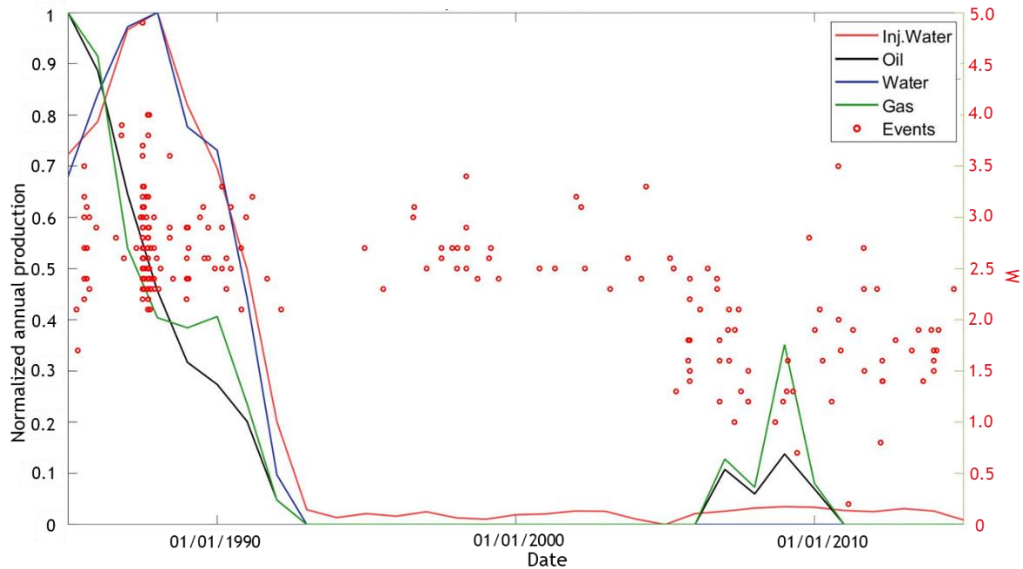


Figure 3.14 – Annual production (oil – black line, water – blue line and gas – green line) and values of injected water (red line) since 1985 to 2015 considering all wells in the field. The red circles identify the seismicity in a circular area of 18 km from Porto San Giorgio.

The periods are:

A: 1985 – 1988 showing an increase of water injection/production. Oil & gas production steadily decreases but maintaining high rates.

B: 1989 – 1992 showing a decrease of water injection/production with a decrease of oil & gas productions to zero rates.

C: 1993 – 2006 showing steady low water injection without oil & gas production.

D: 2007 – 2010 showing steady low water injection with low oil & gas production rates.

E: 2011 - 2015 showing steady low water injection without oil & gas production.

The results of binomial and U-tests are shown in Table 3.4.

Period 1	Period 2	Binomial Test p-value	U - Test p-value
A: 1985 - 1988	B: 1989 - 1992	8.46E-20	0.62
A+B: 1985 - 1992	C: 1993 - 2006	1.18E-32	0.03
C: 1993 - 2006	D: 2007 - 2010	0.035	0.000933
D: 2007 - 2010	E: 2011 - 2015	0.276	0.200806
A+B: 1985 - 1992	C + E: 1993-2006 & 2011-2015	2.55E-35	0.000076
D: 2007 - 2010	C + E: 1993-2006 & 2011-2015	0.056	0.003948

Table 3.4 - Annual results of binomial and U-test. In red are reported the statistically significant results.

Considering the seismicity rate (λ), the medians of magnitude data in each period analyzed and the p-values obtained from the statistical analysis, the results can be synthesized as:

- $\lambda_A > \lambda_B$, a decrease in water production resulted in a decrease of the seismic activity without significantly alter the median magnitude.
- $\lambda_{(A+B)} > \lambda_C$, the interruption of oil & gas production reduced the seismic activity. In general magnitudes showed higher values during injection and production periods.
- $\lambda_C < \lambda_D$, the moderate oil & gas production during the period D caused an increase of seismic activity characterized by weak events.
- No significant difference between λ_D and λ_E and between the medians of magnitude exist. The stop of oil & gas production in period E further did not significantly reduce the seismic activity. The discrepancy between these results and those of B and C periods may probably derive from the time needed for a kind of decay of the seismic activity. C period lasted 14 years whereas E period lasted 5 years.

- $\lambda_{(A+B)} > \lambda_{(C+E)}$, this result indicates a relation between seismicity and production. Both the seismic activity and the median of magnitude were greater during the production period than those during the no-production times.
- $\lambda_{(D)} \geq \lambda_{(C+E)}$, the median of magnitude in D period is lower than the median of the second period. The short period of moderate production did not significantly alter the seismic activity.

The results presented above show a correlation between seismicity and anthropogenic activity, particularly in conjunction with the 1987 sequence, especially moving from periods of production to non-production. This is evident from the results of both tests performed.

3.3.1.2 Analysis of monthly data

The binomial test was performed using the seismic rate data and the Mann – Whitney U test was performed using the magnitude data. The dataset spans since 1985 to March 1992 and correspond to the sum of the production rates of 9 wells (MAT3, MAM4d, MAM5d, MAM6d, MAM8d, MAM9d, MAM10d, MAT11), monthly sampled. The time periods considered were chosen differently based on the industrial parameter to be analyzed. The significance level for the tests is 5%.

The periods selected for each industrial parameter (Figure 3.15) are:

OIL – **A: 01/1985 - 04/1998** showing a decrease of oil production from high to low values.

B: 05/1988 - 03/1992 showing a continue decrease of oil production to very low value but with a gradient lower than in period A.

WATER – **A: 01/1985 - 02/1986** showing low value of water production.

B: 03/1986 - 03/1987 showing an increase of water production from low to high values.

C: 04/1987 - 01/1988 showing a decrease of water production from high to medium values.

D: 02/1988 - 05/1989 showing an increase of water production from medium to very high values.

E: 06/1989 - 03/1992 showing a decrease of water production from very high to low values.

GAS - A: 01/1985 - 08/1987 showing a decrease from very high to medium values.

B: [09/1987 - 04/1988] + [01/1991 - 03/1992] showing steady low values. This period consists of two fragments.

C: 05/1988 - 12/1990 showing medium values

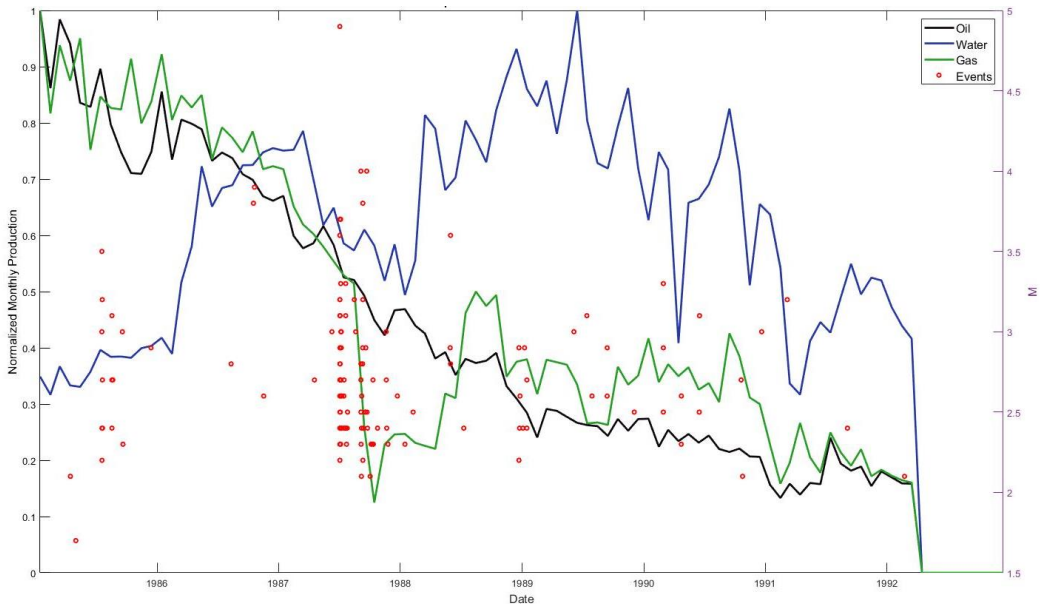


Figure 3.15 – Trend of monthly production technological parameters (oil in black, water in blue and gas in green) from 9 wells in the period 1985 – March 1992. The values are normalized. The red circles indicate the seismicity in a circular area of 18 km from the town of Porto San Giorgio.

Table 3.5 shows the results of the statistical analysis. The binomial test suggests that a decrease of oil production has led to a decrease of seismic

activity. In the case of produced water and gas, there is an increase in the rate of seismic events when their rates decrease. For the periods during which the Mann - Whitney U test was performed, it is found that the medians of magnitude doesn't show a significantly changes when seismic activity increases or decreases. The results of U-test indicate that the null hypothesis, i.e., the two groups of data are not different, is accepted as p-value is greater than 0.05 in all analyzed cases.

	Period 1	Period 2	Bin. Test <i>p-value</i>	U Test <i>p-value</i>
Oil	A _o : [01/1985; 04/1988]	B _o : [05/1988; 03/1992]	5.76 E-18	0.61
Wat	A _w : [01/1985; 02/1986]	B _w : [03/1986; 03/1987]	3.81 E-03	invalid
Wat	B _w : [03/1986; 03/1987]	C _w : [04/1987; 01/1988]	0	invalid
Wat	C _w : [04/1987; 01/1988]	D _w : [02/1988; 05/1989]	1.45 E-29	1
Wat	D _w : [02/1988; 05/1989]	E _w : [06/1989; 03/1992]	0.23	0.44
Wat	A _w : [01/1985; 02/1986]	C _w : [04/1987; 01/1988]	0	0.96
Wat	A _w : [01/1985; 02/1986]	D _w : [02/1988; 05/1989]	0.15	0.95
Wat	A _w : [01/1985; 02/1986]	E _w : [06/1989; 03/1992]	0.01	0.68
Wat	B _w : [03/1986; 03/1987]	D _w : [02/1988; 05/1989]	0.02	invalid
Wat	B _w : [03/1986; 03/1987]	E _w : [06/1989; 03/1992]	0.06	invalid
Wat	C _w : [04/1987; 01/1988]	E _w : [06/1989; 03/1992]	1.89 E-45	0.41
Gas	A _g : [01/1985;08/1987]	B _g : [09/1987-04/1988] & [01/1991-03/1992]	4.16 E-04	0.10
Gas	B _g : [09/1987-04/1988] & [01/1991-03/1992]	C _g : [05/1988;12/1990]	2.75 E-02	0.11
Gas	A _g : [01/1985;08/1987]	C _g : [05/1988;12/1990]	2.60 E-09	0.76

Table 3.5 - Results of binomial and Mann Whitney U-test obtained by considering summarized monthly data from nine wells. Invalid means that the test could not be performed because one of the two groups has less than five samples. In red are reported the statistically significant results.

3.4 Conclusions

The 1987 PSG seismic sequence was analyzed to determine a more accurate knowledge of the seismotectonic of the Central Adriatic offshore. Here, the compressive geological structures delineate the external front of the Apennines as an active seismic zone. This area, characterized by low to moderate seismicity, has been poorly studied and its present seismogenic potential is unclear. To solve the major critical problems, caused by the low azimuthal coverage of the seismic network and by the

absence of digital waveforms, an accurate relocation of the PSG seismic sequence was performed using a nonlinear probabilistic approach and catalog data. The uncertainty related to the source depth was resolved developing a technique that uses the macroseismic intensity field data. The results indicate that the mainshock was located at a 5.7 km depth, and almost all the events were located at up to 15 kilometers from the coast. The earthquake locations depict a thrust fault structure with a northeast vergence and a listric geometry that extends from 5 km to 15 km and shows a fault structure that is indicated as the Porto San Giorgio Seismogenic Thrust (PSGST). The increase in knowledge of this structure help to improve the seismic hazard assessment of the offshore Adriatic. Moreover, the results suggest that the external front of the Apennines is still active and can produce moderate seismicity at shallow depths, as previously proposed by geomorphological studies, seismic profiles, and current stress field studies.

This detailed study of past seismicity in an area subject to hydrocarbon extraction activities is important for subsequent correlation analyses between anthropogenic activities and seismicity.

In this work, seismic and industrial production data were used to verify if the seismicity in the Porto San Giorgio area was affected by the anthropogenic activity generated by the extraction of geo-resources in the Santa Maria a Mare field, between the cities of Porto Sant' Elpidio and Porto San Giorgio. Annual, and monthly production data associated with 11 and 9 wells, respectively, were considered. Statistical analysis was carried out using the binomial test, applied on the seismicity rate, and the Mann Whitney U-test, applied on earthquake magnitude data. The results, evaluated at a 5 percent significance level, show a correlation between seismicity rate and production data in correspondence with the occurrence of the 1987 Porto San Giorgio seismic sequence. This result is also found when analyzing magnitude versus annual production data. Industrial activity appears to be most intense between 1985 and 1988, reaching a peak of produced and injected water in the time of the seismic sequence occurrence.

An important limitation in this study is certainly the lack of a consistent sample of seismic data. Nevertheless, it is worth to note the relevance and the importance of this kind of work to verify the potential link between seismicity and anthropic activity as done in the Porto San Giorgio area for an historical seismic sequence in area poorly studied because of the many complications due to the location offshore, or below the coast, of production and disposal wells. The Adriatic Sea is the largest Italian area for gas exploration and extraction with re-injection of wastewater. It is therefore very important to have a detailed framework of the seismicity, both historical and present, occurring in the proximity of the cultivation concessions to have a better knowledge of the activity of the seismogenic structures present in the area. The location analysis carried out in this work goes in this direction by providing a modern and detailed study of the 1987 Porto San Giorgio seismic sequence, enriching the existing literature (Riguzzi et al., 1989; Console et al., 1992). The statistical analysis, on the other hand, is one of the first studies of its kind carried out in the area. This lack of work in the scientific literature is due to the need for industrial data, which are not freely available. Greater synergy between industry and science can promote free access to industrial data for statistical correlation studies to better discriminate whether a seismic event is natural or anthropogenic in an already tectonically active area.

A potential development of this work is to perform relocation studies for other seismic sequences in the Adriatic Sea, occurred in the vicinity of extraction activities, and subsequent statistical correlation analyses. In addition, the technique developed to derive the magnitude and depth of a seismic event from macroseismic intensity data can be exported to study historical earthquakes for which there are no waveforms or catalogue data.

STUDY OF SEISMICITY IN AREA SUBJECT TO GEOTHERMAL EXPLORATION

Geothermal activities like other that exploit geo-resources do not present zero risk. In fact, they can be the cause of induced/triggered seismicity as they can disrupt the stress conditions to which rocks are subjected (Ellsworth, 2013). In recent years, to increase geothermal production, it has been decided to introduce in this sector, as in oil & gas, the use of non-conventional techniques.

Enhanced Geothermal Systems (EGS) apply the injection of high volumes of pressurized fluid to fracture hot dry rocks to form pathways, new or preexisting, in which water circulates so to enhance the rock permeability (Grigoli et al., 2017; Baisch et al., 2010). The cold water under high pressure is pumped into the hot subsoil, where it heats up and returns to the surface. This process causes micro-seismicity but sometimes, the induced fractures may coalesce into unwanted paths that allow the fluids to reach pre-existing faults, triggering major seismic events (Lasocki & Orlecka-Sikora, 2020). The knowledge of how these fractures propagate in the subsurface is very important to improve production and especially to be able to assess and mitigate the risks associated with the exploitation of geo-resources by fluid injection (Orlecka-Sikora et al., 2019).

The aim of this chapter is to investigate the relationship between injection and a degree of disordering of sources, named ZZ , at the Cooper Basin geothermal field in Australia. The followed methodology is the same as the one developed and applied to study The Geysers geothermal field case (Lasocki & Orlecka-Sikora, 2020). ZZ is a parameter that quantifies the potential of seismicity to build pathways for fluid migration. It is numerically calculated as the average distance between the seismic events in an eight-dimensional parameter space, whose parameters are previously normalized by means of the transformation to equivalent-

dimensions (Lasocki, 2014; see Chapter 2, subsection 2.1.2). As for The Geysers, it is assumed that an important role in linking fractures into unwanted pathways is played by closeness of hypocenters, closeness of radii with origin in the open hole of the injection well on which events locate, and similarity of fracture planes orientations.

4.1 The Cooper Basin geothermal field case study

One of the biggest non-conventional geothermal experiments began in 2002 in the Cooper Basin (Figure 4.1), Australia, by Geodynamics Limited. The field is located in the South of the country near the Queensland border, approximately 900 km NNE of Adelaide (Holl & Barton, 2015). A total of six deep wells (depths 3629–4852 m) were drilled into hot (230° C–264° C) granite basement, known as the Innamincka granite (Hogarth & Holl, 2017). Two of these wells are in the Jalokia and Savina fields and four in the Habanero field (Baisch et al., 2015). Hydraulic stimulation in the Habanero field produced a copious seismic response to fluid injection. One of the largest catalogs of induced seismicity related to similar geothermal experiments was generated (Baisch et al., 2015) with the stimulation of the Habanero 4 well. The first Habanero well was initially stimulated in 2003 and re-stimulated in 2005 with large amounts of fluid, while Habanero wells 2, 3, and 4 were drilled in 2004, 2008, and 2012, respectively (Hogarth et al., 2013). All intersect a large fault forming the reservoir (Figure 4.2, Bendall et al., 2014; Holl & Barton, 2015).

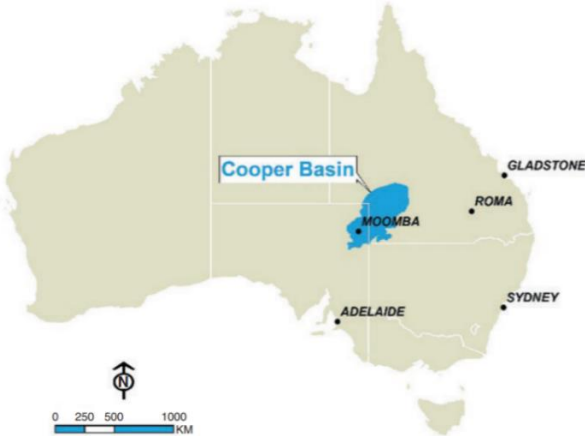


Figure 4.1 - Map of Australia showing Cooper Basin. Source: Lockhart et al. (2018)

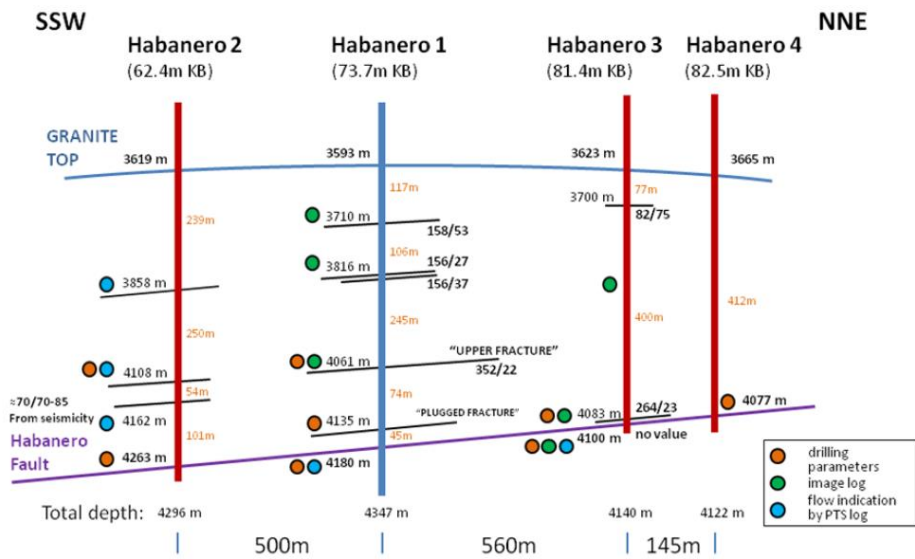


Figure 4.2 - Schematic representation of Habanero wells intersecting the 'Habanero Fault'. The fractures are identified by drilling parameters, image log analysis and flow indication from PTG logging. Source: Holl & Barton (2015)

A small local hydraulic stimulation of the Habanero 4 well began on 14 November 2012 (Mc Mahon & Baisch, 2013) with the aim of improving the hydraulic conductivity of the subsurface. An extensive stimulation started on 17 November of the same year with a total amount of water injected equal to 34000 m³, while the maximum wellhead pressure was of about 50 MPa with an overpressure of 34 MPa observed immediately before injection (Baisch et al., 2015; Holl & Barton, 2015). The industrial operations were monitored by a seismic network of 24 seismic stations (Figure 4.3, Mc Mahon & Baisch, 2013). It recorded more than 27000 events, allowing for the 525 strongest ones the reading of polarities on seismograms and thus the calculation of focal mechanisms. The latter indicated an overthrust on a shallow dipping plane, consistent with the compound fault plane solution determined by studying the seismic response following the re-stimulation of the Habanero 1 well in 2005 (Baisch et al., 2009, 2015). The localized hypocenters for more than 20000 seismic events ($-1.6 \leq M_L \leq 3.0$) are located on a single, subhorizontal fault, known as the 'Habanero Fault' already identified in past stimulations and hydraulically conductive prior to geothermal operations (Hogarth et al.,

2016; Baisch et al., 2006, 2009, 2015). Spatially, the seismicity developed along the north, moving away from the well with increasing time (Figure 4.4, Mc Mahon & Baisch, 2013). In 2013 (April - October), the Habanero 4 and 1 wells gave rise to a closed-loop test in which the first became a production and the second an injector well. The process occurred as part of the Habanero Pilot Project (HPP) for geothermal energy production. Another closed-loop test was conducted in 2008-2009 between Habanero 1 and 3 wells (Hogarth & Bour, 2015; Hogarth et al., 2013).

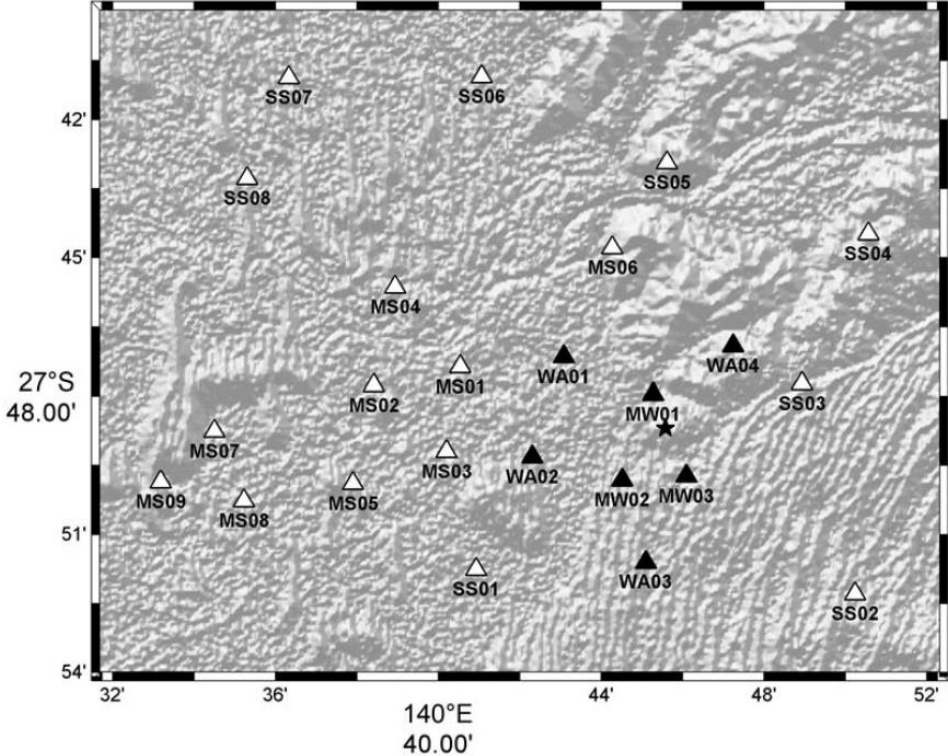


Figure 4.3 - Map of station network. The black triangles indicate the seismic stations for real-time data analysis, the white ones the stations recording in offline mode. The star is the Habanero 4 well. Source: Baisch et al. (2015)

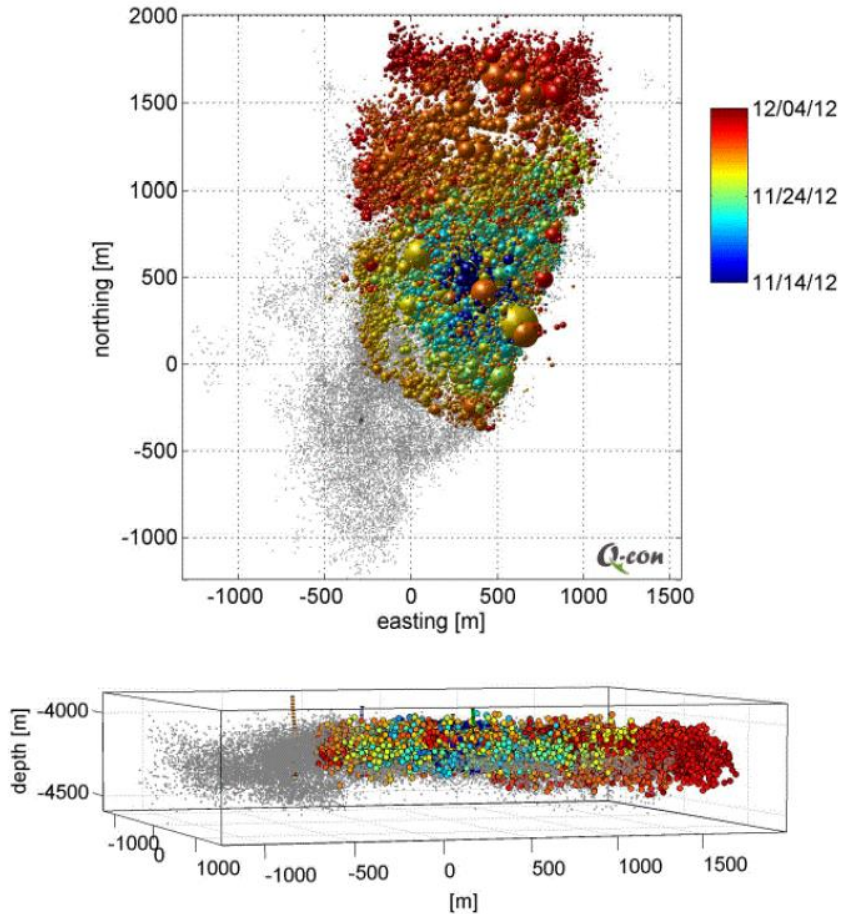


Figure 4.4 - Spatio - temporal distribution of seismicity after Habanero 4 well stimulation. The grey dots indicate previous seismicity while the others are colored in accordance with time in the legend. The size of the spheres is proportional to the events magnitude. Source: Mc Mahon & Baisch (2013)

4.2 Seismic and industrial dataset

To fulfill the purpose of this study, which is to perform a statistical correlation analysis between technological parameters and the degree of disordering of sources, ZZ, industrial and seismic data are needed. They were provided by ReNu Energy Limited (Australia) and Q-con GmbH (Germany) and have been rendered accessible on IS-EPOS platform (IS-EPOS, 2020, https://tcs.ah-epos.eu/#episode:COOPER_BASIN) in the framework of H2020 - Science for Clean Energy (S4CE) project (grant agreement No 764810).

The seismic dataset consists of 20734 events in the period from November 14 to December 4, 2012 (Figure 4.5). The moment magnitude ranges from - 0.3 to 3.1 (Figure 4.6).



Figure 4.5 - Time evolution (step 1 day) of the seismic events occurred in the Cooper Basin geothermal field from November to December 2012.

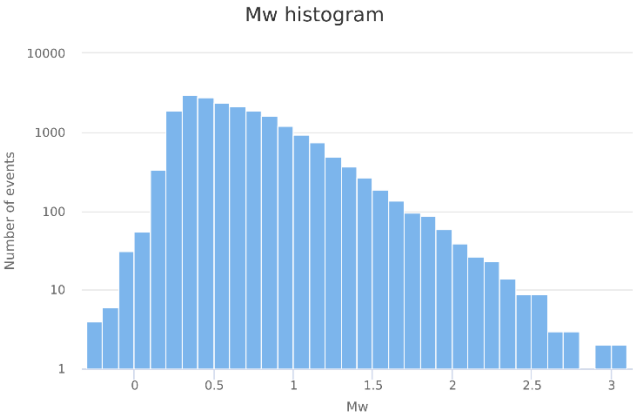


Figure 4.6 - Magnitude distribution of the 20734 seismic events occurred in the Cooper Basin geothermal field from November to December 2012.

As can be seen from Figure 4.5, the occurrence of seismicity is divided into two periods. This study focuses on the second one, which corresponds to the seismic reaction to extensive stimulation in the field. In addition, it is important to extract only the events of sizes above the magnitude of completeness of the catalog (M_c 0.4) to be sure that the analyzed group

comprise statistically all seismic events that actually occurred. In this study the statistical analysis is performed considering a new parameter, ZZ , defined only for the events with known focal mechanisms. Therefore, the initial dataset was filtered by means of the Catalog Filter application, available on the IS-EPOS platform (Orlecka-Sikora et al., 2020), to select only the events of interest in this study. In this way the catalog has been reduced to 489 seismic events (Figure 4.7), with moment magnitude between 0.8 and 3.1 (Figure 4.8). This minimum value of magnitude is obtained after filtering the events on strike, dip and rake. The strongest event with moment magnitude 3.1 occurred on November 27, 2012.

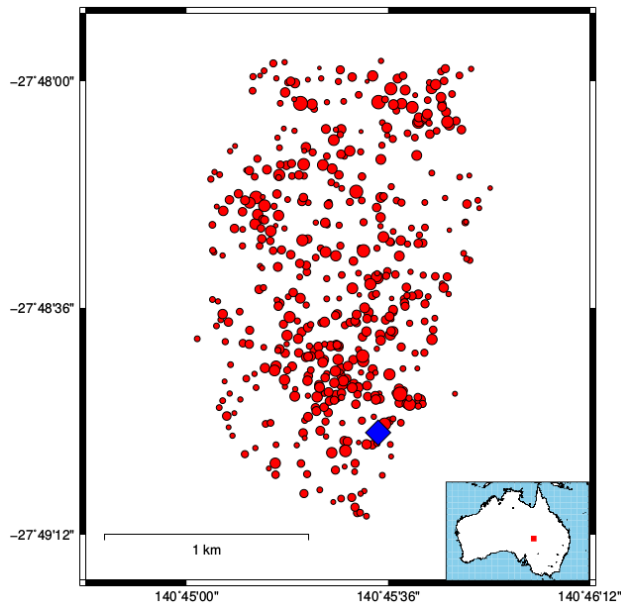


Figure 4.7 - Map of the 489 seismic events used in this study. Circle size is proportional to magnitude. The diamond in blue represents the Habanero 4 well. At the bottom right the map of Australia is shown; the red square on it is the area of interest.

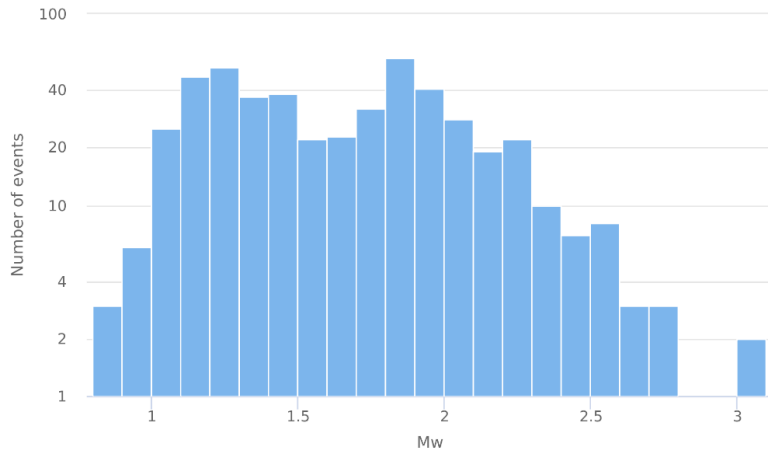


Figure 4.8 - Moment magnitude distribution with step 0.1. On y axis the scale is logarithmic.

An analysis of the obtained seismic catalog shows that the entire seismicity is concentrated in an area of 1 km x 2 km, extending north and westward from the Habanero 4 well. Seismic events located at a depth between 4.0 and 4.4 km with an error on the vertical component between 10 and 143 m. Errors related to latitudinal and longitudinal coordinates are between 6 and 78 m, and between 6 and 83 m, respectively. Finally, the three geometric parameters strike, dip and rake vary between 1° and 342°, 5° and 87°, -180° and 180°, respectively. The distribution of the mentioned seismic parameters is shown in Figure 4.9.

Regarding geothermal activity, the focus in this study is on the case of stimulation of the Habanero 4 well from 17 to 30 November 2012. Technological data available on the IS-EPOS platform, and considered in this work, are related to injection rate and wellhead pressure. The trend of these parameters is shown in Figure 4.10.

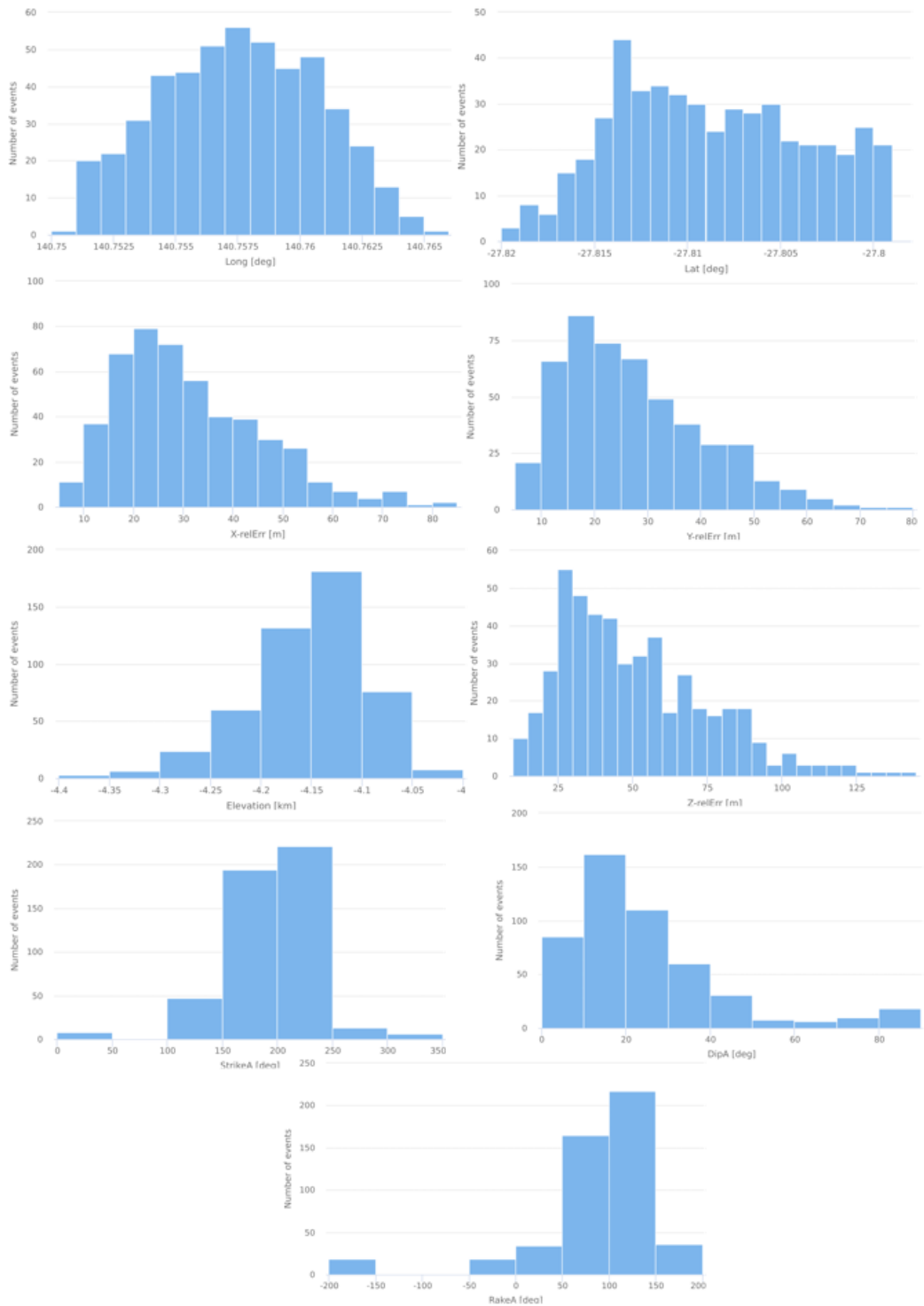


Figure 4.9 – Distribution of earthquake parameters: longitude, latitude, and respective relative errors; elevation and respective relative error; strike, dip, and rake.

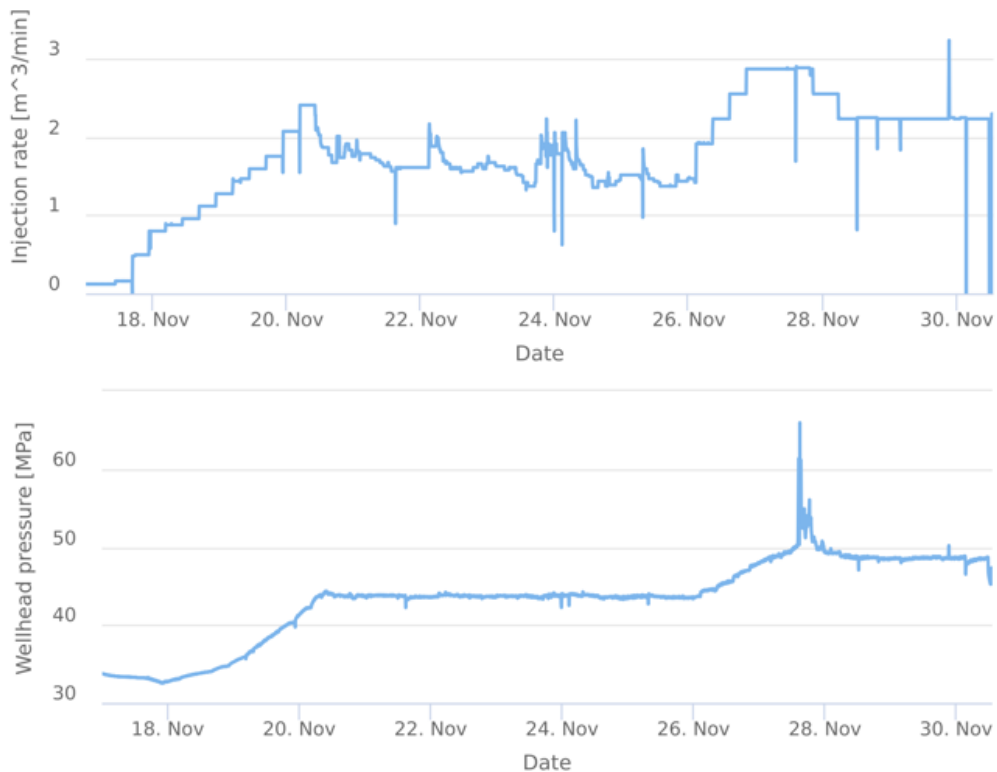


Figure 4.10 - Trend of injection rate and wellhead pressure (17-30 November 2012) in the Habanero 4 well of the Cooper Basin geothermal field.

4.3 Method

The methodology in this work follows the one developed and applied by Lasocki and Orlecka-Sikora (2020) for The Geysers geothermal field case. A new parameter, the degree of disordering of sources, ZZ , quantifies the potential of seismicity to build far-fluid migration pathways. As for The Geysers it is assumed that the potential to construct such paths depends on the proximity of the hypocenters, similarity of fracture planes orientations and closeness of rays with the same initial point at the open hole of Habanero 4 well on which the hypocenters are located.

With these conditions, ZZ was numerically defined and calculated as the average distance between seismic events in an eight - dimensional parameters space consisting of the three hypocentral coordinates, T- and

P-axis plunges, T-axis trend, and polar and azimuthal angles of hypocenters in the spherical system of coordinates with the origin at the open hole of Habanero 4 well. In order to calculate the distance between seismic events in the multi-dimensional space thus defined, it is necessary that all quantities are comparable to each other. For this reason, the equivalent-dimension transformation was used (Lasocki, 2014), which transforms continuous random variables (parameters) of any distribution into the variables uniformly distributed in the interval [0,1]. After the transformation, the eight-dimensional parameter space acquired the Euclidean metric.

Given an ensemble of n seismic events: for each pair of events, (i, j) , the degree of disordering of sources $ZZ(i, j)$ is the sum of three quantities: the distance between hypocenters, $\Delta r(i, j)$, the distance between focal mechanisms, $\Delta m(i, j)$, and the distance between the direction of the rays, $\Delta \phi(i, j)$ on which the two events are located:

$$\begin{aligned}
 ZZ(i, j) &= \sqrt{(\Delta r(i, j))^2 + (\Delta m(i, j))^2 + (\Delta \phi(i, j))^2} \\
 &= \sqrt{\left[\sum_{k=1}^3 (\Delta x_k(i, j))^2 \right] + \left[(\Delta tre_{x_1}(i, j))^2 + \sum_{k=1}^2 (\Delta plu_{x_k}(i, j))^2 \right] + [(\Delta \theta(i, j))^2 + (\Delta \phi(i, j))^2]}
 \end{aligned}$$

Eq. 4.1

In the previous equation:

$$\Delta x_k(i, j) = |x_k(i) - x_k(j)| \quad k = 1, 2, 3 \quad \text{Eq. 4.2}$$

with x_1, x_2, x_3 hypocentral coordinates;

$$\Delta tre_{x_1}(i, j) = 2 \begin{cases} |tre_{X_1}(i) - tre_{X_1}(j)| & \text{if } |tre_{X_1}(i) - plu_{X_1}(j)| \leq 0.5 \\ 1 - |tre_{x_1}(i) - tre_{x_1}(j)| & \text{if } |tre_{x_1}(i) - plu_{x_1}(j)| > 0.5 \end{cases} \quad \text{Eq. 4.3}$$

$$\Delta plu_{x_k}(i, j) = |plu_{X_k}(i) - plu_{X_k}(j)| \quad k = 1, 2 \quad \text{Eq. 4.4}$$

with tre_{x_1} T-axis trend, plu_{x_1} and plu_{x_2} T- and P- axis plunges respectively;

$$\Delta\theta(i,j) = 2 \begin{cases} |\theta(i) - \theta(j)| & \text{if } |\theta(i) - \theta(j)| \leq 0.5 \\ 1 - |\theta(i) - \theta(j)| & \text{if } |\theta(i) - \theta(j)| > 0.5 \end{cases} \quad \text{Eq. 4.5}$$

$$\Delta\varphi(i,j) = 4 \begin{cases} |\varphi(i) - \varphi(j)| & \text{if } |\varphi(i) - \varphi(j)| \leq 0.25 \\ |0.5 - |\varphi(i) - \varphi(j)|| & \text{if } 0.25 < |\varphi(i) - \varphi(j)| \leq 0.75 \\ 1 - |\varphi(i) - \varphi(j)| & \text{if } |\varphi(i) - \varphi(j)| > 0.75 \end{cases} \quad \text{Eq. 4.6}$$

with θ and φ being the polar and azimuthal angles of the ray on which the event is located, respectively. It is important to remember that the trend and polar angle take values in $[0^\circ, 180^\circ]$, the plunge in $[0^\circ, 90^\circ]$ and the azimuthal angle in $[0^\circ, 360^\circ]$. In the transformed space they all take values in $[0, 1]$. Therefore, in the equations 4.3, 4.5 and 4.6 a multiplicative factor to scale the differences of the parameters was inserted.

The calculation of the equations above defined was performed by dividing the 489 seismic events into 50-events windows sliding by 10 events. At the end of the process, the value of ZZ and its components were calculated for n (=50) seismic sources in each of the 45 previously obtained windows:

$$ZZ = \left\{ \sum_{i=1}^{n-1} \sum_{j=i+1}^n ZZ(i,j) \right\} / \frac{n(n-1)}{2} \quad \text{Eq. 4.7}$$

$$\Delta_r = \left\{ \sum_{i=1}^{n-1} \sum_{j=i+1}^n \Delta_r(i,j) \right\} / \frac{n(n-1)}{2} \quad \text{Eq. 4.8}$$

$$\Delta_M = \left\{ \sum_{i=1}^{n-1} \sum_{j=i+1}^n \Delta_m(i,j) \right\} / \frac{n(n-1)}{2} \quad \text{Eq. 4.9}$$

$$\Delta_\phi = \left\{ \sum_{i=1}^{n-1} \sum_{j=i+1}^n \Delta_\phi(i,j) \right\} / \frac{n(n-1)}{2} \quad \text{Eq. 4.10}$$

The variations of these parameters in windows 1:45 are shown in Figures 4.11 - 4.14.

After obtaining in each of the 45 windows the parameters that identify seismicity, it was necessary to calculate in them the average injection rate and the average wellhead pressure. The calculations were performed considering the time periods corresponding to the 50-event window periods, respectively. Because the available technological dataset runs from November 17 to November 30, while the seismic dataset continues

up to December 4, it was possible to divide injection rates and wellhead pressures into only 35 windows (Figure 4.15 and 4.16).

Finally, the statistical analysis between technological parameters and the degree of disordering of sources, ZZ , was carried out by means of the Spearman rank correlation. Moreover, to recognize the contributions of the ZZ components to correlation, statistical analysis was performed also between them and the technological parameters.

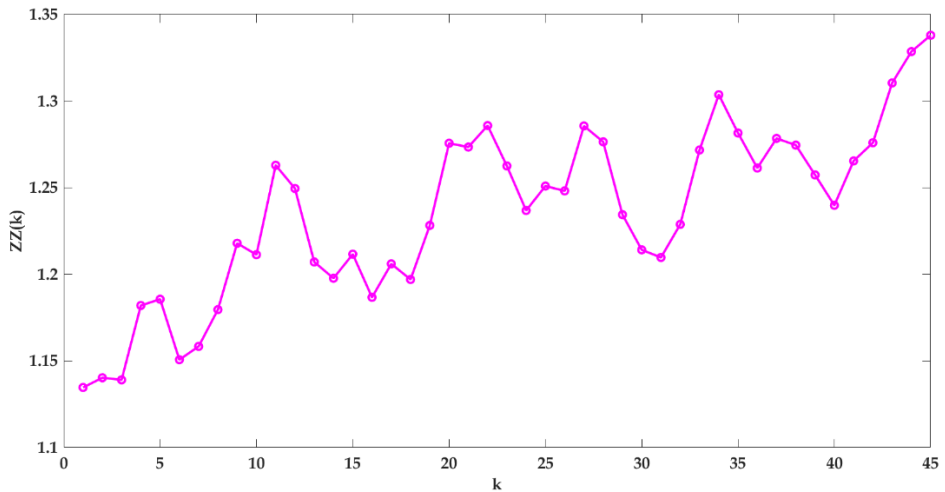


Figure 4.11 - Variation of the ZZ parameter in windows 1:45.

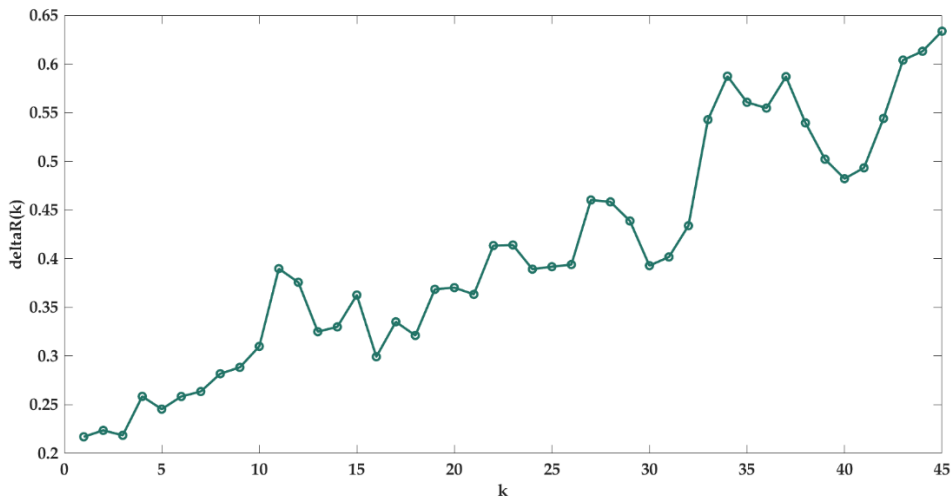


Figure 4.12 - Variation of Δ_r in windows 1:45. This component of the ZZ parameter identifies the differences between hypocentral coordinates.

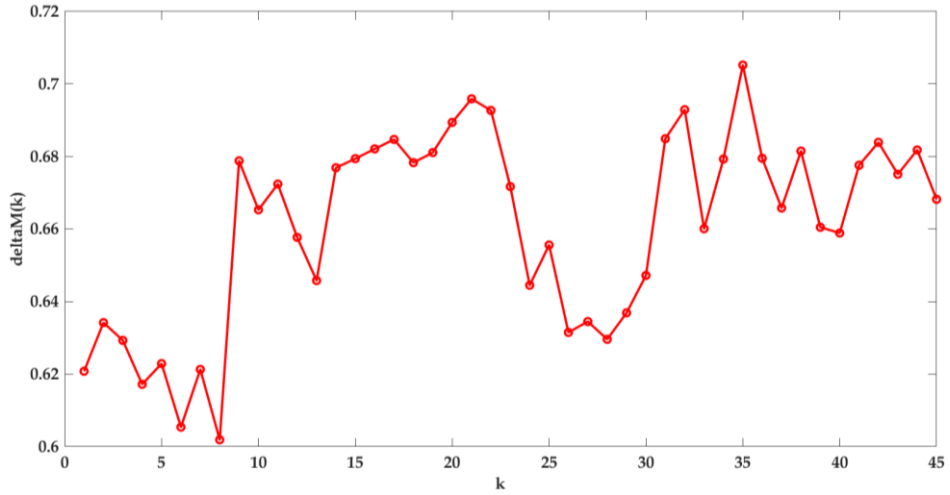


Figure 4.13 - Variation of Δ_m in windows 1:45. This component of the ZZ parameter identifies the differences between focal mechanisms.

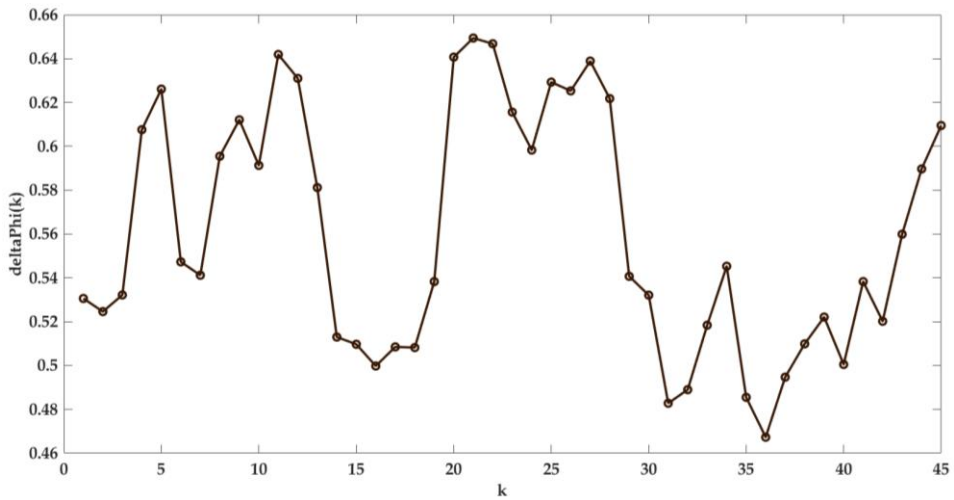


Figure 4.14 - Variation of Δ_ϕ in windows 1:45. This component of the ZZ parameter identifies the differences between the direction of radii from the open hole of the Habanero 4 injection well where the seismic events are located.

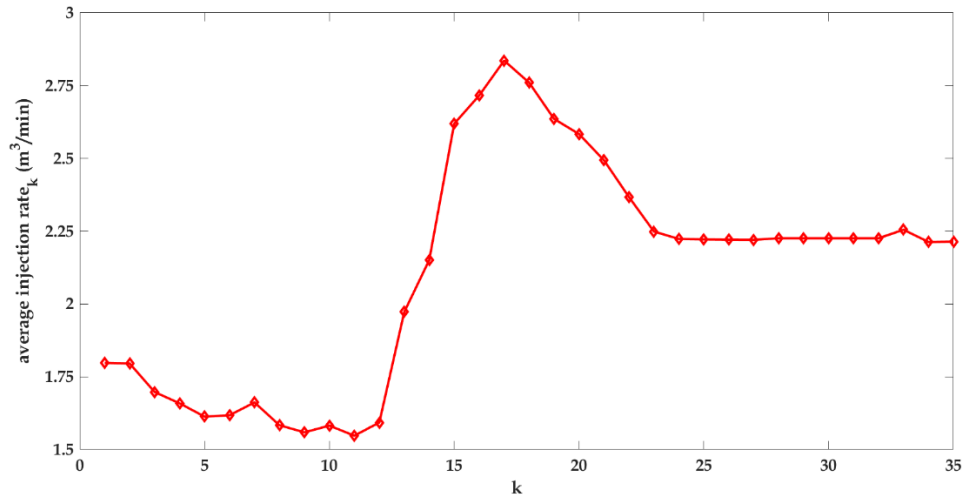


Figure 4.15 - Variation of the average injection rate in windows 1:35.

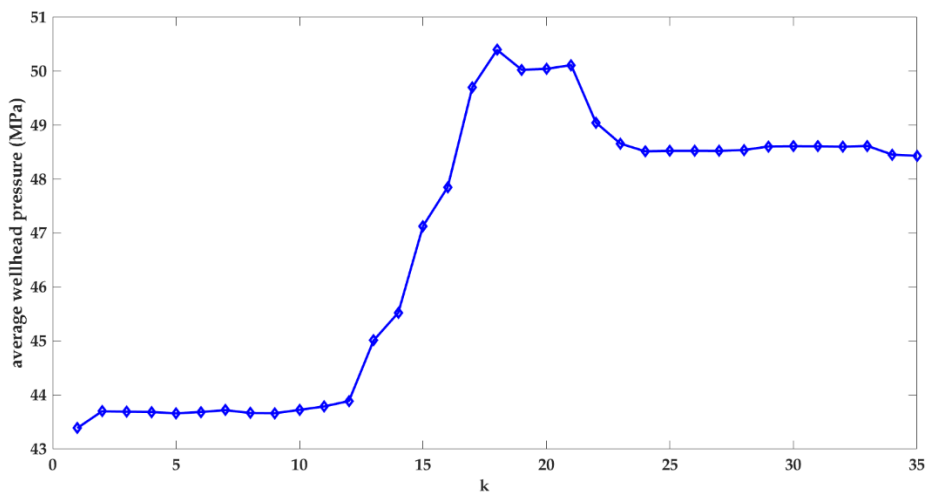


Figure 4.16 - Variation of the average wellhead pressure in windows 1:35.

4.4 Results and discussion

The trends of the technological parameters can be divided into three phases: the first comprising windows 1-10, the second windows 11-24, and the third windows 25-35. To have a meaningful statistical analysis it is necessary to consider quantities that are significantly variable, i.e., for which the standard deviation, which estimates the variability of the data, is greater. This is a demand of the correctness of correlation analysis

because when one variable is correlated with another, whose variations are insignificant, then the result of the correlation is due to chance. For this reason, in each phase, the mean and the standard deviation of injection rate and wellhead pressure were calculated (Table 4.1).

	Phase 1 windows 1-10		Phase 2 windows 11-24		Phase 3 windows 25-35	
	<i>Mean</i>	<i>Std. Dev</i>	<i>Mean</i>	<i>Std. Dev</i>	<i>Mean</i>	<i>Std. Dev</i>
Injection rate (m³/min)	1.66	0.08	2.34	0.41	2.22	0.01
Wellhead Pressure (MPa)	43.66	0.10	47.84	2.37	48.55	0.07

Table 4.1 - Mean and standard deviation of injection rate and wellhead pressure in the three phases of the technological process.

As could be expected from Figure 4.16 the standard deviation takes a high value only for the second phase. Hence, the inclusion values from phases 1 and 3 to the comparisons between the ZZ parameter and the technological parameters would only introduce statistical noise to the correlation analysis obscuring the results. Therefore, in this study, the correlation analysis was carried on only for the second phase (windows 11-24), considering 14 windows for the technological parameters.

In order to study the delays in the seismic response to well stimulation, the Spearman rank correlation was first performed considering a zero-window delay between ZZ and the technological parameters then delaying the ZZ windows, and its components, by one window up to a total delay of 21 windows. Moreover, to better understand the relationship between the injection rate and wellhead pressure, a correlation analysis was performed between these technological parameters as well.

Table 4.2 and 4.3 show the results of the correlation analysis between the injection rate and ZZ and its components, and between the wellhead pressure and ZZ and its components, respectively. Finally, Table 4.4 presents the results obtained by correlating the technological parameters.

Delay (win.)	INJ - ZZ		INJ - Δ_r		INJ - Δ_m		INJ - Δ_ϕ	
	Corr. Coef.	<i>p</i> value	Corr. Coef.	<i>p</i> value	Corr. Coef.	<i>p</i> value	Corr. Coef.	<i>p</i> value
0	-0.39	0.165	-0.47	0.090	0.60	0.025	-0.58	0.032
1	-0.09	0.762	-0.19	0.512	0.60	0.028	-0.25	0.391
2	0.37	0.197	0.22	0.445	0.53	0.052	0.24	0.409
3	0.54	0.048	0.29	0.318	0.41	0.151	0.58	0.032
4	0.63	0.018	0.38	0.176	0.35	0.221	0.77	0.002
5	0.73	0.004	0.41	0.146	0.16	0.573	0.79	0.001
6	0.56	0.038	0.45	0.104	-0.12	0.682	0.56	0.038
7	0.37	0.197	0.48	0.087	-0.45	0.104	0.27	0.341
8	0.09	0.773	0.35	0.215	-0.71	0.006	0.02	0.964
9	-0.18	0.532	0.25	0.383	-0.85	1.79E-04	-0.14	0.627
10	-0.17	0.553	0.29	0.318	-0.78	0.001	-0.09	0.773
11	-0.27	0.341	0.21	0.473	-0.60	0.025	-0.14	0.638
12	-0.23	0.436	0.19	0.512	-0.18	0.532	-0.21	0.473
13	-0.42	0.132	0.09	0.773	0.23	0.436	-0.47	0.09
14	-0.46	0.097	0.04	0.904	0.51	0.067	-0.62	0.021
15	-0.24	0.418	0.15	0.616	0.68	0.009	-0.63	0.019
16	0.05	0.856	0.45	0.104	0.75	0.003	-0.54	0.048
17	0.53	0.052	0.77	0.002	0.61	0.023	-0.39	0.17
18	0.77	0.002	0.87	7.57E-06	0.30	0.295	-0.31	0.281
19	0.50	0.072	0.61	0.024	0.15	0.605	-0.27	0.357
20	0.13	0.649	0.20	0.502	-0.26	0.366	-0.17	0.553
21	-0.24	0.418	-0.20	0.483	-0.31	0.281	-0.13	0.656

Table 4.2 – Results of Spearman rank correlation between injection rate and the degree of disordering of sources, ZZ, and its components.

Delay (win.)	PRES - ZZ		PRES - Δ_r		PRES - Δ_m		PRES - Δ_ϕ	
	Corr. Coef.	<i>p</i> value	Corr. Coef.	<i>p</i> value	Corr. Coef.	<i>p</i> value	Corr. Coef.	<i>p</i> value
0	0.1	0.727	-0.1	0.727	0.63	0.019	-0.02	0.940
1	0.5	0.072	0.36	0.209	0.55	0.044	0.35	0.221
2	0.82	4.66E-04	0.73	0.005	0.35	0.227	0.69	0.008
3	0.63	0.005	0.62	0.02	0.06	0.844	0.75	0.003
4	0.65	0.014	0.66	0.013	-0.14	0.638	0.70	0.007
5	0.54	0.048	0.69	0.008	-0.47	0.09	0.50	0.069
6	0.4	0.16	0.67	0.01	-0.7	0.007	0.32	0.267
7	0.27	0.341	0.62	0.02	-0.76	0.002	0.14	0.627
8	-0.05	0.868	0.63	0.019	-0.78	0.002	-0.16	0.573
9	-0.31	0.274	0.56	0.04	-0.71	0.006	-0.44	0.116
10	-0.37	0.192	0.43	0.128	-0.45	0.112	-0.59	0.029
11	-0.5	0.069	0.28	0.333	-0.02	0.964	-0.68	0.010
12	-0.31	0.288	0.28	0.325	0.34	0.240	-0.64	0.017
13	-0.08	0.785	0.45	0.108	0.67	0.011	-0.68	0.009
14	0.08	0.797	0.54	0.048	0.82	6.24E-04	-0.74	0.004
15	0.22	0.454	0.68	0.009	0.69	0.008	-0.69	0.008
16	0.38	0.176	0.86	6.44E-05	0.59	0.03	-0.46	0.097
17	0.59	0.03	0.8	9.15E-04	0.59	0.029	-0.45	0.104
18	0.48	0.087	0.58	0.032	0.22	0.445	-0.35	0.215
19	0.27	0.357	0.32	0.260	-0.22	0.445	-0.05	0.856
20	0.11	0.716	0.01	0.988	-0.44	0.120	0.31	0.274
21	-0.09	0.773	-0.18	0.542	-0.23	0.436	0.33	0.253

Table 4.3 - Results of Spearman rank correlation between wellhead pressure and the degree of disordering of sources, ZZ, and its components.

<i>Delay (win.)</i>	<i>INJ - PRES</i>	
	<i>Corr. Coef.</i>	<i>p - value</i>
0	0.73	0.005
1	0.88	4.0E-05
2	0.94	0.0 ...
3	0.82	4.66E-04
4	0.49	0.075
5	0.07	0.820
6	-0.50	0.069
7	-0.77	0.002
8	-0.85	1.36E-04
9	-0.91	1.00E-05
10	-0.50	0.072
11	-0.09	0.773

Table 4.4 - Results of Spearman rank correlation between injection rate and wellhead pressure.

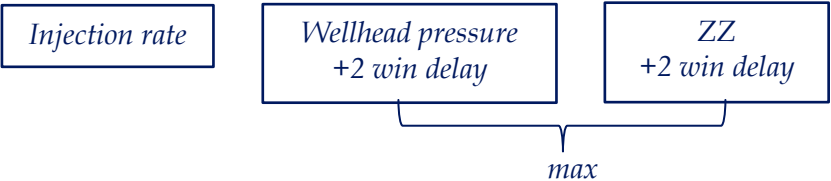
The conclusions were drawn under the standard significance level $\alpha = 0.05$.

The statistical analysis shows that ZZ is significantly correlated with both the injection rate and the wellhead pressure with a delay. In detail, for injection rate and ZZ the correlation coefficient becomes significant for three windows delay and gets the highest correlation at a delay of 5 windows. In correspondence with the latter, the components of ZZ do not exhibit significant correlation values except for the distance between the rays, $\Delta\phi$. This result shows that the degree of disordering of sources depends on the injection rate through a simultaneous effect of the injection rate on all three components - the distance between hypocenters, the conformity of mechanisms, and the distance between the rays on which events are located.

For the wellhead pressure, the correlation with ZZ becomes significant and takes maximum for 2 windows lags. For this lag also Δ_r and Δ_ϕ are significantly correlated with pressure. The correlation is significant up to a delay of 5 windows. Higher wellhead pressure increased the distances between hypocenters and angular dispersion of them with respect to the open hole of Habanero 4 well. This last result is evidenced also for injection rate. Finally, the correlation between injection rate and wellhead pressure shows positive correlation from zero delay up to a delay of three windows, resulting maximum after two windows.

By considering the largest values of the correlation coefficient, it is possible to identify three combinations that maximize the correlation between the technological parameters and the degree of disordering of sources, ZZ:

1. Maximum correlation between the injection rate and the wellhead pressure and between the wellhead pressure and ZZ. This situation occurs when pressure is delayed by two windows with respect to injection and when ZZ is delayed by two windows with respect to pressure. However, the correlation between the injection rate and ZZ is not maximum in such a combination of delays.



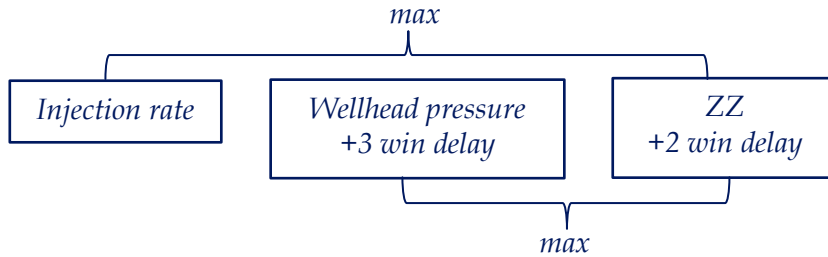
delay = 2-win INJ - PRES Corr. Coef. = 0.94 p - value = 0.0...

delay = 2-win PRES - ZZ Corr. Coef. = 0.82 p - value = 4.66E-04

delay = 4-win INJ - ZZ Corr. Coef. = 0.63 p - value = 0.018

2. Maximum correlation between the injection rate and ZZ and between the wellhead pressure and ZZ. This is the case when the pressure is delayed by three windows relative to the injection and

ZZ is delayed by two windows relative to the pressure. In such a combination the correlation between the injection and ZZ, and the correlation between the pressure and ZZ take maximum, but the correlation between the injection and the pressure is not the largest.

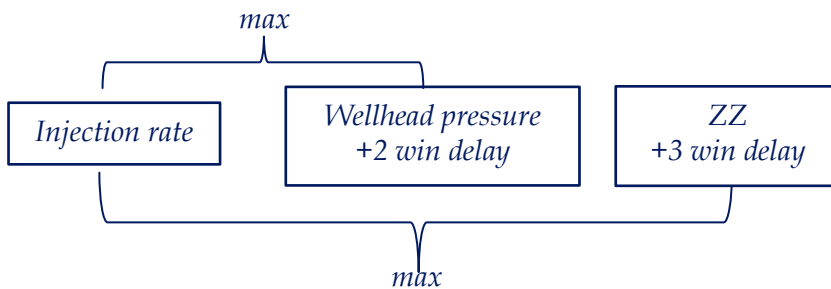


delay = 3-win INJ - PRES Corr. Coef. = 0.82 p - value = 4.66E-04

delay = 2-win PRES - ZZ Corr. Coef. = 0.82 p - value = 4.66E-04

delay = 5-win INJ - ZZ Corr. Coef. = 0.73 p - value = 0.004

3. Maximum correlation between injection rate and pressure and between injection rate and ZZ. This occurs when pressure is delayed by 2 windows with respect to injection and ZZ is delayed by 3 windows with respect to pressure. In such a combination the correlation between the injection and ZZ, and the correlation between the injection and the wellhead pressure take maximum, but the correlation between the pressure and ZZ is not the largest.



delay = 2-win INJ - PRES Corr. Coef. = 0.94 p - value = 0.0...

delay = 3-win PRES - ZZ Corr. Coef. = 0.63 p - value = 0.005

delay = 5-win INJ - ZZ Corr. Coef. = 0.73 p - value = 0.004

Among these possibilities, the first can be considered the best even if not totally optimal because there is not maximum correlation between injection rate and ZZ. The variations of the parameters in these configurations are shown in Figure 4.17.

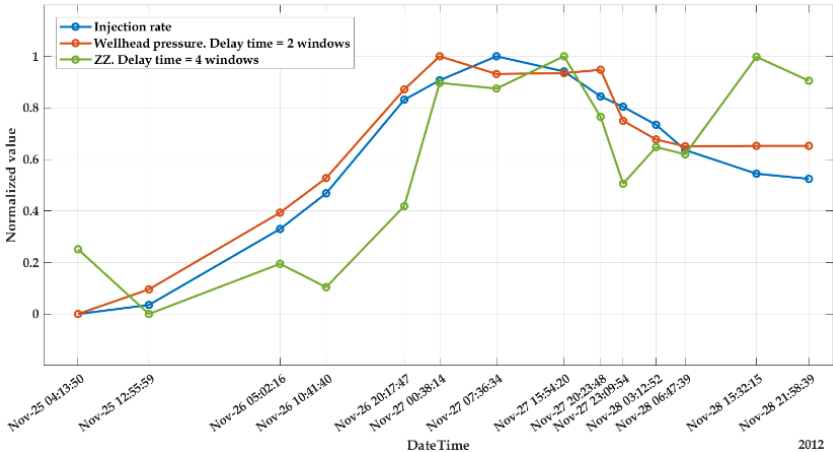


Figure 4.17 - Variation of injection rate, wellhead pressure with a delay of two windows with respect to injection, ZZ with a delay of two windows with respect to wellhead pressure.

As mentioned earlier, in the Cooper Basin geothermal field, the significant correlation between the ZZ parameter and the technological parameters is not immediate but occurs with a certain delay. This means that it takes some time before a seismic response to well stimulation could occur.

Conversely, comparing these results with those of The Geysers, it is possible to see that in the latter site the seismic response already occurred at zero delay and all the components of ZZ were highly positively correlated with injection rate (Lasocki & Orlecka-Sikora, 2020). These two geothermal sites are significantly different. At The Geysers, geothermal energy production has been carried on in a sedimentary rock since the 1960s. In the Cooper Basin the reservoir rock is granitic, rigid, and of low permeability and was intact before the stimulation.

Despite these differences, in both sites it turned out that the higher the injection rate - the wellhead pressure was, the less probable was the creation of undesired fluid migration pathways. ZZ was positively

correlated with injection rate/wellhead pressure; thus, the potential to build unwanted paths for fluid migration was negatively correlated.

4.5 Conclusions

In this study, a statistical analysis using the Spearman rank correlation was performed to explore the relationship between seismic and anthropogenic activity in the Cooper Basin geothermal field in Australia. A new parameter, ZZ , in a multi-dimensional space, defines the potential of seismicity to build far-reaching pathways for fluid migration. The statistical analysis showed intriguing results regarding the delay between the injection rate, wellhead pressure and the seismic reaction, expressed by ZZ , to technological parameters changes. The best positive correlation was obtained when pressure was delayed with respect to injection by 2 windows, ZZ was delayed with respect to injection by 5 windows, and when ZZ was delayed with respect to pressure by 2 windows.

This means that contrary to what one might imagine, high injection rates and wellhead pressures result in a displacement of seismic events in the eight-dimensional space considered, i.e., they are related to a lower potential to build unwanted paths for fluid migration. This result is the same obtained in The Geysers geothermal field (Lasocki & Orlecka-Sikora, 2020), so it suggests that such correlation may be a global feature of rock fracturing caused by pressurized fluid injections. Increasing knowledge of this type of seismicity and mechanism in geothermal fields (i.e., creation of unwanted pathways) can help mitigate the hazard and risks associated with this kind of anthropogenic activity.

A further future development of this work is to repeat the analysis considering windows of the same time length with a constant time shift since the consecutive windows used for the correlation test are not separated one from another of the same time.

In addition, the application of this methodology, already validated for the Cooper Basin and The Geysers case studies, can be extended to other sites where unconventional geothermal activity is carried out. Undesirable pathways for fluid migration can also arise where there is unconventional

oil and gas extraction through the fracking technique. It is therefore interesting to be able to apply the methodology to a case of fracking to investigate if it can lead to results like those found for geothermal sites. To be able to carry out all the studies mentioned, it is very important to have industrial information, such as injected volumes and pressures, as well as a wide seismic dataset. The lack of either of these two elements represents a strong limitation for this type of study.

**A MULTI-HAZARD RISK ANALYSIS OF
AN INDUSTRIAL PLANT:
THE SAN POTITO AND COTIGNOLA
GAS STORAGE FIELD**

The exploitation of energy geo-resources involves impacts on the surrounding environment (see Chapter 1). It is, therefore, important to analyze the possible phases of the industrial project: construction, operation, site closure, and post-abandonment, to be able to assess, mitigate, and predict the risks that these activities may entail (Garcia-Aristizabal et al., 2017). At the same time, this study is important to assess the effects of NaTech (Natural Hazard Triggering Technological Disaster) events.

All industrial facilities in which the quantities of hazardous substances exceed certain values listed in the Seveso III Directive (European Union, 2012) are subject to the preparation of the safety report in which NaTech risk studies must also be included, identifying possible natural hazards (Krausmann et al., 2017). These facilities include natural gas storage sites that allow to store the gas (e.g., methane) in underground geological structures from which the gas is withdrawn when required and introduced into the national network. The gas may be hosted in depleted gas fields, deep aquifers, or cavities within underground saline formations, and the storage is defined as conventional, semi-conventional, or special, respectively (Mazzini et al., 2018).

Gas storage sites, like other industrial systems that use natural gas, are currently widespread as this energy resource is widely used to generate electricity, for industrial and domestic uses. They are made up of many elements, mainly pipelines of different sizes that connect sites even very distant from each other. Damage to pipelines can cause gas leakage that

can generate fires and give rise to a chain of disasters involving economic, human life, and environmental damage. It is, therefore, very important to make risk estimates by analyzing the impacts of the natural hazards, in particular earthquakes, on industrial equipment and components as pipelines (Lanzano et al., 2013; 2014).

In this chapter, a bow-tie approach (see Chapter 2, subsection 2.3) was considered for a multi-hazard risk analysis of pipelines used in the San Potito and Cotignola gas storage site (Italy), operated by Edison Stoccaggio S.p.A.. In particular, the quantitative resolution of the Fault Tree is defined by using the MERGER application (Garcia-Aristizabal et al., 2019) while the Event Tree is considered only in qualitative terms. The annual probability of occurrence of a Top Event identified as the spill of gas from one of the analyzed pipelines is determined. The annual rate of damages due to the occurrence of an earthquake or material fatigue were initially considered as Basic Events.

All the information mentioned in the following paragraphs about the gas storage site are taken from the safety report of *Edison Stoccaggio S.p.A.*, according to Art. 8 D.Lgs. 17 agosto 1999, n. 334 e s.m.i., January 2015 edition, concerning the gas storage plant of San Potito and Cotignola (RA), provided within the PhD collaboration.

5.1 The San Potito and Cotignola gas storage field

The San Potito and Cotignola gas storage field is in the Emilia-Romagna region (Italy), in the province of Ravenna (Figure 5.1). Like the other storage facilities in Italy, it was built within exhausted gas fields. In particular, the San Potito gas field was depleted in January 2000 and the Cotignola gas field in February 2003. In 2009, the concession for the San Potito and Cotignola storage site was granted to Edison Stoccaggio S.p.A. by the Italian Ministry of Economic Development. Edison Stoccaggio S.p.A. converted the fields from production to methane storage and unified them in a single site that became operational in 2013. The whole plant consists of several elements, such as the reservoir, a treatment and compression facility, cluster areas and wells, internal pipelines and flow-lines connecting the central facility and the clusters (Figure 5.2).



Figure 5.1 - Map of the area where the San Potito and Cotignola gas storage field is located. Source: Edison Stoccaggio S.p.A. (www.edisonstoccaggio.it)

The central unit is in San Potito in the municipality of Bagnacavallo while the three clusters are located among the municipalities of Bagnacavallo, Cotignola and Faenza containing a total of eleven wells. Moreover, the storage site is connected to the national network managed by Snam Rete Gas through the Castel Bolognese interconnection point, in the province of Ravenna, owned by Edison Stoccaggio S.p.A. In turn, the interconnection point is connected to the storage site through a methane

pipeline of about 22 km, along which there are other facilities necessary for gas movement.

The activity of the storage site consists of cyclical phases of injection and supply. Between April and October, the natural gas coming from the national transportation network is compressed to a higher pressure than that present in the reservoir to inject it into the storage wells, after being appropriately cleaned of solid and liquid substances.

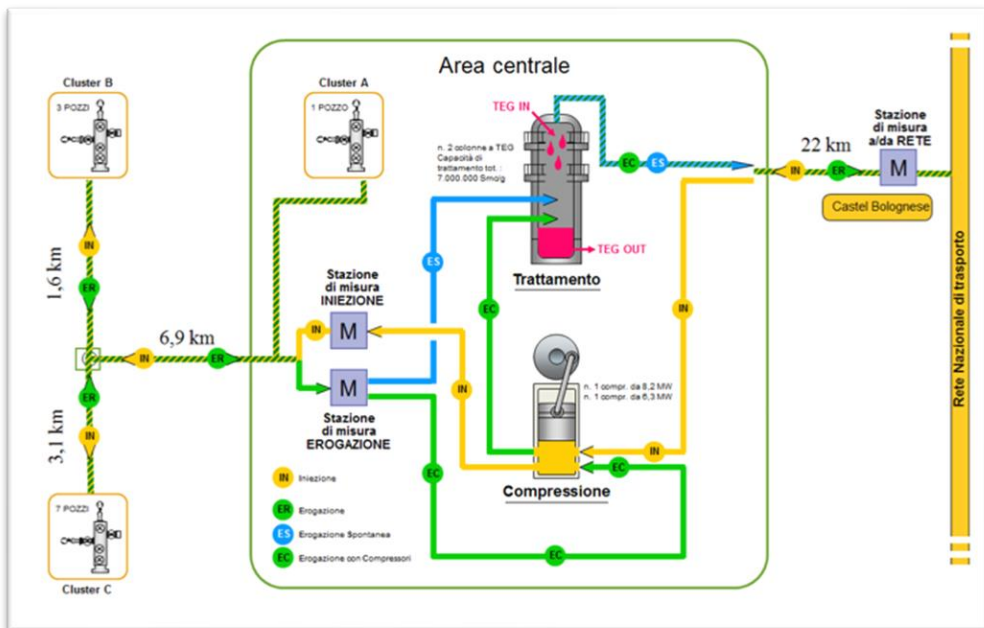


Figure 5.2 - Schematization of San Potito and Cotignola gas storage facility. The figure shows the treatment and compression central facility, connected to the clusters by pipelines and flow-line. Moreover, it is connected to the interconnection point of Castel Bolognese (on the right) from which the gas is introduced in or withdrawn from the national transport network. Clusters A, B and C contain 1, 3 and 7 wells, respectively. In the figure IN (yellow line) stands for injection, ER (green and yellow grooved line) for supply, EC (green line) for supply with compressors and ES (blue line) for spontaneous supply. TEG in fuchsia indicate the treatment of the gas with triethylene glycol used for dehydration. Source: Edison Stoccaggio S.p.A. (www.edisonstoccaggio.it)

During the period from October to April, the gas is withdrawn from the wells. Once the gas arrived at the central facility, if necessary, it is compressed and then separated from the strata water and any solid substances. At the end, it is introduced into the national transportation

network. The supply of gas can also occur spontaneously when the pressure at which it is found allows the direct release into the national transport network without passing through the compression phase (Figure 5.2).

5.2 Risk pathway scenario

The first task of a multi-hazard risk assessment is to elaborate a risk pathway scenario, with a first qualitative analysis. This procedure is not always simple as it must take into consideration multiple factors, such as the possible initial hazards (e.g., natural, mechanical, anthropogenic), the elements of the facility that may be damaged and how failure may propagate in them. Moreover, for a complete analysis it is necessary to consider the risk receptors, such as the environmental elements, the ecosystem, the infrastructures, and people (Garcia-Aristizabal et al., 2019). Whereas routine operations produce easily manageable and limited impacts, system failures or additional extreme natural events with low probability of occurrence can produce severe consequences. When there is a natural hazard, the occurrence of catastrophic events could spread with a domino effect, i.e., NaTech events, amplifying the damage due to the natural event (Capuano et al., 2017; Gasparini et al., 2016). The quantitative multi-hazard risk analysis is developed through a bow-tie approach that consists of two parts: Fault Tree (FT) and Event Tree (ET) that are connected to each other by the critical or Top Event (TE). The FT is built starting from the TE with a backward mechanism to consider the possible causes (basic events) that generated the criticality. At the same time, the TE is the starting point to build the ET in which the impacts resulting from the accident are analyzed. The assessment of the bow-tie structure is based on the probabilities assigned to the basic events and at the nodes of the ET (Capuano et al., 2017).

In this work, the study case is the San Potito and Cotignola gas storage field that consists, as above mentioned, of three clusters in which the storage wells are located and a central facility where gas treatment and compression operations take place. Scientific literature shows that the elements of a plant most prone to earthquake damage in a gas storage site

are the pipelines, whose role is very important and strategic since they allow the transport of gas on a large and small scale (Lanzano et al., 2013; 2014). The impacts related to the damage of a gas pipeline can generate very catastrophic and unexpected incidents, leading to significant economic and environmental damages and in extreme cases to loss of human life.

In this framework, the fault tree is performed considering as basic events two hazards: natural earthquakes and material fatigue that can originate, as top event, the spill of gas from a pipeline located in a cluster of the gas storage site (Figure 5.3). The environmental element affected by the spill of gas is the air, that can be considered the first risk receptor of the analysis, while the impacts on the final risk receptors, are derived by the construction of the event tree. Gas escaping from pipelines may or not ignite, resulting in the first case in a flash or jet fire according to the ignition timing (Figure 5.4). The damages to the surrounding environment (e.g., communities and ecosystems) depends on a series of factors, including the direction of fire propagation and the presence or absence of inhabited areas, industrial zones, etc.

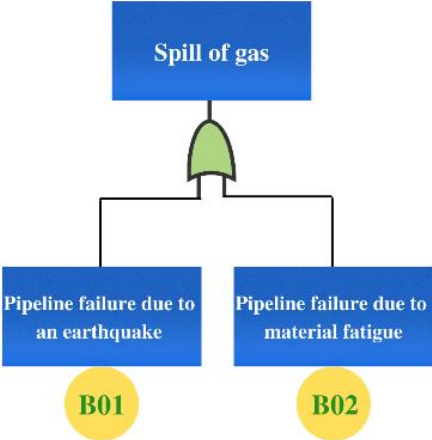


Figure 5.3 - Fault tree in which there are two basic events (B01 and B02), and the top event is the spill of gas in the air.

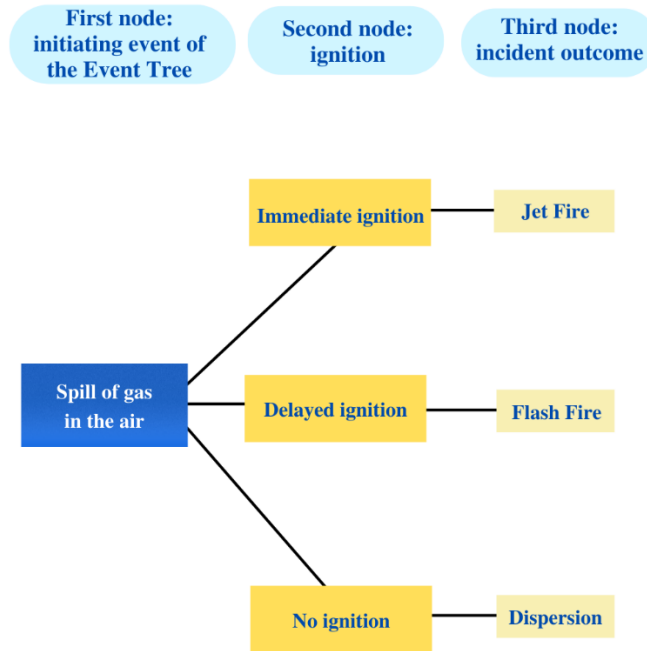


Figure 5.4 - Simplified Event Tree in which there are three nodes: the spill of gas in the air as initiating event (i.e., the top event of the Fault Tree), the ignition and the incident outcome.

5.3 Earthquake - related failure of an asset

In order to calculate the probability of occurrence of the top event, with the MERGER application, the annual rate of earthquake failure, for the selected asset and for a particular damage state, must be defined. This quantity is expressed by the combination of the fragility function and the slope of the seismic hazard curve (Eads et al., 2012). Let the intensity measure of the shaking, i.e., Peak Ground Acceleration (PGA), $F(s)$ the fragility function calculated as a function of PGA, and $G(s)$ the annual frequency of exceedance of a given PGA, then the earthquake-related failure of an asset can be expressed by the following integral (e.g., Porter, 2021; Nahar et al., 2020; Eads et al., 2012)

$$\lambda = \int_0^{\infty} -F(s) \frac{dG(s)}{ds} ds \quad \text{Eq. 5.1}$$

Since $G(s)$ in the present case is available for discrete values, this integral can be calculated numerically as follows (Porter, 2021):

$$\begin{aligned}\lambda &= \sum_{i=1}^n \left(F_{i-1} G_{i-1} (1 - \exp(m_i \Delta s_i)) - \frac{\Delta F_i}{\Delta s_i} G_{i-1} \left(\exp(m_i \Delta s_i) \left(\Delta s_i - \frac{1}{m_i} \right) + \frac{1}{m_i} \right) \right) = \\ &= \sum_{i=1}^n (F_{i-1} a_i - \Delta F_i b_i) \end{aligned} \quad \text{Eq. 5.2}$$

in which

$$\begin{aligned}\Delta s_i &= s_i - s_{i-1} & \Delta F_i &= F_i - F_{i-1} & m_i &= \frac{\ln(G_i/G_{i-1})}{\Delta s_i} & i &= 2, \dots, n \\ a_i &= G_{i-1} (1 - \exp(m_i \Delta s_i)) & b_i &= \frac{G_{i-1}}{\Delta s_i} \left(\exp(m_i \Delta s_i) \left(\Delta s_i - \frac{1}{m_i} \right) + \frac{1}{m_i} \right)\end{aligned}$$

As can be seen from the previous equations, to calculate lambda it is necessary to get the expected PGAs in the area of interest as defined by the seismic hazard analysis and the fragility function of the particular asset to be analyzed.

5.3.1 Seismic hazard analysis

The estimation of the occurrence rate of exceeding the maximum probable acceleration at a given location in a predefined time interval is carried out by seismic hazard analysis. Its results are very important in mitigating the effects of earthquakes as it allows engineers to design and construct safe buildings (Lanzano et al., 2017; Convertito & Faenza, 2015; Zollo & Emolo, 2011). Generally, the analysis is performed starting from the knowledge of 1) the seismogenic structures, 2) the attenuation laws, 3) the maximum amplitude of ground motion, 4) the rate of occurrence and 5) the magnitude distribution of seismicity (Zollo & Emolo, 2011).

For the whole Italian territory, MPS04 (Stucchi et al., 2004) is the national seismic hazard model, defined for different exceedance probabilities in 50 years (Meletti & Montaldo, 2007). In fact, the National Institute of Geophysics and Volcanology (INGV) calculated hazard curves for each node of the national reference grid and released the Italian seismic hazard map (Stucchi et al., 2004). Therefore, in this work, MPS04 is used to calculate, using the mesh method, the intensity parameter (PGA) in each of the three clusters of which the San Potito and Cotignola gas storage site is composed.

The mesh method consists in considering the four grids' nodes of MPS04 closest to the site of interest, X, and then evaluating the distances between the nodes and X (Figure 5.5). They are calculated starting from the knowledge of the coordinates (latitude and longitude, expressed in radians) of the points between which the distance is to be calculated, knowing the mean Earth's radius R

$$d = R \cdot \arccos [\sin (lat\beta) \cdot \sin(lata\alpha) + \cos (lat\beta) \cdot \cos (lata\alpha) \cdot \cos (lon\alpha - lon\beta)]$$

Eq. 5.3

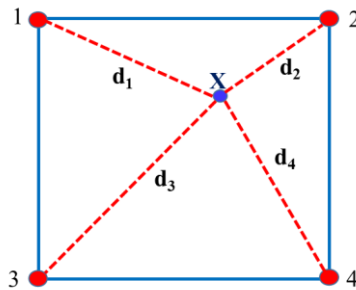


Figure 5.5 - Graphical schematization of the mesh used to calculate the value of the intensity parameter at point X, known the value that it assumes in nodes 1, 2, 3 and 4 and the distances d_i .

Given the values of the intensity parameter p in the four nodes adjacent to point X and the distances previously calculated, it is possible to obtain the intensity parameter p at point X as follows

$$p = \frac{\sum_{i=1}^4 \frac{p_i}{d_i}}{\sum_{i=1}^4 \frac{1}{d_i}}$$

Eq. 5.4

In this work, as mentioned above, the intensity parameter p represents the PGA derived from seismic hazard curve calculated at cluster points A, B, and C, respectively, for each available annual frequency of exceedance. The PGA values obtained are shown in Tables 5.1 - 5.3, while the hazard curves PGA - annual frequency of exceedance are shown in Figures 5.6 - 5.8.

PGA (g)	Annual frequency of exceedance
0.055	0.0332
0.070	0.0199
0.081	0.0139
0.094	0.0099
0.108	0.0071
0.127	0.0050
0.182	0.0021
0.240	0.0010
0.326	0.0004

Table 5.1 – PGA values (expressed in g) and annual frequency of exceedance for the point cluster A of coordinates (11.9472°, 44.4203°).

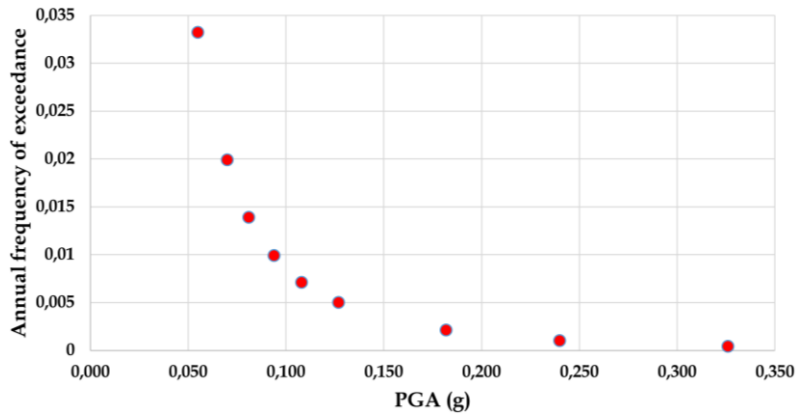


Figure 5.6 – Seismic hazard curve in term of annual frequency of exceedance of PGA for the point Cluster A of coordinates (11.9472°, 44.4203°).

PGA (g)	Annual frequency of exceedance
0.059	0.0332
0.075	0.0199
0.088	0.0139
0.101	0.0099
0.116	0.0071
0.136	0.0050
0.189	0.0021
0.243	0.0010
0.327	0.0004

Table 5.2 – PGA values (expressed in g) and annual frequency of exceedance for the point cluster B of coordinates (11.9692°, 44.3617°).

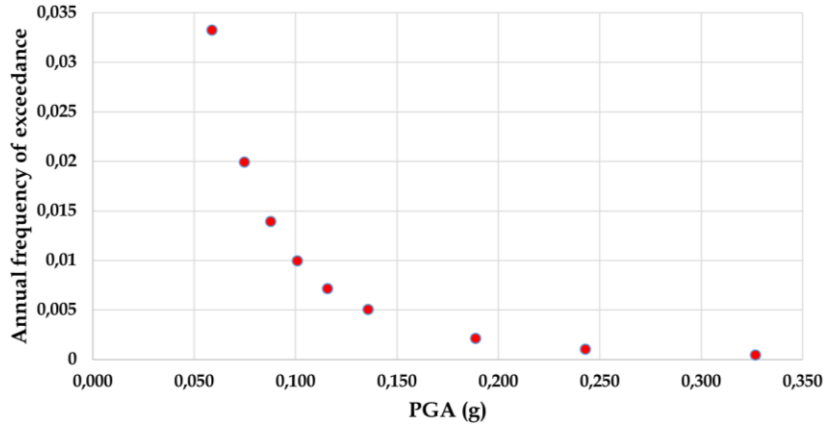


Figure 5.7 – Seismic hazard curve in term of annual frequency of exceedance of PGA for the point Cluster B of coordinates (11.9472°, 44.4203°).

PGA (g)	Annual frequency of exceedance
0.061	0.0332
0.078	0.0199
0.091	0.0139
0.105	0.0099
0.120	0.0071
0.140	0.0050
0.194	0.0021
0.248	0.0010
0.328	0.0004

Table 5.3 – PGA values (expressed in g) and annual frequency of exceedance for the point Cluster C of coordinates (11.9194°, 44.3710°).

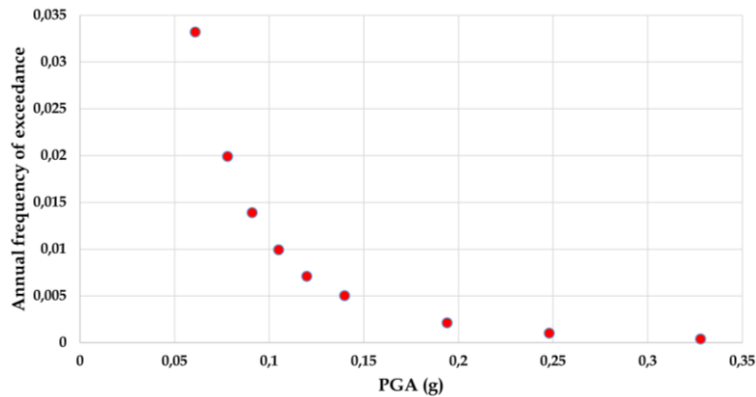


Figure 5.8 – Seismic hazard curve in term of annual frequency of exceedance of PGA for the point Cluster C of coordinates (11.9194°, 44.3710°).

5.3.2 Earthquake-related fragility and failure of gas pipelines

The probability of exceedance a particular damage state under environmental excitations (e.g., seismic events) is expressed by the fragility function and the so-called fragility curves (Porter, 2021; Rosti et al., 2021; Nazri, 2018). They are derived by observing what has happened in the past as a result of the natural event through a best fit of available data and allowing to estimate the damage of civil and industrial buildings and equipment in the future (Lanzano et al., 2013).

The fragility curves have a log-normal trend, expressed with the intensity parameter on the x-axis and the probability on the ordinates (Porter et al., 2021). Mathematically, the fragility function is expressed by a conditional probability, which in the general form is given by (e.g., Nazri, 2018; Billah & Alam, 2014)

$$Fragility = P[LS|IM = y] \quad Eq.5.5$$

in which LS indicates the limit or damage state (DS), IM is the intensity measure (e.g., PGA, the peak ground velocity PGV, the spectral acceleration, etc.) and y is the realized condition of IM. This generic equation was solved by researchers in analytically slightly different ways (Nazri, 2018). In this work the following formulation, reported in Lanzano et al. (2014), was used:

$$F(IM) = \frac{1}{2} \left[1 + erf \left(\frac{\ln(IM) - \ln(\mu)}{\beta\sqrt{2}} \right) \right] \quad Eq.5.6$$

with μ and β representing respectively the mean and standard deviation of the best-fit distribution.

At San Potito and Cotignola gas storage site, three case studies were identified concerning the failure of gas pipelines located at the three clusters of the gas field:

1st case study: Cluster A - partial natural gas pipeline failure, setup - supply San Potito;

2nd case study: Cluster B – partial natural gas pipeline failure - setup: injection/supply Cotignola;

3rd case study: Cluster C – partial natural gas pipeline failure - setup: injection/supply Cotignola.

In order to perform the calculation, it was necessary to extract from literature the values for the fragility coefficients (mean and standard deviation). In the present case, the mean and standard deviation for a low damage state $DS \geq DS1$ are 0.58g and 0.17g, respectively (Lanzano et al., 2014). The fragility curves shown in Figures 5.9 – 5.11 were derived by solving equation 5.6 for all values of PGA previously calculated. Once the values of fragility and frequencies of exceedance of PGA are known, it is possible, through equation 5.2, to calculate the annual rate of earthquake-related failure for kilometer of the gas pipeline. Finally, since it is very important to perform an analysis that really captures the element of the plant involved in the study, it was necessary to make a proportion to calculate lambda for the exact pipelines' lengths (Table 5.4).

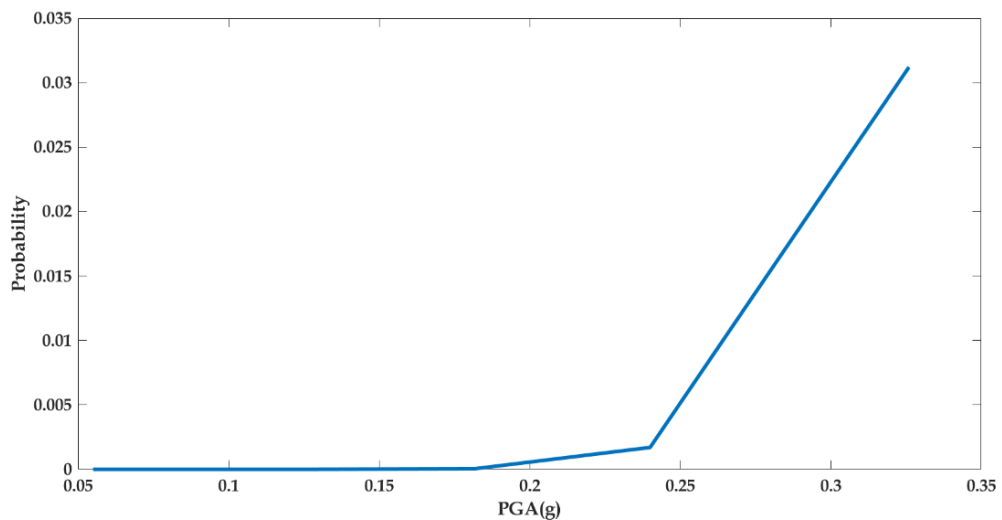


Figure 5.9 -Earthquake-related fragility curve calculated for a natural gas pipeline in the 1st case study (Cluster A) of the gas storage site.

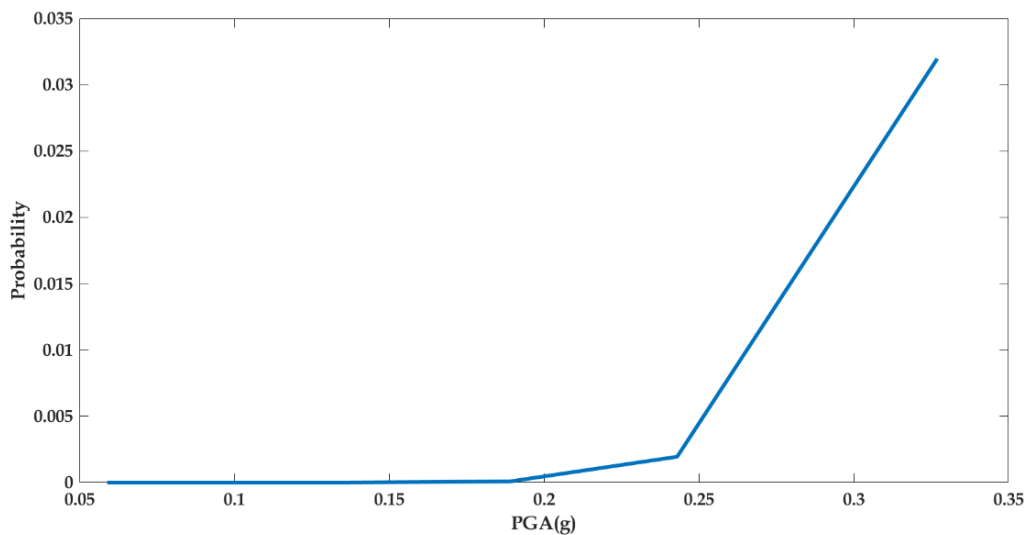


Figure 5.10 - Earthquake-related fragility curve calculated for a natural gas pipeline in the 2nd case study (Cluster B) of the gas storage site.

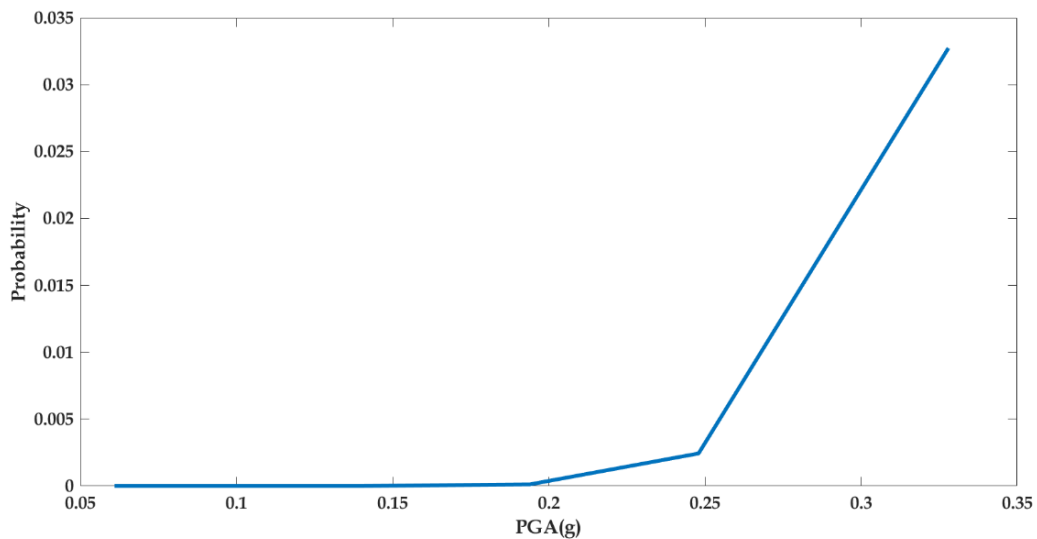


Figure 5.11 - Earthquake-related fragility curve calculated for a natural gas pipeline in the 3rd case study (Cluster C) of the gas storage site.

	λ for km of pipeline	Pipeline length (m)	Effective value of λ
1st case study: Cluster A	9.45 e-06	60	5.67 e-07
2nd case study: Cluster B	9.91e-06	40	3.97e-07
3rd case study: Cluster C	1.06e-05	40	4.23e-07

Table 5.4 - Values of the annual rate of failure (λ) due to an earthquake for the pipelines considered in each case study of the gas storage site.

5.4 Fault Tree analysis

The computational resolution of the Fault Tree in Figure 5.3 was performed by using the MERGER application (Garcia-Aristizabal et al., 2019) available on the IS-EPOS platform (Orlecka-Sikora et al., 2020). The basic events studied, as explained in paragraph 5.2, are two: the pipeline failure due to an earthquake and the pipeline failure due to material fatigue. In the first case, the annual rate of failure was calculated considering the fragility of the pipelines and the value of PGA in the point Cluster of the field considered. In the second case, the failure value is taken from the safety report of the San Potito and Cotignola gas storage site, provided in the framework of the doctoral collaboration.

The calculation of the annual occurrence probability of the top event (i.e., spill of gas from a pipeline) was evaluated considering an “or” Boolean operator assuming that either one of the two basic events will occur individually or that both will occur. The top event results at each of the three cluster points provide very low annual occurrence probability values. Table 5.5 shows the values obtained for the best estimate (median value) and the uncertainty limits (5th and 95th percentile values) while histograms of the results are shown in Figures 5.12-5.14. They were obtained by considering 500 iterations and a homogeneous Poisson process³ for the occurrence of the basic events.

³ A Poisson process is a counting process with rate $\lambda > 0$. The number of events in any time interval t is independent and occurs following a Poisson distribution with mean λt .

	P top event / yr (50 th perc)	P top event / yr (5 th perc)	P top event / yr (95 th perc)
Cluster A	0.0001	6.70e-06	0.0004
Cluster B	1.1793e-05	9.5652e-07	5.1957e-05
Cluster C	1.25e-05	1.3913e-06	4.9196e-05

Table 5.5 - Values of the annual probability of occurrence of the top event, considering the 50th, 5th and 95th percentiles in each cluster of the gas storage site.

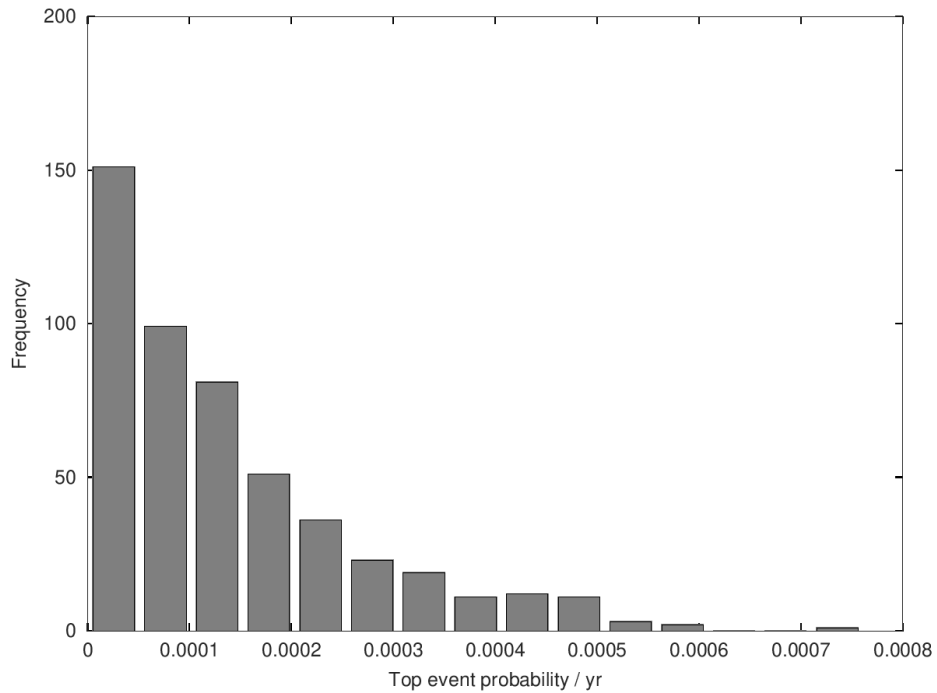


Figure 5.12 - Results of the annual probability of occurrence of the top event obtained in cluster A of the gas storage site.

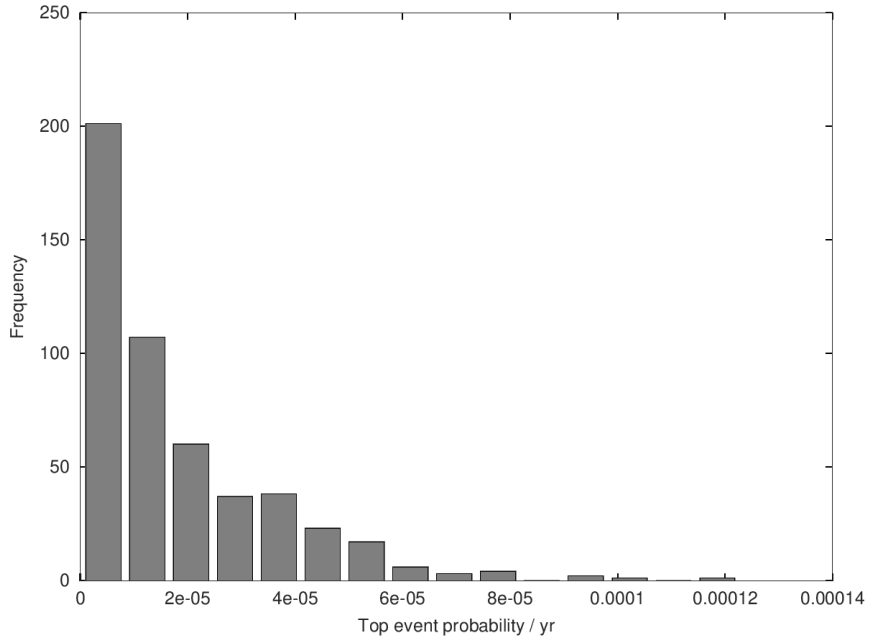


Figure 5.13 – Results of the annual probability of occurrence of the top event obtained in cluster B of the gas storage site.

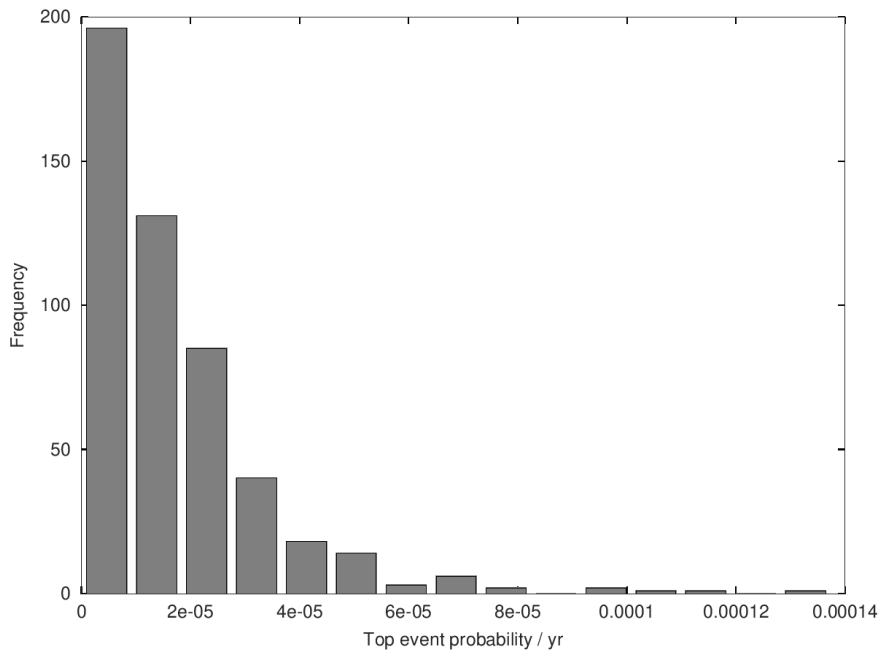


Figure 5.14 – Results of the annual probability of occurrence of the top event obtained in cluster C of the gas storage site.

5.5 Conclusions

A careful multi-hazard risk assessment is important to develop new strategies to prevent and mitigate accidents, especially when considering natural events, including rare ones, as initial hazards. The impact of a natural phenomenon, such as an earthquake, on an industrial plant can originate very serious consequences that can severely affect the whole society. A multi-hazard risk analysis on the gas storage site of San Potito and Cotignola, in Emilia-Romagna (Italy), was performed considering as assets of the study the gas pipelines located in each of the three clusters that the site is composed. The Fault Tree was computationally solved through the MERGER application allowing to calculate the annual occurrence probability of the top event, i.e., spill of gas in the air from a pipeline. Since at the current stage the MERGER application does not allow to perform the full analysis the Event Tree has been assumed qualitatively. A quantitative solution would allow estimating the magnitude of the consequences, which is highly dependent on the elements exposed to risk, e.g., houses, hospitals, schools, natural reserves, and other industrial plants.

The analysis of the Event Tree is the focus of a future development of this work, but the idea is to also re-analyse the Fault Tree considering more initial natural hazards and other elements of the storage facility. In view of the mitigation of risks resulting from events with a low probability of occurrence, scenarios that take into account extreme climatic events will be considered in a future work. The methodology is also exportable to other industrial facilities, both onshore and offshore.

The multi-hazard risk analysis is site-specific, so it is necessary to have detailed information on the industrial plant, but this is not always easy due to the industry's secrecy of data. Another major limitation is the multidisciplinary nature of this study, which leads to NaTech incidents being overlooked even though they are very important. It is necessary to search a synergy between scientists and industries and between professionals with different skills (e.g., seismology, engineering, climatology...) to carry out a detailed multi-hazard risk analysis in order

to prevent and mitigate damages. The consequences affect not only the industrial plant itself, i.e., the companies that operate it, but also the entire surrounding area, compromising the safety of people living near the industrial site in case of accident. In this context, it is important to consider whether it is ethical for industries to keep data confidential or is more appropriate to allow free access to carry out such analyses.

CONCLUSIONS

The increasing exploitation of energy geo-resources raises important questions concerning the risks related to the industrial activities. It is well known, globally, that in the last decades many anthropogenic seismic events, also called triggered or induced earthquakes, have occurred in areas where hydrocarbon extraction fields, wastewater injection fields, geothermal plants, gas or CO₂ storage sites are carried out. They have become an important issue for scientists, policy makers and society as they can generate even large damages especially in densely populated region. At the same time, the occurrence of a natural or induced earthquake can cause industrial accidents, generating cascading events that can amplify the damage of the natural event itself.

In this perspective, the study of NaTech and TechNa events proves to be of particular importance to develop a deeper knowledge and elaborate strategies for risk prevention and mitigation. This is consistent with the goals of the Sendai Framework 2015-2030 and the UN 2030 Agenda, which aim to achieve public education about the risk generated by natural disasters and the implementation of scientific methodologies that lead to drawing updated risk maps. The purpose of this thesis was the study of TechNa and NaTech events through the application of different and relevant methodologies (i.e., seismicity characterization, statistical correlation analysis multi-hazard risk assessment) to expand the scientific knowledge about the interaction between industrial plant management and seismicity. Three case study consisting with possible episodes of induced/triggered seismicity in areas of exploitation of energy geo-resources and an industrial accident triggered by a natural hazard (i.e., an earthquake) have been analyzed.

The study of current and past seismicity is very important to improve the knowledge of the seismic potential of active geological structures to perform correct analyses for seismic risk assessment, especially in areas of geo-resources exploitation. This is the case of the Porto San Giorgio offshore area (Italy) studied in this thesis work in which hydrocarbon

fields are located. The seismic sequence that occurred in the area from July to December 1987, which began with a mainshock of local magnitude 5, was relocated using a probabilistic approach. The earthquake location results showed that it developed between 5 km and 15 km depth and within 15 km from the coast depicting a thrust-fault structure with a northeast vergence and a listric geometry. The mainshock depth, most debated in the scientific literature, was derived through the decisive development of a technique that uses macroseismic intensity data to infer the earthquake depth and its magnitude. This analysis provides a depth for the mainshock of 5.7 km. This study has improved the knowledge of seismotectonic structures of the central Adriatic offshore area outlining that the external Apennine front is still active and able to generate seismicity at shallow depths. The importance of this study consists in the analysis of past instrumental seismicity with modern and innovative techniques in a poorly studied area whose seismogenic potential is not well understood. These limitations are due to poor azimuthal coverage of the seismic network and absence of waveforms. Moreover, the relocation analysis is important for the subsequent statistical study that was performed using binomial and Mann-Whitney tests to evaluate the possible correlation between seismicity and anthropogenic activity in the period 1985-2015. The results showed that statistically significant values were obtained in correspondence with the 1987 seismic sequence. This result provides only an indication of a possible triggering of seismicity due to anthropogenic activity.

As above mentioned, any kind of exploitation of energy geo-resources can generate risks even if clean and renewable forms of energy are considered, such as geothermal energy. In fact, the increasing adoption of unconventional methods such as Enhanced Geothermal Systems (EGS) challenges the scientific community and civil society about the possible consequences that such facilities may generate. It is well known that hydraulic fracturing of impermeable rocks has the potential to generate microseismicity as part of the process to form pathways in which water can circulate. However, if they reach pre-existing faults, they can also give rise to major events felt by the population, especially if these plants are

located in the vicinity of highly urbanized areas, as happened in Basel in 2006. Understanding the relationship between the injection rates or pressures at which these fluids are injected into the subsurface and seismicity turns out to be an important challenge in helping companies with risk mitigation and prevention. In this thesis work, the stimulation effect of the Habanero 4 well at the Cooper Basin geothermal field, which occurred in November 2012, is analyzed in detail. Seismicity recorded during that period and a few days after the end of stimulation consists of 489 seismic events with moment magnitude greater than 0.8. To understand which relationship exists between anthropogenic and seismic activity a Spearman's correlation test was performed between technological parameters, i.e., injection rate and wellhead pressures, and a new quantity, called ZZ , which represents the degree of disordering of sources and quantifies the potential for seismicity to build undesirable pathways for fluid migration. It was calculated as the average distance between the seismic events in a multidimensional space. This was possible considering the innovative method of transformation to Equivalent Dimensions (Lasocki, 2014) that overcomes the difficulty of comparing seismic parameters whose metrics are different. The results obtained in this work for the Cooper Basin geothermal field indicate that higher values of injection rate and wellhead pressures inhibit the creation of these pathways. The procedure used, was previously developed, and implemented by Lasocki and Orlecka-Sikora (2020) to study The Geyser geothermal field. Although the two geothermal fields have different geology and stimulation, the statistical tests provide the same results, evidencing that ZZ is positively correlated with the technological parameters so the potential for building unwanted pathways decreases as the volumes of fluids injected and pressures of fluids increase. This suggests that this may be a common feature of all geothermal sites. Obviously, the study of other sites using the same procedure may lead, in the case of similar conclusions, to the strengthening of this statement. In addition, it is important to learn how fractures propagate as a result of well stimulation in order to understand how to improve the industrial apparatus and prevent any future risks with warning systems.

Although industrial plants produce well-being in society, it must be considered the risks associated with them and that may originate from the anthropogenic activity itself or due to the occurrence of a natural disaster. An earthquake is, for example, an unforeseen natural event that can damage the industrial plant itself with leakage from the elements of the plant of toxic substances that, in turn, can give rise to fires or explosions generating cascading events with risky consequences for the population, the environment and the economy. In this thesis work, a multi-hazard risk analysis was performed on the San Potito and Cotignola gas storage site in Emilia-Romagna (Italy). In particular, the earthquake and the material fatigue of the pipeline were considered as initial hazards of an incident. Following a bow-tie approach, the probability of annual occurrence of the critical event defined as the leakage of gas from a pipeline of the plant was calculated. The results were obtained by solving the Fault Tree using the MERGER application (Garcia-Aristizabal, 2019) available on the IS-EPOS platform (Orlecka-Sikora et al., 2020). This probabilistic tool is very important to perform complex multi-hazard risk analyses considering different pathways scenarios and natural hazard.

A major limitation encountered in this work to study the correlation analysis in the Porto San Giorgio area is related to the presence of a sparsely sampled data due to the use of seismic data from a complete catalog for magnitudes greater than 2. This is explained by the absence of seismic stations in the Adriatic Sea and a national network with few stations on the coast until the early 2000s. For these reasons, location studies in this area are not straightforward although they are important in an area subject to exploitation of energy geo-resources. Correlation studies between seismic and anthropogenic activity are even rarer in this area. The studies carried out in this work for Porto San Giorgio and Cooper Basin are of course feasible only if industrial information, such as volumes and pressures of injected fluids, and a large seismic dataset are available. In the first case, access to the data is constrained by the industries that tend not to make them freely accessible, thus preventing this type of study. The same problem of secrecy of information is encountered in the case of multi-hazard/risk analysis. Since they are site-

specific studies, it is important to know in detail the industrial plant and its components to be able to correctly identify which accidental event could occur and with which probability. Cooperation between scientists and industry is needed to perform these types of analyses especially considering rare events because, unlike routine operations, they can produce unexpected risks for which the level of preparation and safety is not adequate. Moreover, they require multidisciplinary knowledge and therefore are currently uncommon although of great importance for risk mitigation.

In the future, it might be desirable to perform relocation studies for other seismic sequences occurring in the Adriatic Sea in the vicinity of industrial activities to increase knowledge of the activity of the seismogenic structures present in these areas. Then it will be possible to understand the link between seismicity and anthropogenic activity. The methodology used for the correlation analysis considering the Cooper Basin geothermal site can be exported in the future to study cases of induced seismicity at other industrial sites. These can be either geothermal or hydrocarbon extraction using the fracking technique, since in this case, too, microfractures are intentionally created for circulation of the fluid. Finally, the preliminary study carried out in this work for the San Potito and Cotignola gas storage site can be extended by assessing the consequences that the accident may generate and quantifying the damage it causes. In such a study, it is very important to first consider the exposed elements present in the area and then assess the risks on multiple levels: environmental, economic, and social. A further development could be the assessment of different natural hazards such as extreme weather events in a perspective of safeguarding and mitigating risk in an era in which global climate change is disrupting economies and entire societies.

In conclusion, the entire thesis work constitutes for each case study an innovative work that can expand the scientific literature about the mitigation of environmental risks. In particular, these three case studies provide a discussion of different industrial and environmental aspects related to the exploitation of geo-resources through the use of modern and

innovative methodologies. Future developments will further enrich the knowledge useful to develop strategies in the prevention and mitigation of environmental risks related to the exploitation of geo-resources.

Appendix A

This appendix contains additional material (Figures and Tables) of chapter 3. It provides more detailed information on the macroseismic dataset used, the tests performed to verify the correctness of the macroseismic analysis, and the station corrections used in the relocation analysis of the Porto San Giorgio 1987 seismic sequence.

Table A.1 - Macroseismic intensity data of Porto San Giorgio (PSG) mainshock (3 July 1987, 10:21.57 UTC). Data obtained from the Bollettino Macrosismico of the Istituto Nazionale di Geofisica (ING) (Gasparini *et al.*, 1988). MCS, Mercalli-Cancani-Sieberg.

<i>Place</i>	<i>Latitude</i>	<i>Longitude</i>	<i>Elevation (m)</i>	<i>Macroseismic intensity (MCS)</i>
CAMPOFILONE	43.078	13.814	202	7
LAPEDONA	43.109	13.772	263	7
PORTO SAN GIORGIO	43.18	13.794	4	7
PEDASO	43.097	13.841	5	6-7
CIVITANOVA ALTA	43.316	13.681	160	6
CIVITANOVA MARCHE	43.307	13.73	3	6
COSSIGNANO	42.983	13.688	400	6
CUPRA MARITTIMA	43.024	13.86	4	6
FERMO	43.161	13.716	319	6
FRONTINO	43.764	12.377	519	6
MAGLIANO DI TENNA	43.138	13.586	293	6
MASSIGNANO	43.05	13.798	255	6
MONSAMPIETRO MORICO	43.067	13.556	289	6
MONTE GIBERTO	43.091	13.631	322	6
MONTE SAN GIUSTO	43.236	13.595	236	6
MONTE URANO	43.202	13.673	247	6
MONTE VIDON COMBATTE	43.05	13.631	393	6
MONTERUBBIANO	43.085	13.716	463	6
MORESCO	43.085	13.732	405	6

PETRIOLO	43.221	13.466	271	6
PONZANO DI FERMO	43.102	13.659	248	6
PORTO SANT'ELPIDIO	43.257	13.761	4	6
POTENZA PICENA	43.366	13.621	237	6
RIPATRANSONE	42.999	13.762	494	6
SAN SEVERINO MARCHE	43.229	13.178	235	6
SANT'ANGELO IN PONTANO	43.099	13.398	473	6
SANT'ELPIDIO A MARE	43.229	13.686	251	6
SPINETOLI	42.888	13.773	176	6
SULMONA	42.047	13.929	405	6
TORRE SAN PATRIZIO	43.184	13.608	224	6
LORO PICENO	43.166	13.416	436	5-6
ACQUASANTA TERME	42.77	13.41	411	5
ALBA ADRIATICA	42.827	13.93	5	5
ASCOLI PICENO	42.853	13.578	154	5
BARBARA	43.579	13.025	219	5
BELMONTE PICENO	43.091	13.54	312	5
CAMERANO	43.53	13.551	231	5
CASTELDELCI	43.791	12.155	618	5
CASTELLALTO	42.677	13.818	481	5
ELICE	42.518	13.968	259	5
ESANATOGLIA	43.251	12.948	446	5
FORCE	42.963	13.491	689	5
GIULIANOVA	42.752	13.958	68	5
GROTTAMMARE	42.98	13.872	4	5
GROTTAZZOLINA	43.111	13.603	222	5
MALTIGNANO	42.832	13.687	307	5
MARTINSICURO	42.885	13.914	2	5
MONSANO	43.563	13.25	191	5
MONTALTO DELLE MARCHE	42.988	13.609	513	5
MONTE SAN PIETRANGELI	43.192	13.578	241	5
MONTEFIORE DELL'ASO	43.051	13.751	412	5
MONTEGIORGIO	43.13	13.537	411	5

MONTELUPONE	43.343	13.568	272	5
MONTEPRANDONE	42.919	13.835	266	5
MORRO D'ORO	42.663	13.92	210	5
ORTEZZANO	43.031	13.609	322	5
PETRITOLI	43.067	13.656	358	5
POLLENZA	43.267	13.348	341	5
RAPAGNANO	43.161	13.593	314	5
RECANATI	43.403	13.55	293	5
SAN BENEDETTO DEL TRONTO	42.934	13.893	6	5
SAN GIUSTINO	43.549	12.175	336	5
SANT'AGATA FELTRIA	43.864	12.209	607	5
SANT'ANGELO IN VADO	43.664	12.412	359	5
SELLANO	42.888	12.927	640	5
TORTORETO	42.804	13.914	239	5
URBANIA	43.668	12.523	273	5
USSITA	42.944	13.136	744	5
CAMPOROTONDO DI FIASTRONE	43.131	13.265	335	4-5
CASTEL DI LAMA	42.873	13.707	201	4-5
CASTORANO	42.993	13.424	562	4-5
CELLINO ATTANASIO	42.586	13.859	443	4-5
CITTÀ SANT'ANGELO	42.518	14.06	317	4-5
MONTEGRIMANO	43.866	12.473	536	4-5
SERVIGLIANO	43.08	13.492	216	4-5
TERAMO	42.659	13.704	265	4-5
TREIA	43.311	13.312	342	4-5
ACQUACANINA	43.029	13.175	734	4
ANCARANO	42.837	13.742	293	4
ANCONA	43.603	13.508	16	4
APPIGNANO	43.364	13.347	199	4
ARI	42.291	14.262	289	4
ARQUATA DEL TRONTO	42.772	13.296	777	4
BELFORTE ALL'ISAURO	43.716	12.377	344	4
BELFORTE DEL CHIENTI	43.163	13.238	347	4
BOLOGNANO	42.217	13.961	276	4

<i>BUCCHIANICO</i>	42.304	14.181	371	4
<i>BUGNARA</i>	42.022	13.862	580	4
<i>BUSSI SUL TIRINO</i>	42.21	13.826	344	4
<i>CAMPLI</i>	42.726	13.686	393	4
<i>CANTALICE</i>	42.466	12.904	660	4
<i>CANZANO</i>	42.646	13.804	448	4
<i>CAPPELLE SUL TAVO</i>	42.464	14.104	122	4
<i>CARAMANICO TERME</i>	42.157	14.003	650	4
<i>CASOLI</i>	42.117	14.292	378	4
<i>CASTEL DI IERI</i>	42.114	13.743	519	4
<i>CASTIGLIONE A CASAURIA</i>	42.235	13.9	350	4
<i>CERRETO D'ESI</i>	43.32	12.985	276	4
<i>CESSAPALOMBO</i>	43.108	13.258	434	4
<i>CIVITELLA DEL TRONTO</i>	42.772	13.668	589	4
<i>COLLECORVINO</i>	42.459	14.015	253	4
<i>COLLEDARA</i>	42.54	13.681	430	4
<i>COLLEDIMACINE</i>	42.004	14.201	770	4
<i>COLLEDIMEZZO</i>	41.986	14.383	424	4
<i>COLLEPIETRO</i>	42.74	13.863	227	4
<i>COLONNELLA</i>	42.872	13.867	303	4
<i>CORRIDONIA</i>	43.248	13.51	255	4
<i>CORTINO</i>	42.622	13.509	1050	4
<i>CRECCHIO</i>	42.297	14.327	209	4
<i>CUGNOLI</i>	42.268	14.042	251	4
<i>FABRIANO</i>	43.336	12.905	325	4
<i>FALCONARA MARITTIMA</i>	43.626	13.399	5	4
<i>FARA FILIORUM PETRI</i>	42.249	14.186	210	4
<i>FOSSACESIA</i>	42.244	14.481	140	4
<i>FRANCAVILLA AL MARE</i>	42.412	14.301	19	4
<i>GENGA</i>	43.429	12.935	322	4
<i>LAMA DEI PELIGNI</i>	42.042	14.188	669	4
<i>LORETO APRUTINO</i>	42.433	13.988	294	4
<i>MAGLIANO DE MARSÌ</i>	42.092	13.363	728	4
<i>MONTAZZOLI</i>	41.948	14.43	850	4

<i>MONTECOPIOLO</i>	43.841	12.36	915	4
<i>MONTECOSARO</i>	43.316	13.636	252	4
<i>MONTEGALLO</i>	43.525	13.478	240	4
<i>MONTELABBATE</i>	43.849	12.79	65	4
<i>MONTEMONACO</i>	42.899	13.327	988	4
<i>MONTESILVANO</i>	42.515	14.151	5	4
<i>MORROVALLE</i>	43.314	13.58	245	4
<i>MOSCUFO</i>	42.428	14.055	246	4
<i>NAVELLI</i>	42.237	13.73	760	4
<i>NOVAFELTRIA</i>	43.894	12.29	275	4
<i>NUMANA</i>	43.512	13.622	56	4
<i>OSIMO</i>	43.486	13.483	265	4
<i>PENNA SAN GIOVANNI</i>	43.056	13.426	630	4
<i>PENNA SANT'ANDREA</i>	42.593	13.772	413	4
<i>PENNE</i>	42.457	13.928	438	4
<i>PERGOLA</i>	43.563	12.837	265	4
<i>PESCARA</i>	42.464	14.214	4	4
<i>PESCIASSEROLI</i>	41.808	13.789	1167	4
<i>PIANELLA</i>	42.398	14.05	236	4
<i>PICCIANO</i>	42.474	13.991	170	4
<i>PIORACO</i>	43.178	12.986	441	4
<i>POLLUTRI</i>	42.137	14.594	180	4
<i>PRATA D'ANSIDONIA</i>	42.277	13.61	846	4
<i>PRATOLA PELIGNA</i>	42.098	13.875	342	4
<i>RAIANO</i>	42.102	13.814	390	4
<i>ROCCA SAN GIOVANNI</i>	42.25	14.466	155	4
<i>ROCCA SANTA MARIA</i>	42.686	13.528	1073	4
<i>SAN PAOLO DI JESI</i>	43.454	13.174	224	4
<i>SAN PIO DELLE CAMERE</i>	42.286	13.656	830	4
<i>SAN VALENTINO IN ABRUZZO</i>	42.233	13.987	457	4
<i>SANT'ANGELO IN LIZZOLA</i>	43.827	12.803	280	4
<i>SEFRO</i>	43.146	12.949	497	4
<i>SILVI</i>	42.555	14.114	3	4
<i>SPOLTORE</i>	42.227	14.422	247	4

STAFFOLO	43.432	13.187	441	4
TOLLO	42.339	14.319	152	4
TORRICELLA SICURA	42.658	13.656	437	4
URBINO	43.726	12.636	485	4
VALLE CASTELLANA	42.735	13.498	625	4
CASTELFIDARDO	43.463	13.55	199	3
CASTELLI	42.212	14.43	255	3
CASTELVECCHIO SUBEQUO	42.13	13.731	490	3
CIVITELLA CASANOVA	42.364	13.889	400	3
CORINALDO	43.649	13.048	203	3
CROGNALETO	42.215	14.027	480	3
FANO ADRIANO	42.552	13.538	745	3
FARINDOLA	42.441	13.824	530	3
FERMIGNANO	43.675	12.647	200	3
FILETTO	42.226	14.245	403	3
FIUMINATA	43.188	12.932	479	3
GIULIANO TEATINO	42.305	14.278	272	3
GUARDIAGRELE	42.19	14.222	576	3
GUBBIO	43.352	12.577	522	3
ISOLA DEL GRAN SASSO D'IT	42.501	13.661	415	3
LANCIANO	42.23	14.39	265	3
MIGLIANICO	42.359	14.292	125	3
MONTECALVO IN FOGLIA	43.811	12.632	345	3
MONTEREALE	42.522	13.246	945	3
MONTONE	43.363	12.327	482	3
MONTORIO AL VOMANO	42.582	13.629	263	3
NOCCIANO	42.332	13.984	301	3
NORCIA	42.793	13.094	604	3
ORSOGNA	42.219	14.283	430	3
PARRANO	42.863	12.106	441	3
PASCELUPO	43.399	12.752	529	3
PENNABILLI	43.817	12.265	629	3
PENNADOMO	42.005	14.326	430	3
PENNAPIEDIMONTE	42.151	14.195	669	3
PESARO	43.905	12.905	11	3

<i>PETRIANO</i>	43.78	12.734	327	3
<i>PIETRACAMELA</i>	42.523	13.554	1005	3
<i>PIOBBICO</i>	43.008	13.263	730	3
<i>POGGIO SAN VICINO</i>	43.375	13.079	509	3
<i>PRECI</i>	42.879	13.039	596	3
<i>ROCCACASALE</i>	42.124	13.888	450	3
<i>ROSCIANO</i>	42.321	14.044	242	3
<i>SAN DEMETRIO NE VESTINI</i>	42.288	13.558	662	3
<i>SAN GIORGIO DI PESARO</i>	43.718	12.981	201	3
<i>SAN LORENZO IN CAMPO</i>	43.604	12.947	209	3
<i>SAN MARCELLO</i>	43.1	13.069	587	3
<i>SANT'IPPOLITO</i>	43.02	13.345	546	3
<i>SASSOFERRATO</i>	43.434	12.858	386	3
<i>SCHEGGIA</i>	43.403	12.668	580	3
<i>SCURCOLA MARSICANA</i>	42.064	13.342	700	3
<i>SERRA SANT'ABBONDIO</i>	43.491	12.772	536	3
<i>SERRAVALLE DI CHIANTI</i>	43.073	12.955	647	3
<i>SERRUNGARINA</i>	43.747	12.875	209	3
<i>TOSSICIA</i>	42.545	13.648	409	3
<i>URBISAGLIA</i>	43.196	13.377	310	3
<i>VALLO DI NERA</i>	42.754	12.865	467	3
<i>VALTOPINA</i>	43.057	12.754	366	3
<i>VICOLI</i>	42.341	13.898	445	3

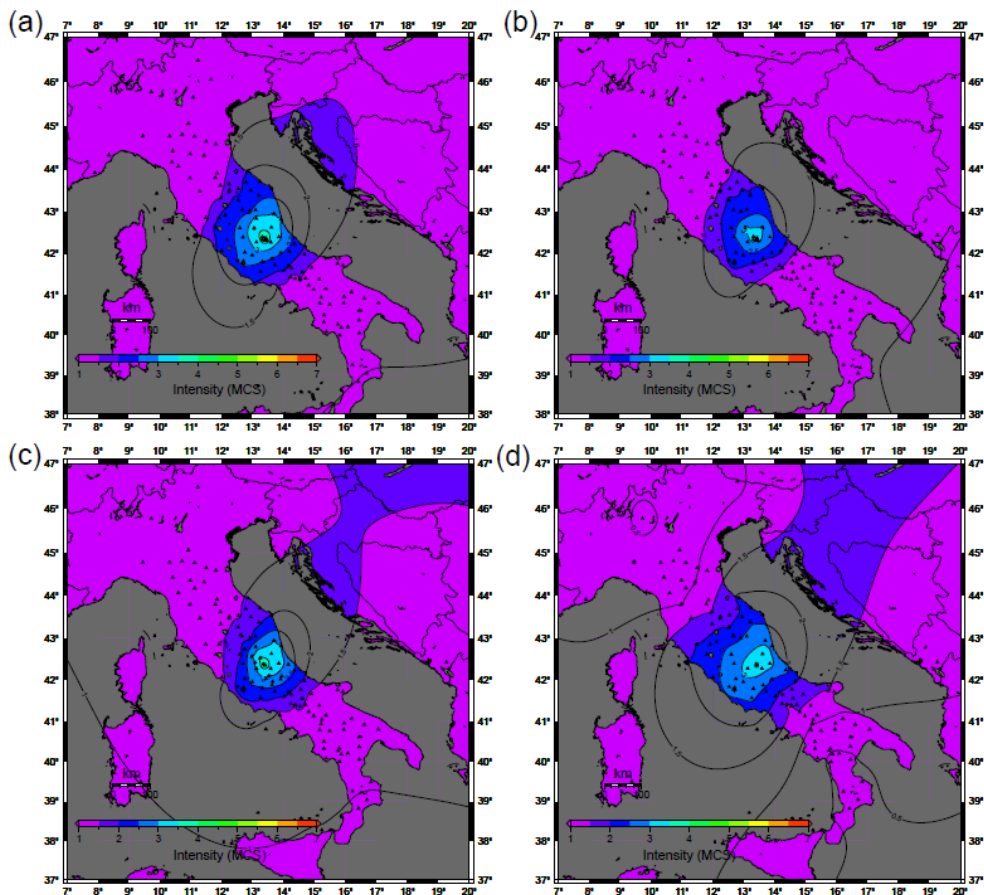


Figure A.1 - Tests on instrumental earthquakes of the 2009 L'Aquila seismic sequence to verify the reliability of the methodology to get information about depth and magnitude of pre-instrumental earthquake from the macroseismic intensity field. Three tests were performed selecting three instrumental earthquakes of the 2009 L'Aquila seismic sequence (M 6.1), with a magnitude comparable to the 1987 M 5 PSG earthquake. For each test, after fixing the epicenter location (calculated by Chiaraluce et al., 2011), the magnitude and the depth of the earthquakes were retrieved using the intensity data through a grid-searching technique, as explained in chapter 3. The results are compared with the final earthquake relocations obtained by Chiaraluce et al. (2011). The magnitude–depth values were explored with a sampling step equal to 0.2 and 1 km, respectively, using the velocity model and the $M_L - M_W$ relation reported in Scognamiglio et al. (2009). Instrumental intensities are derived from the INGV shakemap webpage. The selected events are (1) M_W 5.0 earthquake (a; test 1) that

occurred on 9 April 2009 at 19:38:16 (UTC) nearby Capitignano (Province of L'Aquila, AQ), (2) M_W 4.8 earthquake (b, test 2) that occurred on 13 April 2009 at 21:14:24 (UTC) nearby Capitignano, (3) M_W 5.0 earthquake (c; test 3) that occurred on 6 April 2009 at 23:15:36 (UTC), nearby Pizzoli (AQ). In (d), a synthetic macroseismic intensity field for an earthquake of M_W 5.2 and depth 9 km is reported (solution of test 3). As shown in Table A.2, the results of the three tests show a common solution (M_W 5.2 and depth 9 km; e.g., panel d) that is comparable to real solutions in terms of depth and magnitude, with differences in depth equal to 1.4, 2, and 0.22 km for tests 1, 2, and 3, respectively. The differences are related to the intrinsic uncertainties of the method, and in part, to the sampling selected for the magnitude - depth exploration. These tests, performed using instrumental intensity data, show that our method correctly retrieved the real depth and magnitude of the earthquakes, with the largest error equal to 0.2 and to 2 km, for magnitude and depth, respectively. The rms values between real and synthetic macroseismic data are reported in Table A.2.

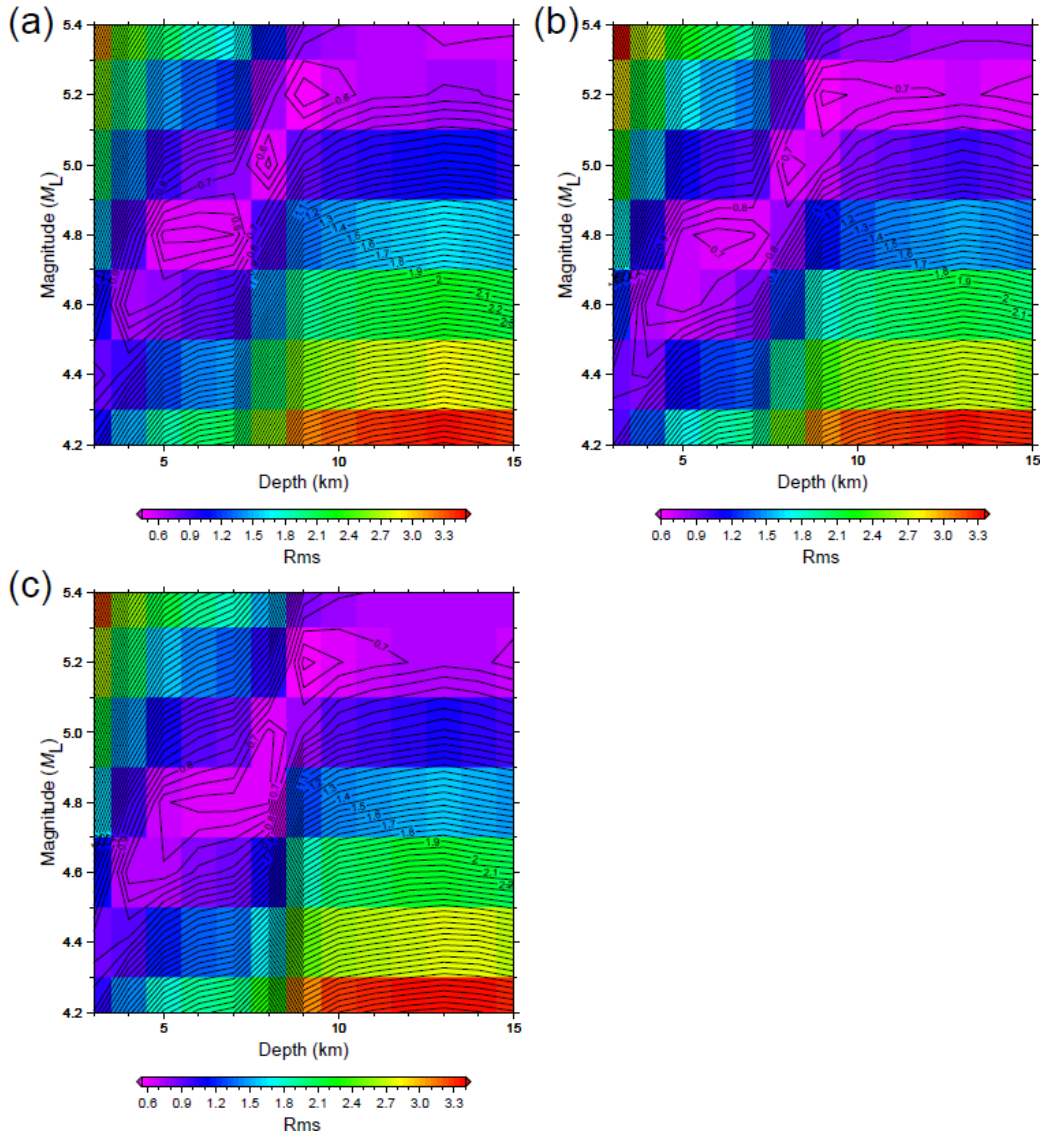


Figure A.2 - Results of the grid searching for (a) test 1, (b) test 2, and (c) test 3. The real and synthetic macroseismic maps are compared evaluating the rms value between real and synthetic intensity data for each combination of magnitude - depth values. See Figure A.1 and Table A.2 for details.

Table A.2 - The final solutions of grid-searching for the three tests are reported. Columns 2-4 show the real depths and magnitudes derived from Chiaraluce et al. (2011). Columns 5 - 7 shows depths and magnitudes recovered by inverting macroseismic intensity data. The root mean square (rms) values are reported in column 8.

	M_L	M_w	Depth (km)	M_L	M_w	Depth (km)	RMS
Test 1	5.0	5.0	7.60	5.2	5.0	9.0	0.41
Test 2	5.0	4.8	7.04	5.2	5.0	9.0	0.63
Test 3	5.0	5.0	8.78	5.2	5.0	9.0	0.57

Table A.3 - Cumulative delay list for P and S phases at each station. The cumulative delay is given by the sum of the average residuals. These values are used as the station corrections.

Station	Phase	Total Correction (s)	Standard Deviation (s)
ALP	P	-0.62	0.52
ALP	S	-0.46	0.62
AMC	P	-0.25	0.37
AMC	S	0.32	0.66
AQU	P	0.63	0.91
AQU	S	-0.16	0.85
ARV	P	-0.12	0.39
ARV	S	0.15	0.78
ASS	P	-0.46	0.59
ASS	S	-0.12	0.91
AZ9	P	1.14	0.40
BAI	P	-0.38	0.68
BDI	P	0.02	0.60
BOB	P	0.94	0.66
BRT	P	-0.69	0.22
BRY	P	0.50	0.25
BSS	P	-0.01	0.16
BVT	P	1.32	1.04
BVT	S	-1.90	0.59
CDM	P	-1.03	0.67
CEY	P	0.52	0.84
CEY	S	0.05	0.21
CMR	P	-0.28	0.40

CMR	S	-0.14	1.11
CO9	P	0.11	1.04
CO9	S	-2.58	-1.00
CP9	P	0.25	0.68
CP9	S	0.49	-1.00
CRE	P	0.36	0.53
CRE	S	0.18	0.65
CTI	P	-0.56	0.62
CTI	S	-1.74	0.55
DUI	P	0.54	0.38
DUI	S	-1.08	0.05
FG2	P	-0.03	0.39
FG4	P	0.23	0.65
FIR	P	0.81	1.04
FOI	P	-0.57	0.16
FOI	S	-2.29	-1.00
FVI	P	-0.59	0.14
HCY	P	0.63	0.30
HCY	S	0.40	0.20
HVA	P	0.23	0.83
HVA	S	0.48	0.64
LJU	P	0.45	0.47
LJU	S	-1.36	0.92
MAO	P	0.05	0.37
MC8	P	-0.02	0.38
MC8	S	0.00	0.44
MCO	P	0.14	0.36
MCO	S	0.36	0.63
MGR	P	-0.05	0.19
MME	P	0.33	0.60
MNS	P	-0.10	0.60
MNS	S	0.11	0.73
MS1	P	-0.45	0.72
MSC	P	0.45	0.11
OVO	P	1.48	-1.00
PE1	P	-0.32	0.53
PGD	P	0.62	0.51
PGD	S	-2.08	1.06
PII	P	0.14	0.90
PRG	P	-3.66	-1.00
PS9	P	0.67	0.39
PTJ	P	0.37	0.86
PTJ	S	-1.54	-1.00

RBL	P	-0.44	0.47
RDP	P	0.25	0.67
RMP	P	0.13	0.42
SAL	P	0.10	0.34
SAL	S	-2.07	-1.00
SAR	P	1.83	0.44
SDI	P	0.26	0.48
SDI	S	-0.90	0.56
SGG	P	0.22	0.24
SGO	P	-0.30	0.44
SGO	S	0.26	-1.00
SOR	P	-0.08	0.31
SS9	P	1.07	0.64
SS9	S	-0.83	0.81
TR9	P	0.89	0.60
TRI	P	-0.61	0.40
TRI	S	-0.95	-1.00
VBY	P	0.89	0.68
VBY	S	0.53	-1.00
VEA	P	1.46	1.05
VOY	P	-0.65	0.32
VOY	S	-1.21	0.80
ZAG	P	-0.08	0.45
ZAG	S	-0.89	-1.00

Bibliography

Ahmed, T. (2010). Principles of Waterflooding, Chapter 14 in *Reservoir Engineering Handbook (Fourth Edition)*, Gulf Professional Publishing, 909-1095, <https://doi.org/10.1016/B978-1-85617-803-7.50022-5>

Argnani, A., G. Barbacini, M. Bernini, F. Camurri, M. Ghielmi, G. Papani, F. Rizzini, S. Rogledi, and L. Torelli (2003). Gravity tectonics driven by Quaternary uplift in the Northern Apennines: insights from the La Spezia-Reggio Emilia Geo-Transect, *Quat. Int.* **101-102**, 13-26, doi: [10.1016/S1040-6182\(02\)00088-5](https://doi.org/10.1016/S1040-6182(02)00088-5)

Argnani, A., and F. Gamberi (1995). Stili strutturali al fronte della catena appenninica nell'Adriatico centro-settentrionale, *Studi Geol. Camerti Vol Spec* **1995/1**, 19-27

Baisch S., E. Rothert, H. Stang, R. Vörös, C. Koch, and A. McMahon (2015). Continued Geothermal Reservoir Stimulation Experiments in the Cooper Basin (Australia). *Bulletin of Seismological Society of America* **105**, no. 1, 198-209, doi: [10.1785/0120140208](https://doi.org/10.1785/0120140208)

Baisch S., R. Vörös, E. Rothert, H. Stang, R. Jung, and R. Schellschmidt (2010). A numerical model for fluid injection induced seismicity at Soultz-sous-Forêts, *International Journal of Rock Mechanics & Mining Sciences* **47**, no. 3, 405-413, doi:[10.1016/j.ijrmms.2009.10.001](https://doi.org/10.1016/j.ijrmms.2009.10.001)

Baisch S., R. Vörös, R. Weidler, and D. Wyborn (2009). Investigation of Fault Mechanisms during Geothermal Reservoir Stimulation Experiments in the Cooper Basin, Australia. *Bulletin of Seismological Society of America* **99**, no. 1, 148-158, doi: [10.1785/0120080055](https://doi.org/10.1785/0120080055)

Baisch, S., R. Weidler, R. Vörös, D. Wyborn, and L. de Graaf (2006). Induced Seismicity during the Stimulation of a Geothermal HFR Reservoir in the Cooper Basin, Australia. *Bulletin of Seismological Society of America* **96**, no. 6, 2242-2256, doi: [10.1785/0120050255](https://doi.org/10.1785/0120050255)

Bally, A., L. Burbi, C. Cooper, and R. Ghelardoni (1986). Balanced sections and seismic reflection profiles across the Central Apennines, *Mem. Soc. Geol. It.*, **35**, 257-310

BC Oil and Gas Commission (2014). Investigation of observed seismicity in the Montney Trend

Bendall B., R. Hogarth, H. Holl, A. McMahon, A. Larking, and P. Reid (2014). Australian Experiences in EGS Permeability Enhancement – A Review of 3 Case Studies. *Proceedings, Thirty-Ninth Workshop on Geothermal Reservoir Engineering*, Stanford University, California, February 24 – 26

Bertello, F., R. Fantoni, R. Franciosi, V. Gatti, M. Ghielmi, and A. Pugliese (2010). From thrust and fold belt to foreland; hydrocarbon occurrences in Italy, in Vining, B.A., Pickering, S.C. (Eds.), *Petroleum Geology: From Mature Basin to New Frontiers*. 7th Petroleum Geology Conference, Geol. Soc., 113-126

Bertotti, G., R. Capozzi, and V. Picotti (1997). Extension controls Quaternary tectonics, geomorphology and sedimentation of the N-Apennines foothills and adjacent Po Plain (Italy), *Tectonophysics* **282**, 291-301

Billah, A., and M. Alam (2014). Seismic Fragility Assessment of Highway Bridges: A State-of-the-Art Review. *Structure and Infrastructure Engineering*, 1–29. <https://doi.org/10.1080/15732479.2014.912243>.

Braun, T., S. Cesca, D. Kühn, A. Martirosian-Janssen, and T. Dahm (2018). Anthropogenic seismicity in Italy and its relation to tectonics: State of the art and perspectives, *Anthropocene* **21**, 80-94, ISSN 2213-3054, <https://doi.org/10.1016/j.ancene.2018.02.001>.

Caciagli, M., R. Camassi, S. Danesi, S. Pondrelli, and S. Salimbeni (2015). Can We Consider the 1951 Caviaga (Northern Italy) Earthquakes as Noninduced Events?, *Seismol. Res. Lett.* **86**, no. 5, 1-10, doi: [10.1785/0220150001](https://doi.org/10.1785/0220150001).

Campedel, M. (2008). Analysis of major industrial accidents triggered by natural events reported in the principal available chemical accident databases. *European Commission Joint Research Centre. EUR-Scientific and Technical Research Report: JRC42281. OPOCE*, ISSN: 1018-5593.

Capuano et al. (2017). Report finale del progetto ARGO (Analisi dei Rischi naturali e antropogenici delle piattaforme petrolifere Off-shore, MISE)

Carannante, S., G. Monachesi, M. Cattaneo, A. Amato, and C. Chiarabba (2013). Deep structure and tectonics of the northern-central Apennines as seen by

regional-scale tomography and 3-D located earthquakes, *J. Geophys. Res. Solid Earth* **118**, 5391–5403, doi: [10.1002/jgrb.50371](https://doi.org/10.1002/jgrb.50371).

Casero, P., and S. Bigi (2013). Structural setting of the Adriatic basin and the main related petroleum exploration plays, *Mar. Pet. Geol.* **42**, 135-147, <https://doi.org/10.1016/j.marpetgeo.2012.07.006>

Casero, P. (2004). Structural setting of petroleum exploration plays in Italy, *Special volume of the Italian geological Society for the IGC* **32**, 189-199

Castello, B., G. Selvaggi, C. Chiarabba, and A. Amato (2006). *CSI Catalogo della sismicità Italiana 1981-2002, versione 1.1*, Istituto Nazionale di Geofisica e Vulcanologia – Centro Nazionale Terremoti, Roma, Italy (in Italian).

Chatelain, J.L. (1978). Etude fine de la sismicité en zone de collision continentale à l'aide d'un réseau de stations portables: la région Hindu-Kush-Pamir, *Thèse de 3^{ème} cycle*, Université Paul Sabatier, Toulouse.

Chatelain, J. L., S. W. Roecker, D. Hatzfeld, and P. Molnar (1980). Microearthquake seismicity and fault plane solutions in the Hindu Kush region and their tectonic implications, *J. Geophys. Res.* **85**, 1365-1378.

Chiarabba, C., and A. Frepoli (1997). Minimum 1D velocity models in Central and Southern Italy: a contribution to better constrain hypocentral determinations, *Annali di Geofisica* **XL**, N. 4, 937-954.

Chiaraluce, L., R. Di Stefano, E. Tinti, L. Scognamiglio, M. Michele, E. Casarotti, M. Cattaneo, P. De Gori, C. Chiarabba, A. Monachesi, L. Lombardi, L. Valoroso, D. Latorre, and S. Marzorati (2017a). The 2016 Central Italy seismic sequence: A first look at the mainshocks, aftershocks, and source models, *Seismol. Res. Lett.* **88**, no. 3, doi:[10.1785/0220160221](https://doi.org/10.1785/0220160221).

Chiaraluce, L., R.M. Barchi, S. Carannante, C. Collettini, F. Mirabella, C. Pauselli, and L. Valoroso (2017b). The role of rheology, crustal structures and lithology in the seismicity distribution of the northern Apennines, *Tectonophysics* **694**, 280-291, doi:[10.1016/j.tecto.2016.11.011](https://doi.org/10.1016/j.tecto.2016.11.011).

Chiaraluce, L. (2012). Unravelling the complexity of Apenninic extensional fault systems: A review of the 2009 L'Aquila earthquake (Central Apennines, Italy). *Journal of Structural Geology*, **42**, 2-18.

Chiaraluce, L., L. Valoroso, D. Piccinini, R. Di Stefano, and P. De Gori (2011). The anatomy of the 2009 L'Aquila normal fault system (central Italy) imaged by high resolution foreshock and aftershock locations, *J. Geophys. Res.* **116**, no. B12311, doi: [10.1029/2011JB008352](https://doi.org/10.1029/2011JB008352).

Console, R., R. Di Giovambattista, P. Favali, and G. Smriglio (1992). Seismogenic structures activated during the 1987 seismic sequences along the Adriatic coast, *Geophys. J. Int.* **108**, 379-386.

Convertito, V., and L. Faenza (2015) Earthquake Recurrence. In: Beer M., Kougioumtzoglou I.A., Patelli E., Au SK. (eds) Encyclopedia of Earthquake Engineering. Springer, Berlin, Heidelberg, https://doi.org/10.1007/978-3-642-35344-4_236

Convertito, V., and N. A. Pino (2014). Discriminating among distinct source models of the 1908 Messina Straits earthquake by modelling intensity data through full wavefield seismograms, *Geophys. J. Int.* **198**, no. 1, 164-173, <https://doi.org/10.1093/gji/ggu128>

Cozzani, V., G. Gubinelli, G. Antonioni, G. Spadoni, and S. Zanelli (2005). The assessment of risk caused by domino effect in quantitative area risk analysis, *Journal of Hazardous Materials* **127**, no. 1-3, 14-30 doi:[10.1016/j.jhazmat.2005.07.003](https://doi.org/10.1016/j.jhazmat.2005.07.003)

Coutant, O. (1989). Program of Numerical Simulation AXITRA. Res. Report LGIT, Grenoble, in French.

Cruz, A.M., E. Krausmann, N. Kato and S. Girgin (2017). Reducing Natech Risk: Structural Measures, Chapter 13 in *Natech Risk Assessment and Management – Reducing the Risk of Natural-Hazard Impact on Hazardous Installations*, Elsevier, 205-225

Cruz, A.M., and M.C. Suarez-Paba (2019). Advances in Natech research: An overview, *Progress in Disaster Science* **1**, 100013 <https://doi.org/10.1016/j.pdisas.2019.100013>

Dayal, A.M. (2017). Hydraulic Fracturing, Chapter 6 in *Shale gas Explor. Environ. Econ. Impacts*, 95-111, <http://dx.doi.org/10.1016/B978-0-12-809573-7.00006-8>

De Pater, C.J., and S. Baisch (2011). Geomechanical Study of Bowland Shale Seismicity – Synthesis Report. Prepared for Cuadrilla Resources.

Deichmann, N., and D. Giardini (2009). Earthquakes Induced by the Stimulation of an Enhanced Geothermal System below Basel (Switzerland). *Seismological Research Letters* **80**, no. 5, 784-798, doi: [10.1785/gssrl.80.5.784](https://doi.org/10.1785/gssrl.80.5.784)

De Michele, G. (2014). L'energia che verrà, *Ambiente Rischio Comunicazione. Quadrimestrale di analisi e monitoraggio ambientale*. **No risk no energy**, no. 9, 50-57 (in Italian)

Di Bucci, D., and S. Mazzoli (2002). Active tectonics of the Northern Apennines and Adria geodynamics: new data and a discussion, *Journal of Geodynamics* **34**, no. 5, 687-707

DISS Working Group (2018). Database of Individual Seismogenic Sources (DISS), Version 3.2.1: A compilation of potential sources for earthquakes larger than M 5.5 in Italy and surrounding areas. <http://diss.rm.ingv.it/diss/>, Istituto Nazionale di Geofisica e Vulcanologia; doi: [10.6092/INGV.IT-DISS3.2.1](https://doi.org/10.6092/INGV.IT-DISS3.2.1)

Dogliani, C. (1993). Some remarks on the origin of the foredeeps, *Tectonophysics* **228**, no. 1-2, 1-20

Eads, L., Miranda, E., Krawinkler, H., and D. Lignos (2012). Improved estimation of collapse risk for structures in seismic regions. In *Proceedings of the 15th World Conference on Earthquake Engineering*, Lisbon, Portugal, 24–28 September 2012.

Ehrlich, P.R., and J.P. Holdren (1972). A Bulletin Dialogue on the 'Closing Circle': Critique: One-Dimensional Ecology, *Bulletin of the Atomic Scientists* **28**, no. 5, 16-27, doi: [10.1080/00963402.1972.11457930](https://doi.org/10.1080/00963402.1972.11457930)

Eiken, O., Ringrose, C., Hermanrud, B., Nazarian, B., Torp, T.A., and L. Høier (2011). Lessons learned from 14 years of CCS operations: Sleipner, in Salah and Snøhvit, *Energy Procedia* **4**, 5541-5548, doi:[10.1016/j.egypro.2011.02.541](https://doi.org/10.1016/j.egypro.2011.02.541)

Ellsworth, W.L. (2013). Injection-Induced Earthquake, *Science* **341**, no. 6142, doi:[10.1126/science.1225942](https://doi.org/10.1126/science.1225942)

Emolo, A., G. Iannaccone, A. Zollo, and A. Gorini (2004). Inferences on the source mechanisms of the 1930 Irpinia (Southern Italy) earthquake from simulations of the kinematic rupture process, *Ann. Geophys.* **47**, no. 4, doi: <https://doi.org/10.4401/ag-3372>

European Union (2012). Directive 2012/18/EU of the European Parliament and of the Council of 4 July 2012 on the control of major-accident hazards involving

dangerous substances, amending and subsequently repealing Council Directive 96/82/EC. *Off. J. Eur. Union.* 197, 1

Evans, K.F., A. Zappone, T. Kraft, N. Deichmann, and F. Moia (2011). A survey of the induced seismic responses to fluid injection in geothermal and CO₂ reservoirs in Europe, *Geothermics* **41**, 30-54, doi:[10.1016/j.geothermics.2011.08.002](https://doi.org/10.1016/j.geothermics.2011.08.002)

Faenza, L., and A. Michelini (2010). Regression analysis of MCS intensity and ground motion parameters in Italy and its application in ShakeMap, *Geophys. J. Int.*, **180**, no. 3, 1138-1152.

Fisher, R. A. (1954) *Statistical Methods for Research Workers*. Edinburgh: Oliver and Boyd.

Florez, M.A., and G.A. Prieto (2017). Precise relative earthquake depth determination using array processing techniques, *J. Geophys. Res. Solid Earth* **122**, 4559- 4571, doi:[10.1002/2017JB014132](https://doi.org/10.1002/2017JB014132)

Font, Y., Kao, H., Lallemand, S., Liu, C.-S. and L.-Y. Chiao (2004). Hypocentral determination offshore Eastern Taiwan using the Maximum Intersection method. *Geophys. J. Int.* **158**, 655-675

Foulger, G.R., M.P. Wilson, J.G Gluyas, B.R. Julian and R.J. Davies (2018). Global review of human-induced earthquakes. *Earth-Science Reviews* **178**, 438-514, <http://dx.doi.org/10.1016/j.earscirev.2017.07.008>

Frepoli, A., and A. Amato (1997). Contemporaneous extension and compression in the Northern Apennines from earthquake fault-plane solutions, *Geophys. J. Int.*, **129**, no. 2, 368-388, <https://doi.org/10.1111/j.1365-246X.1997.tb01589.x>

Gambini, R., R. Thomas, and S. Morandi (1997). Inversion tectonics on the central Adriatic Sea, *FIST, Geitalia*, 5-9

Garcia-Aristizabal, A., J. Kocot, R. Russo, and P. Gasparini (2019). A probabilistic tool for multi-hazard risk analysis using a bow-tie approach: application to environmental risk assessments for geo-resource development projects. *Acta Geophys.* **67**, 385-410, doi: [10.1007/s11600-018-0201-7](https://doi.org/10.1007/s11600-018-0201-7)

Garcia-Aristizabal A., Capuano P., Russo R., and P. Gasparini (2017). Multi-hazard risk pathway scenarios associated with unconventional gas

development: identification and challenges for their assessment. *Energy Proc.* **125**, 116–125, <https://doi.org/10.1016/j.egypro.2017.08.087>

Gasparini, C., Anzidei, M., Maramai, A., Murru, M., Riguzzi, F., Tertulliani, A., Cardoni, M., Del Mese, S., Vannucci, C., Vecchi, M. and A. Massucci (1988), *Bollettino macrosismico 1987*. Istituto Nazionale di Geofisica, Roma, 47 pp.

Gasparini, P., Di Ruocco, A., Garcia-Aristizabal, A., Basco, A., Teofilo, G., and I. Antoncetti (2016). Approccio Multi-Rischio alla valutazione degli effetti di eventi NATECH, Conference Paper, VGR 2016 – Valutazione e gestione del rischio degli insediamenti civili ed industriali (Roma)

Gasparini, P., G. Vannucci, D. Tripone, and E. Boschi (2010). The Location and Sizing of Historical Earthquakes Using the Attenuation of Macro seismic Intensity with Distance, *Bull. Seismol. Soc. Am.* **100**, no. 5A, 2035-2066

Ghisetti, F., and L. Vezzani (2002). Normal faulting, transcrustal permeability and seismogenesis in the Apennines (Italy), *Tectonophysics* **348** (1-3), 155-168.

Grasso, J.R., and G. Wittlinger (1990). Ten years of seismic monitoring over a gas field area. *Bulletin of the Seismological Society of America* **80**, no. 2, 450-473.

Greco, P. (2014). L'equilibrio tra rischio e intelligenza, *Ambiente Rischio Comunicazione. Quadrimestrale di analisi e monitoraggio ambientale*. **No risk no energy**, no. 9, 4-5 (in Italian)

Grigoli, F., L. Scarabello, M. Böse, B. Weber, S. Wiemer, and J. F. Clinton (2018). Pick- and waveform-based techniques for real-time detection of induced seismicity, *Geophys. J. Int.* **213**, no. 2, 868–884, <https://doi.org/10.1093/gji/ggy019>

Grigoli, F., S. Cesca, E. Priolo, A. P. Rinaldi, J. F. Clinton, T. A. Stabile, B. Dost, M. G. Fernandez, S. Wiemer, and T. Dahm (2017). Current challenges in monitoring, discrimination, and management of induced seismicity related to underground industrial activities: A European perspective. *Rev. Geophys.*, 55, no. 2, 310–340, doi:[10.1002/2016RG000542](https://doi.org/10.1002/2016RG000542)

Gruppo di Lavoro CSTI, 2005, Catalogo Strumentale dei Terremoti Italiani dal 1981 al 1996 (Versione 1.1), http://gaspy.df.unibo.it/paolo/gndt/Versione1_1/Leggimi.htm

Havskov, J., Bormann, P., and J. Schweitzer (2009 online). Earthquake location, in Bormann, P. (Ed.), *New Manual of Seismological Observatory Practice (NMSOP)*, Postdam: Deutsches GeoForschungsZentrum GFZ, 1-28, https://doi.org/10.2312/GFZ.NMSOP_r1_IS_11.1

Havskov, J., and L. Ottemöller (2010). *Routine Data Processing in Earthquake Seismology: With sample data, exercises and software*. New York: Springer. https://doi.org/10.1007/978-90-481-8697-6_6

Hogarth R., and H.G. Holl (2017). Lessons Learned from the Habanero EGS Project. *GRC Transactions* **41**

Hogarth R., S. Baisch, H.G. Holl, R. Jeffrey, and R. Jung (2019). *European Geothermal Congress*, Strasbourg, France, 19-24 September

Hogarth, R., and D. Bour (2015). Flow Performance of the Habanero EGS Closed Loop. *Proceedings World Geothermal Congress*, Melbourne, Australia, 19-25 April

Hogarth R., H. Holl, and A. McMahon (2013). Flow Testing Results from Habanero EGS Project. *Proceedings Australian Geothermal Energy Conferences*, Brisbane, Australia, 14 - 15 November

Hogarth R., H. Holl, and A. McMahon (2013). Production, injection and closed-loop testing at Habanero EGS Project. *35th New Zealand Geothermal Workshop: 2013 Proceedings*, Rotorua, New Zealand, 17-20 November

Holl, H.G., and C. Barton (2015). Habanero Field - Structure and State of Stress. *Proceedings World Geothermal Congress*, Melbourne, Australia, 19-25 April

Holland, A.A. (2013). Earthquakes Triggered by Hydraulic Fracturing in South-Central Oklahoma. *Bulletin of the Seismological Society of America* **103**, no. 3, 1784-1792, doi: [10.1785/0120120109](https://doi.org/10.1785/0120120109)

Huang, K., G. Chen, Y. Yang and P. Chen (2020). An innovative quantitative analysis methodology for Natech events triggered by earthquakes in chemical tank farms. *Safety Science* **128**, 104744, <https://doi.org/10.1016/j.ssci.2020.104744>

Husen, S., and J.L. Hardebeck (2010). Earthquake location accuracy, Community Online Resource for Statistical Seismicity Analysis, doi: [10.5078/corssa-55815573](https://doi.org/10.5078/corssa-55815573)

Improta, L., S. Bagh, P. De Gori, L. Valoroso, M. Pastori, D. Piccinini, C. Chiarabba, M. Anselmi and M. Buttinelli (2017). Reservoir Structure and Wastewater-Induced Seismicity at the Val d'Agri Oilfield (Italy) Shown by Three-Dimensional Vp and Vp/Vs Local Earthquake Tomography. *Journal of Geophysical Research: Solid Earth* **122**, no. 11, 9050-9082, <https://doi.org/10.1002/2017JB014725>

International Seismological Centre (ISC) (2016). International Seismological Centre On-line Bulletin, <http://www.isc.ac.uk>, International Seismological Centre, Thatcham, United Kingdom, <http://doi.org/10.31905/D808B830> (last accessed February 2019)

Kagan, Y. Y. (2002). Seismic moment distribution revisited: I. Statistical results, *Geophys. J. Int.* **148**, no. 3, 540-541, doi: [10.1046/j.1365-246x.2002.01594.x](https://doi.org/10.1046/j.1365-246x.2002.01594.x)

Khakzad, N., Khan, F., and P. Amyotte (2013). Quantitative risk analysis of offshore drilling operations: a Bayesian approach, *Saf. Sci.* **57**, 108-117

Khakzad, N., Khakzad, S., and F. Khan (2014). Probabilistic risk assessment of major accidents: application to offshore blowouts in the Gulf of Mexico, *Nat. Hazards* **74**, no. 3, 1759-1771

Kennett, B.L.N. (Compiler and Editor) (1991). *IASPEI 1991 Seismological Tables*. Bibliotech, Canberra, Australia, 167 pp.

Kijko, A., Lasocki, S. and G. Graham (2001). Nonparametric seismic hazard analysis in mines, *Pure appl. Geophys.* **158**, 1655-1676

Krausmann, E., S. Girgin and A. Necci (2019). Natural hazard impacts on industry and critical infrastructure: Natech risk drivers and risk management performance indicators. *International Journal of Disaster Risk Reduction* **40**, 101163, <https://doi.org/10.1016/j.ijdr.2019.101163>

Krausmann, E. and A.M. Cruz (2017). Past Natech Events, Chapter 2 in *Natech Risk Assessment and Management – Reducing the Risk of Natural-Hazard Impact on Hazardous Installations*, Elsevier, 3-31

Krausmann, E. (2017). Natech Risk and Its Assessment, Chapter 7 in *Natech Risk Assessment and Management – Reducing the Risk of Natural-Hazard Impact on Hazardous Installations*, Elsevier, 105-118

Krausmann, E., A.M. Cruz, B. Affeltranger (2010). The impact of the 12 May 2008 Wenchuan earthquake on industrial facilities. *J. Loss Prev. Process. Ind.* **23**, no.2, 242-248, <https://doi.org/10.1016/j.jlp.2009.10.004>

Lanzano, G., Basco, A., Pellegrino, A.M., and E. Salzano (2017). Natural Hazard Characterization in *Natech Risk Assessment and Management – Reducing the Risk of Natural-Hazard Impact on Hazardous Installations*, Elsevier, 69-88

Lanzano, G., Salzano, E., Santucci de Magistris F., and G. Fabbrocino (2014). Seismic vulnerability of gas and liquid buried pipelines. *Journal of Loss Prevention in the Process Industries* **28**, 72-78, <https://doi.org/10.1016/j.jlp.2013.03.010>

Lanzano, G., Salzano, E., Santucci de Magistris F., and G. Fabbrocino (2013). *Reliability Engineering and System Safety* **117**, 73-80, <http://dx.doi.org/10.1016/j.ress.2013.03.019>

Lasocki, S., and B. Orlecka-Sikora (2020). High Injection Rates Counteract Formation of Far-Reaching Fluid Migration Pathways at The Geysers Geothermal Field. *Geophysical Research Letters* **47**, e2019GL086212, <https://doi.org/10.1029/2019GL086212>

Lasocki, S. (2014). Transformation to equivalent dimensions – a new methodology to study earthquake clustering. *Geophys. J. Int.* **197**, 1224 – 1235, doi: [10.1093/gji/ggu062](https://doi.org/10.1093/gji/ggu062)

Lavecchia, G., Adinolfi, G. M., de Nardis, R., Ferrarini, F., Cirillo, D., Brozzetti, F., ... & Zollo, A. (2017). Multidisciplinary inferences on a newly recognized active east-dipping extensional system in Central Italy. *Terra Nova*, **29**, no. 1, 77-89.

Lavecchia, G., F. Brozzetti, M. Barchi, M. Menichetti, and J. V. Keller (1994). Seismotectonic zoning in east-central Italy deduced from an analysis of the Neogene to present deformations and related stress fields, *GSA Bulletin*, **106**, no. 9, 1107-1120.

Lavecchia, G., P. Boncio, and N. Creati (2003). A lithospheric-scale seismogenic thrust in central Italy. *Journal of Geodynamics* **36**, 79-94, doi: [10.1016/S0264-3707\(03\)00040-1](https://doi.org/10.1016/S0264-3707(03)00040-1)

Lay, T., and T.C. Wallace (1995). *Modern Global Seismology*. Academic Press.

Leone, U. (2014). Editoriale, *Ambiente Rischio Comunicazione. Quadrimestrale di analisi e monitoraggio ambientale*. **No risk no energy**, no. 9, 2-3 (in Italian)

Leptokarpoulos, K., S. Cielesta, M. Staszek, D. Olszewska, G. Lizurek, J. Kocot, S. Lasocki, B. Orlecka-Sikora, M. Strerzel and T. Szeplienic (2019). IS-EPOS: a platform for anthropogenic seismicity research. *Acta Geophysica* **67**, 299-310, <https://doi.org/10.1007/s11600-018-0209-z>

Leptokarpoulos, K., Staszek, M., Lasocki, S., Martínez-Garzón, P., and G. Kwiatek (2018). Evolution of seismicity in relation to fluid injection in the North-Western part of The Geysers geothermal field. *Geophysical Journal International* **212**, no. 2, 1157–1166, <https://doi.org/10.1093/gji/ggx481>

Lockhart D.A., E. Riel, M. Sanders, A. Walsh, G.T. Cooper, and M. Allder (2018). Play-based exploration in the southern Cooper Basin: a systematic approach to exploration in a mature basin. *The APPEA Journal* **58**, 825-832, <https://doi.org/10.1071/AJ17138>

Lomax, A., J. Virieux, P. Volant, and C. Berge-Thierry (2000). Probabilistic earthquake location in 3D and layered models: introduction of a Metropolis-Gibbs method and comparison with linear locations, in *Advances in Seismic Event Location* Thurber, C.H & Rabinowitz (eds.), (p. 101-134). Kluwer, Amsterdam, 101-134.

Lomax, A., Michelini, A., and A. Curtis (2009). Earthquake Location, Direct, Global-SearchMethods. In *Encyclopedia of Complexity and Systems Science*, Part 5, 2449-2473, ed. Meyers, A., Springer, New York, doi: [10.1007/978-0-387-30440-3_150](https://doi.org/10.1007/978-0-387-30440-3_150)

López-Comino, J.A., S. Cesca, J. Jarosławski, N. Montcoudiol, S. Heimann, T. Dahm, S. Lasocki, A. Gunning, P. Capuano and W.L. Ellsworth (2018). Induced seismicity response of hydraulic fracturing: results of a multidisciplinary monitoring at the Wysin site, Poland, *Scientific Reports*, **8**, 1-14, doi:[10.1038/s41598-018-26970-9](https://doi.org/10.1038/s41598-018-26970-9)

Maesano, F. E., G. Toscani, P. Burrato, F. Mirabella, C. D'Ambrogi, and R. Basili (2013). Deriving thrust fault slip rates from geological modeling: examples from the Marche coastal and offshore contractional belt, Northern Apennines, Italy, *Mar. Pet. Geol.* **42**, 122-134, doi:[10.1016/j.marpetgeo.2012.10.008](https://doi.org/10.1016/j.marpetgeo.2012.10.008)

Mann, H.B., and D.R. Whitney (1947). On a Test of Whether one of Two Random Variables is Stochastically Larger than the Other, *The Annals of Mathematical Statistics* **18**, 50-60

Mazzini, C., Agenzia Regionale Prevenzione Ambientale, Corpo Nazionale dei Vigili del Fuoco, Istituto Nazionale Assicurazioni Infortuni sul lavoro, Istituto Superiore per la Protezione e la Ricerca Ambientale, Ufficio Nazionale Minerario per gli Idrocarburi e le Georisorse, Regione Lombardia, Università di Bologna - Dip. Ingegneria Civile, Chimica, Ambientale e dei Materiali (2018). Gli stoccaggi sotterranei di gas naturale - Linee Guida per la valutazione dei Rapporti di Sicurezza.

Mazzoli, S., C. Macchiavelli, and A. Ascione (2014). The 2013 Marche offshore earthquakes: new insights into the active tectonic setting of the outer northern Apennines, *J. Geol. Soc. London* **171**, 457-460, <http://dx.doi.org/10.1144/jgs2013-091>

McMahon, A., and S. Baisch (2013). Case study of the seismicity associated with the stimulation of the enhanced geothermal system at Habanero, Australia. *Proceedings Australian Geothermal Energy Conferences*, Brisbane, Australia, 14-15 November

McKillup, S., and M. Darby-Dyar (2010). *Geostatistics explained. An introductory guide for earth scientists*. Cambridge University Press, London

Meletti, C., and V. Montaldo (2007). Deliverable D2, Valutazioni di ag (16mo, 50mo e 84mo percentile) con le seguenti probabilità di superamento in 50 anni: 81%, 63%, 50%, 39%, 30%, 22%, 5%, 2%, rispettivamente corrispondenti a periodi di ritorno di 30, 50, 72, 100, 140, 200, 1000 e 2500 anni.

Montone, P., M. T. Mariucci, and S. Pierdominici (2012). The Italian present-day stress map, *Geophys. J. Int.* **189**, 705-716, doi: [10.1111/j.1365-246X.2012.05391.x](https://doi.org/10.1111/j.1365-246X.2012.05391.x)

Montone, P., M. T. Mariucci, S. Pondrelli, and A. Amato (2004). An improved stress map for Italy and surrounding regions (central Mediterranean), *J. Geophys. Res.: Solid Earth* **109**, no. B(10), <https://doi.org/10.1029/2003JB002703>

Moser, T.J., T. van Eck and G. Nolet (1992). Hypocenter determination in strongly heterogeneous earth models using the shortest path method., *J. Geophys. Res.* **97**, 6563-6572.

Mysiak, J., Surminski, S., Thieken, A., Mechler, R., and J. Aerts (2015). Sendai Framework for Disaster Risk Reduction – success or warning sign for Paris?, *Natural Hazards and Earth System Science*, **3**, 3955–3966, DOI: [10.5194/nhessd-3-3955-2015](https://doi.org/10.5194/nhessd-3-3955-2015)

Nahar, T.T., Rahman, M.M., and D. Kim (2020). PSHRisk-Tool: A Python-Based Computational Tool for Developing Site Seismic Hazard Analysis and Failure Risk Assessment of Infrastructure, *Appl. Sci.*, **10**, no. 21: 7487. <https://doi.org/10.3390/app10217487>

National Research Council (2013). Induced Seismicity Potential in Energy Technologies. Washington, DC: *The National Academies Press*. <https://doi.org/10.17226/13355>

Nazri, F.M. (2018). Seismic Fragility Assessment for Buildings due to Earthquake Excitation, *SpringerBriefs in Computational Mechanics*, https://doi.org/10.1007/978-981-10-7125-6_2

Nicol, A., Gerstenberger M., Bromley, C., Carne, R., Chardot, L., Ellis, S., Jenkins, C., Siggins, T., and P. Viskovic (2013). Induced seismicity; observations, risks and mitigation measures at CO₂ storage sites, *Energy Procedia* **37**, 4749-4756, doi: [10.1016/j.egypro.2013.06.384](https://doi.org/10.1016/j.egypro.2013.06.384)

Orlecka-Sikora, B., S. Lasocki, J. Kocot, et al. (2020). An open data infrastructure for the study of anthropogenic hazards linked to georesource exploitation. *Sci Data* **7**, no. 89, [doi: 10.1038/s41597-020-0429-3](https://doi.org/10.1038/s41597-020-0429-3)

Orlecka-Sikora, B., S. Cielesta, and S. Lasocki (2019). Tracking the development of seismic fracture network from The Geysers geothermal field. *Acta Geophysica* **67**, 341-350, <https://doi.org/10.1007/s11600-018-0202-6>

Orlecka-Sikora, B. and S. Lasocki, S. (2005). Nonparametric characterization of mining induced seismic sources. in *Proceedings of the Sixth Int. Symp. on Rockburst and Seismicity in Mines*, 2005 March 9–11, Australia, Nedlands, eds Potvin, Y. & Hudyma, M., pp. 555–560. Australian Centre for Geomechanics.

Pierdominici, S., O. Heidbach (2012). Stress field of Italy – mean stress orientation at different depths and wave-length of the stress pattern, *Tectonophysics* 532-535, 301-311, doi: [10.1016/j.tecto.2012.02.018](https://doi.org/10.1016/j.tecto.2012.02.018)

- Podvin, P. and I. Lecomte (1991). Finite difference computation of traveltimes in very contrasted velocity models: a massively parallel approach and its associated tools, *Geophys. J. Int.* **105**, 271-284.
- Pondrelli, S., S. Salimbeni, G. Ekström, A. Morelli, P. Gasperini, and G. Vannucci (2006). The Italian CMT dataset from 1977 to the present, *Phys. Earth Planet. In.* **159**, 286-303
- Popper, K. R. (1968). *The Logic of Scientific Discovery*. London: Hutchinson.
- Porter, K. (2021). A Beginner's Guide to Fragility, Vulnerability, and Risk in *Encyclopedia of Earthquake Engineering*, Springer-Verlag Berlin Heidelberg, doi: [10.1007/978-3-642-36197-5_256-1](https://doi.org/10.1007/978-3-642-36197-5_256-1)
- Raleigh, C.B., J.H. Healy, and J.D. Bredehoeft (1976). An experiment in earthquake control at Rangely, Colorado, *Science* **191**, no. 4233, 1230-1237, doi: [10.1126/science.191.4233.1230](https://doi.org/10.1126/science.191.4233.1230)
- Rapporto di Sicurezza San Potito e Cotignola (2015). Rapporto di Sicurezza ai sensi dell'Art. 8 D. Lgs. 17 agosto 1999, n.334 e s.m.i., Edison Stoccaggio S.p.A.
- Riguzzi, F., A. Tertulliani, and C. Gasparini (1989). Study of Seismic Sequence of Porto San Giorgio (Marche) - 3 July 1987, *Il nuovo cemento* **12 (C)**, no. 4, 453-466.
- Rosti, A., Del Gaudio, C., Rota, M. et al. (2021). Empirical fragility curves for Italian residential RC buildings, *Bull. Earthquake Eng.* **19**, 3165-3183, <https://doi.org/10.1007/s10518-020-00971-4>
- Rovida A., M. Locati, R. Camassi, B. Lolli, and P. Gasperini (2016). CPTI15, the 2015 version of the Parametric Catalogue of Italian Earthquakes. Istituto Nazionale di Geofisica e Vulcanologia, <http://doi.org/10.6092/INGV.IT-CPTI15>
- Rubinstein, J., and A.B. Mahani (2015). Myths and Facts on Wastewater Injection, Hydraulic Fracturing, Enhanced Oil Recovery, and Induced Seismicity. *Seismological Research Letters* **86**, no. 4, 1-8, doi: [10.1785/0220150067](https://doi.org/10.1785/0220150067)
- Sardanelli, F., and G. Di Leo (2008). *Biostatistica in Radiologia, progettare, realizzare e scrivere un lavoro scientifico radiologico*, Springer-Verlag Mailand, doi: [10.1007/978-88-470-0605-8](https://doi.org/10.1007/978-88-470-0605-8)

Schneider, F., Kläy, A., Zimmermann, A.B., Buser, T., Ingalls, M., and P. Messerli (2019). How can science support the 2030 Agenda for Sustainable Development? Four tasks to tackle the normative dimension of sustainability, *Sustainability Science* **14**, 1593–1604, doi: [10.1007/s11625-019-00675-y](https://doi.org/10.1007/s11625-019-00675-y)

Scognamiglio, L., E. Tinti, and A. Michelini (2009). Real-Time Determination of Seismic Moment Tensor for the Italian Region, *Bull. Seismol. Soc. Am.* **9**, no. 4, 2223–2242, doi: [10.1785/0120080104](https://doi.org/10.1785/0120080104)

Scrocca, D., E. Carminati, C. Doglioni, and D. Marcantoni (2007). Slab Retreat and Active Shortening along the Central-Northern Apennines, in *Thrust Belts and Foreland Basins. Frontiers in Earth Sciences*, edited by Lacombe O., Roure F., Lavé J., Vergés J., 471-487, Springer, Berlin, Heidelberg, https://doi.org/10.1007/978-3-540-69426-7_25

Shepherd, M. (2009). Factors influencing recovery from oil and gas fields, in *Oil field production geology*, AAPG Memoir **91**, 37–46, doi:[10.1306/13161187M913372](https://doi.org/10.1306/13161187M913372)

Silverman, B.W. (1986). Density Estimation for Statistics and Data Analysis, Monograph, CRC Press, 175 pp.

Sirovich, L., and F. Pettenati (2001). Test of source-parameter inversion of the intensities of a 54,000-death shock of the seventeenth century in Southeast Sicily, *Bull. Seismol. Soc. Am.* **91**, no. 4, 792-811.

Sirovich, L., F. Pettenati, and C. Chiaruttini (2001). Test of source-parameter inversion of intensity data, *Natural Hazards* **24**, no. 2, 105-131.

Soliani, L. (2008). I test non parametrici più usati nelle discipline scientifiche, Uni.Nova editore, pp.828

Spearman, C. (1904). The proof and measurement of association between two things, *The American Journal of Psychology* **15**, no. 1, 72–101, <https://doi.org/10.2307/1412159>

Stabile, T.A., V. Serlenga, C. Satriano, M. Romanelli, E. Gueguen, M.R. Gallipoli, E. Ripepi, J.M. Saurel, S. Panebianco, J. Bellanova and E. Priolo (2020). The INSIEME seismic network: a research infrastructure for studying induced seismicity in the High Agri Valley (southern Italy). *Earth Syst. Sci. Data* **12**, no. 1, 519-538, <https://doi.org/10.5194/essd-12-519-2020>

Steinberg, L.J., and A.M. Cruz (2004). When natural and technological disasters collide: lessons from the Turkey earthquake of August 17, 1999. *Nat. Hazards Rev.* **5**, no. 3, 121-130.

Stucchi M., Meletti C., Montaldo V., Akinci A., Faccioli E., Gasperini P., Malagnini L., Valensise G. (2004). Pericolosità sismica di riferimento per il territorio nazionale MPS04 [Data set]. Istituto Nazionale di Geofisica e Vulcanologia (INGV), <https://doi.org/10.13127/sh/mps04/ag>

Taylor, J.R. (1999) Introduzione all'analisi degli errori. Lo studio delle incertezze nelle misure fisiche (Seconda edizione), Zanichelli.

Tarantola, A. (2005). Inverse Problem Theory and Methods for Model Parameter Estimation, Siam.

Tarantola, A., and B. Valette (1982). Inverse problems = quest for information, *J. Geophys. Res.* **50**, 159-170.

UN (2015b). Sendai Framework for Disaster Risk Reduction 2015–2030, A/CONF.224/CRP.1, 18 March 2015

UNISDR (2017). Words into Action Guidelines, National Disaster Risk Assessment – Governance Systems, Methodologies and Use of Data. *United Nations Office for Disaster Risk Reduction*, Geneva

Valensise, G., and D. Pantosti (2001). The investigation of potential earthquake sources in peninsular Italy: a review, *J. Seismol.* **5**, no. 3, 287-306.

Valensise, G. (1987). Determinazione simultanea di parametri ipocentrali di eventi sismici regionali e parametri della struttura crostale nell'area italiana, PhD thesis, 'La Sapienza' Università di Roma

van Thienen-Visser, K., and J. Breunese (2015). Induced seismicity of the Groningen gas field: History and recent developments. *The Leading Edge*, 664-671, <http://dx.doi.org/10.1190/tle34060664.1>

Vannoli, P., G. Vannucci, F. Bernardi, B. Palombo, and G. Ferrari (2015). The Source of the 30 October 1930 Mw 5.8 Senigallia (Central Italy) Earthquake: A Convergent Solution from Instrumental, Macroseismic, and Geological Data, *Bull. Seismol. Soc. Am.* **105**, no. 3, 1548-1561, <https://doi.org/10.1785/0120140263>

Vannoli, P., R. Basili, and G. Valensise (2004). New geomorphic evidence for anticlinal growth driven by blind-thrust faulting along the northern Marche coastal belt (central Italy), *J. Seismol.* **8**, no. 3, 297-312, <https://doi.org/10.1023/B:JOSE.0000038456.00574.e3>

Waldhauser, F., and W. L. Ellsworth (2000). A double-difference earthquake location algorithm: Method and application to the northern Hayward fault, *Bull. Seismol. Soc. Am.* **90**, 1353-1368.

Wilson, M.P., G.R. Foulger, J.G. Gluyas, R.J. Davies, and B.R. Julian (2017). HiQuake: The Human-Induced Earthquake Database. *Seismological Research Letters* **88**, no. 6, 1560-1565, <https://doi.org/10.1785/0220170112>

Yamamura, E. (2012). Experience of technological and natural disasters and their impact on the perceived risk of nuclear accidents after the Fukushima nuclear disaster in Japan 2011: A cross-country analysis, *The Journal of Socio - Economics* **41**, no. 4, 360-363, <https://doi.org/10.1016/j.socec.2012.04.002>

Yang, M., Khan, F.I., and L. Lye (2013). Precursor-based hierarchical Bayesian approach for rare event frequency estimation: a case of oil spill accidents, *Process. Saf. Environ. Prot.* **91**, no. 5, 333-342, <https://doi.org/10.1016/j.psep.2012.07.006>

Yeo, I.W., M.R.M. Brown, S. Ge, and K.K. Lee (2020). Causal mechanism of injection-induced earthquakes through the Mw 5.5 Pohang earthquake case study, *Nature Communications* **11**, 2614, doi:[10.1038/s41467-020-16408-0](https://doi.org/10.1038/s41467-020-16408-0)

Zhou, H. (1994). Rapid 3-D hypocentral determination using a master station method, *J. Geophys., Res.* **99**, 15439-15455

Zollo, A., and A. Emolo (2011). *Terremoti e Onde*. Napoli: Liguori Editore.

Web references

Catalogo della Sismicità Italiana (CSI, Catalogue of Italian Seismicity): <https://csi.rm.ingv.it/> (last accessed June 2019)

Catalogo Parametrico dei Terremoti Italiani (CPTI15): <http://emidius.mi.ingv.it/CPTI15-DBMI15/> (last accessed June 2019)

Edison Stoccaggio S.p.A.: www.edisonstoccaggio.it (last accessed June 2021)

European-Mediterranean Regional Centroid-Moment Tensors:
<http://rcmt2.bo.ingv.it/> (last accessed June 2019)

INGV - National Earthquake Center: <http://cnt.rm.ingv.it/> (last accessed January 2021)

IS EPOS (2020), Episode: COOPER BASIN, https://tcs.ah-epos.eu/#episode:COOPER_BASIN, doi:10.25171/InstGeoph_PAS_ISEPOS-2020-001 (last accessed April 2021)

ISIDe Working Group (2007). Italian Seismological Instrumental and Parametric Database (ISIDe). Istituto Nazionale di Geofisica e Vulcanologia (INGV), <https://doi.org/10.13127/ISIDE> (last accessed May 2017)

Italian Ministry of Economic Development: www.unimig.mise.gov.it (last accessed April 2021)

Swiss Seismological Service (SED) ETH Zurich: <http://www.seismo.ethz.ch> (last accessed March 2021)

The Human Induced Earthquake Database (HiQuake):
<https://inducedearthquakes.org/> (last accessed March 2021)

The NonLinLoc Software Guide: <http://alomax.free.fr/nlloc> (last accessed April 2021)

Thematic Core Service – Anthropogenic Hazards (TCS - AH): <https://tcs.ah-epos.eu/> (last accessed March 2021)

ViDEPI Visibilità dei dati afferenti all'attività di esplorazione petrolifera in Italia:
www.videpi.com/videpi/videpi.asp (last accessed June 2019)

La borsa di dottorato è stata cofinanziata con risorse del
Programma Operativo Nazionale Ricerca e Innovazione 2014-2020 (CCI 2014IT16M2OP005),
Fondo Sociale Europeo, Azione I.1 “Dottorati Innovativi con caratterizzazione Industriale”



UNIONE EUROPEA
Fondo Sociale Europeo

